LIGHT COLOURED COOL ASPHALT PAVEMENTS

LIGHT COLOURED COOL ASPHALT PAVEMENTS

JOHN VANDERMEULEN, B.Eng.

A THESIS

SUBMITTED TO THE DEPARTMENT OF CIVIL ENGINEERING

AND THE SCHOOL OF GRADUATE STUDIES

OF MCMASTER UNIVERSITY

IN PARTIAL FULFILMENT OF THE REQUIREMENTS

FOR THE DEGREE OF

MASTER OF APPLIED SCIENCE

Master of Applied Science (2014)	McMaster University
(Civil Engineering)	Hamilton, Ontario, Canada

TITLE:	LIGHT COLOURED COOL ASPHALT PAVEMENTS
AUTHOR:	John vanderMeulen B.Eng., (Civil Engineering) McMaster University, Hamilton, Ontario, Canada
SUPERVISOR:	Dr. Peijun Guo
NUMBER OF PAGES:	xv, 115

Abstract

The black colour of an asphalt pavement causes it to reach very high temperatures throughout the summer months. Asphalt binder is a temperature dependent material, so these high temperatures can result in damage to the road surface.

This report explores the use of light coloured surface coatings to decrease the temperature of an asphalt pavement. A field testing method was developed to compare the effect of several surface materials on temperature. To support this field test, a method was developed to characterize the surface colour (albedo) through the use of a simple light meter. As well, the durability of the surface coatings applied to asphalt pavement surfaces was examined using the Wet Track Abrasion Test, and methods for further testing were suggested.

A numerical model was developed in Abaqus to predict the temperature effects based on the surface colour and climate conditions. This model can be used to predict the temperature in an asphalt concrete pavement at the surface and throughout the depth of the pavement. Two versions of this model were created: A complete model, which is used when all climate data is available, and a simplified model, which uses estimated values to replace any data that is not available

The temperature difference between white and black painted asphalt concrete surfaces was found to be as much as 17°C. Using light coloured surfaces with albedo

values in the range of 0.2 to 0.3 yielded a temperature decrease of approximately 7 to 10°C as compared to a black painted surface. Microclimate effects were found to be significant; wind speed can drastically affect the temperature of a pavement.

The use of hydrated lime in conjunction with a polymer modified asphalt surface course yielded good results for both temperature reduction and durability. It should be considered for future work.

Acknowledgements

Thanks to Dr. Peijun Guo and Dr. John Emery for their support and encouragement throughout the course of my research.

To my research assistant Zahra Alkazwini, thanks for your great work. I couldn't have finished without you.

Thanks to Scott Crowley and Thomas Dziedziejko from AME for donating materials with known material properties. This was invaluable for saving time and allowing consistency across test specimens.

Thanks to Shiloh Canconstruct and MITACS from providing equipment and funding.

Lastly, thanks to NSERC and OGS for providing funding.

Notation and abbreviations

Mathematical Symbols:

Symbol	Units	Name
α	–	Albedo
q	W/m^2	Heat flux
T	°C	Temperature
E	W/m^2	Incident longwave radiation
ϵ	–	Emissivity
σ	$W \cdot m^{-2} \cdot {}^{\circ}C^{-4}$	Stefan-Boltzmann constant
h_c	–	Convection Coefficient
h_r	–	Radiation Coefficient

Abbreviations:

Term	Meaning
IR	Infrared
HMA	Hot Mix Asphalt
UHI	Urban Heat Island
LTPP	Long Term Pavement Performance
BPN	British Pendulum Number

Contents

List of Tables

List of Figures

Chapter 1

Introduction

The majority of paved roads are constructed using asphalt concrete. This material has a black colouring, which in warm temperatures can cause the material to become much hotter than ambient air temperatures. This research studies the effects of the surface colour on the thermal profile of the asphalt concrete.

1.1 Temperature dependence of asphalt concrete

Asphalt binder is a derivative of bitumen. In an asphalt concrete pavement, the asphalt binder remains a thick, viscous fluid. As such, the material properties are subject to change with temperature. As the temperature of an asphalt pavement increases, the binder softens, expands and becomes more ductile, which can lead to surface damage such as rutting and bleeding. At low temperatures, the binder shrinks as well as becoming more brittle, which can lead to cracking in the road. As a consequence of this temperature dependent behaviour, asphalt concrete pavement roads are designed based on the maximum and minimum expected pavement temperatures.

Asphalt binder is graded to perform within these boundaries. Having a large spread between the maximum and minimum temperatures, such as in Ontario, may require more expensive binder to provide adequate durability. If the maximum temperature can be decreased, this may allow for more durable and cost effective designs.

1.2 Influence of surface colour on temperatures

The colour of a material exposed to sunlight affects the temperature it reaches. Dark colours absorb more solar energy, which causes higher temperatures; light colours absorb less solar energy, which causes lower temperatures. The colour of a surface can be characterized by a parameter called albedo, which is the fraction of the incident sunlight that the surface reflects. This is a value between 0 and 1 which describes the amount of solar energy reflected from the surface. An albedo value of 0 indicates that all incident light is absorbed; this corresponds to a black colour. A value of 1 means that all incident light is reflected; this corresponds to a white colour. The expected albedo for a black asphalt concrete surface is in the range of 0.04 to 0.16 (Pomerantz *et al.*, 2000).

1.3 Economics, durability, and environmental benefits

Lowering the maximum temperature that an asphalt pavement experiences can allow for the use of less expensive asphalt binder and/or a less expensive aggregate mix without sacrificing the performance of the pavement. As well, because the pavement layers do not experience as high temperatures, damage such as rutting and bleeding may be diminished. This can lead to a more durable and longer lasting road. More durability requires less maintenance, which can save costs. At the same time, less maintenance results in less use of new asphalt binder, which is a very energy intensive material with a large environmental footprint (Chen *et al.*, 2010).

1.4 Urban Heat Island effect

Continuing on with the environmental benefits, light coloured pavements may decrease the Urban Heat Island (UHI) effect . The UHI effect is the increase in temperatures in a built up urban area as compared to a less developed rural area. Many man-made materials used in an urban environment tend to absorb more solar radiation than natural materials, which causes an increase in temperature. Because asphalt pavement is generally dark in colour, it has a significant influence on the UHI. By using a lighter coloured asphalt pavement, the UHI effect will be diminished (Pomerantz *et al.*, 1999; Yilmaz *et al.*, 2008).

1.5 Summary of objectives

The research in this thesis has components of both physical experiments and numerical modelling. The objectives are summarized below.

- To show the effect of surface albedo on the temperature of pavements;
- To test different materials for suitability as a light coloured surface coating, including both temperature effects and durability;

- To develop a model to predict surface temperatures based on local climate data and the surface albedo;
- To refine the model to allow prediction of surface temperatures at any location based only on readily available data from sources such as Environment Canada;
- To use the model to predict the vertical temperature profile of a pavement and compare it to the existing BELLS3 method.

1.6 Organization of the thesis

This thesis consists of nine chapters. After the introductory chapter, Chapter 2 covers a review of the relevant literature. Chapter 3 covers details of the materials used for this research as well as the preparation of test specimens. Chapter 4 covers the development of a simple method for determining the albedo of a surface. Chapter 5 covers the field testing procedures for determining the temperature effects of surface coatings with varying albedos. In Chapter 6, the durability of the various surface coatings is explored. Chapter 7 covers the development of a model for predicting temperatures within an asphalt pavement and Chapter 8 covers the results of model simulations under various conditions. Finally, Chapter 9 covers the results and conclusions made throughout the process of this applied research.

Chapter 2

Literature review

Considerable research has been performed on the use of light coloured pavements for decreasing surface temperatures. Most of this research covers the use of various surface coatings and material properties which increase the albedo of the surface. There has also been work done on the estimation of surface and profile temperatures of the pavement.

2.1 Existing methods for modifying the surface colour of asphalt concrete pavement

Work has been done at McMaster by Abu-Halimeh (2007) on determining the temperature effects of different concentrations of hydrated lime applied to the asphalt concrete surface. The decrease in temperatures as compared to untreated black asphalt concrete was found to be as much as 14°C. The albedo of the hydrated lime was not measured, nor was the durability of the lime coating.

As described by Emery *et al.* (2014), hydrated lime has been successfully used in some real world pavement projects. The application of lime was tested on three racetracks paved with conventional asphalt concrete pavement. The temperatures were lowered, but there are some concerns about the durability. In another project, two taxiways at Toronto Pearson International Airport were repaired with a layer of hydrated lime coated asphalt concrete pavement. The asphalt binder used is polymer modified, which helps to bind the hydrated lime to the pavement surface and improve the durability. After 7 years, the taxiway remains a lighter colour than the surrounding untreated asphalt pavement surfaces. Hydrated lime was also successfully demonstrated in the construction of the Da'an to Jiliao Expressway in China.

Work has also been done on other methods for creating a light coloured surface. Feng and Zhang (2009) used a number of different paints mixed with glass particles as surface coatings. The results show decreased temperatures compared to an untreated surface. Skid resistance was also tested, using the British Pendulum Number (BPN). It was found that the paint reduces the skid resistance, but for most of the tested surfaces skid resistance satisfies the requirements. The problem with this surface coating material is the durability, as the expected life is only 2 months. One of the coatings tested was a material that had been successfully used in Japan (Kinouchi *et al.*, 2004). This one had the most favourable results and much longer durability, but the cost was much too high for widespread use.

In a study by Wang *et al.* (2013), a polymer composite was developed, consisting of an acrylic or epoxy resin filled with nano particles of TiO_2 or $TiNO_2$. This composite is applied to the asphalt concrete surface as an overlay. As with the work by Feng and Zhang (2009), the skid resistance was tested using the BPN method. The results are improved skid resistance compared to conventional asphalt concrete. When the temperatures are considered, it was found that the polymer consisting of acrylic resin and TiO_2 nano particles provide the best result, a drop of 12.9°C. There are some concerns over the cost of this method and the long term durability was not examined.

Another method that has been used to change the surface colour is to replace the asphalt binder in the surface course with a synthetic resin binder. A study by Lee *et al.* (1985) use a synthetic binder of light yellow colour which is tinted with various pigments. The resulting asphalt concrete reportedly has similar materials properties to conventional asphalt concrete. This project is conducted purely for cosmetic reasons, so details on the thermal performance are not available.

The last common method for making a lighter coloured asphalt pavement is to use light coloured aggregates such as limestone or marble. The surface of the freshly laid asphalt is then mechanically abraded to expose the natural colour of the aggregate (Tran *et al.*, 2009). This can be very effective in areas where good quality light coloured aggregates are available.

The use of portland cement concrete pavements can also be considered, as they naturally have a much higher albedo than asphalt concrete. Levinson and Akbari (2002) state that the albedo for a portland cement concrete pavement can be between 0.18 and 0.39.

2.2 Existing models for predicting temperatures

Different models have been developed to predict temperature in asphalt concrete pavements. Most models assume some nominal surface albedo and do not include environmental effects such as wind.

Gui *et al.* (2007) developed a one-dimensional heat transfer model for surface temperature of asphalt pavement. The model results closely match the results from the data of a single field test, but the model has not been compared to other data to examine its reliability. This model has been used to simulate the effects of various parameters including albedo. It is found that increasing albedo causes a significant decrease in the surface temperature. The magnitude of temperature may not be reliable, as the simulation only has the reference of a single albedo.

A two-dimensional heat transfer model was developed by Yavuzturk *et al.* (2005). This model can be used to predict surface temperatures and the temperatures at different depths. The results of this model are compared to LTPP data and Superpave algorithms. The comparison showed acceptable results. Changes in albedo are not considered in this model. Suggestions for improvement for this model include using a dedicated weather station near the test surface to get more accurate weather data.

Currently two models are mostly used in the industry. The first is the Long-Term Pavement Performance (LTPP) program (Mohseni, 1998), which has developed a model to predict the maximum and minimum surface temperatures as well as to determine binder grade. The second model is the BELLS3 model (ASTM, 2006a), which is used for predicting the temperature profile with depth in the pavement based on the surface temperature.

2.2.1 Long-Term Pavement Performance Program (LTPP)

The FHWA/TRB LTPP program uses data records over a period of several years at locations across North America (Mohseni, 1998). Based on this data, a model has been developed to predict the maximum and minimum surface temperatures of asphalt concrete pavement at any location across North America. This model does not take into account the surface albedo.

The pavement temperature information from the LTPP program and model have been compiled into a software package called LTPPBind. LTTPBind is used to select the correct performance grade PG binder to use in a Superpave HMA mix design, by taking into account the climate data at a specific location and pavement temperatures. This program is available for download from the U.S. Federal Highway Administration (Mohseni, 2005).

2.2.2 BELLS3

The BELLS3 method (ASTM, 2006a) was developed as a simple method to estimate the temperatures at any depth in an asphalt pavement structure (with some depth limitations). This data are commonly used for calculations in deflection testing for tests such as the Falling Weight Deflectometer.

There are minimal data and computational requirements to use the BELLS3 model. The input parameters for this model are surface temperature, the depth below the surface where the temperature is to be estimated, previous day average temperature, and the time of day. This data can be entered into a simple equation to get the estimate. This method does not take into account the material properties or design of the pavement. Because the model is so simplified, there may be some significant error in the estimate. The results of the new model developed herein will be compared to the BELLS3 method in Section 8.5.

2.3 Methods for characterizing the surface colour

Most of the work on the use of light coloured pavement does not give a method for quantitatively characterizing the colour of the pavement surface. What is most important about the colour is how much solar radiation it reflects, so the best way to characterize the colour is to use the albedo or solar reflectance. Both of these terms have a similar meaning; they measure the fraction of solar radiation that is reflected.

Standard methods have been developed to determine the albedo of a surface. ASTM E1918 (ASTM, 2006b) makes use of a pyranometer. This device measures incoming and reflected solar radiation simultaneously. The difficulty with using this method is that it requires a large flat surface and a clear sunny day to get accurate results. This method is not ideal for determining the albedo of small size test specimens, but this is not a problem for determining the albedo of a road surface. Levinson *et al.* (2010) compared a number of other methods for determining the albedo. Using the pyranometer method (ASTM, 2006b), as mentioned above, yields acceptable results under correct conditions. A modified method for using a pyranometer, dubbed "E1918A", by Akbari *et al.* (2008) is a non-ASTM method. This method allows for the use of a smaller diameter specimen.

Another method, ASTM E903 (ASTM, 2012), uses a solar spectrophotometer. This device provides its own calibrated light source. The use of this instrument is relatively simple. Because it only records the albedo of a small area, about 10mm^2, it is best for a uniform surface. This equipment can only be used to analyze small specimens, so for large surfaces a test coupon must be removed. A further complication of ASTM E903 is that the equipment is large, immobile, and expensive.

The last method covered in the Levinson *et al.* (2010) study is the use of a Solar

Spectrum Reflectometer, following ASTM C1549 (ASTM, 2009). The Solar Spectrum Reflectometer is a small, portable device, which is operated by placing the aperture directly on the surface of the specimen. All four of the above methods can yield acceptable results when used correctly.

2.4 Urban Heat Island Effect

The Urban Heat Island (UHI) effect describes the increase of temperatures in built up urban areas in comparison to less developed areas. One of the main contributors to UHI effect is that dark coloured surfaces, with a low albedo, absorb more energy than most natural surfaces (Pomerantz *et al.*, 1999). This can be mitigated by replacing dark surfaces, such as asphalt pavements and roofs, with lighter colour surfaces.

Santamouris (2007) has studied the UHI effect in various cities across Europe. The increase of temperature in urban areas is found to be between 2 and 9°C. This increase in temperature is associated with an increase in cooling loads on buildings and peak energy demand. The use of light coloured materials was suggested as a method for mitigating the UHI effect. The use of portland cement concrete (PCC) pavement may be considered as an option as it naturally has a higher albedo, between 0.18 and 0.39 (Levinson and Akbari, 2002).

Yilmaz *et al.* (2008) have compared the surface temperatures and air temperatures at 2m above the surface between asphalt pavement, soil, and grass. The data were recorded at an airbase in Erzurum, Turkey. Only data from clear, calm days were recorded. The average surface temperature difference between asphalt pavement and soil was 6.5°C and between asphalt pavement and grass was 11.8°C. The average air temperature difference at 2m above the surface is 5.2°C between asphalt pavement and soil and 7.5°C between asphalt pavement and grass.

There is some debate over whether there are any tangible benefits to the use of light coloured asphalt pavement for mitigation of the UHI effect. Yang *et al.* (2013) claim that there is a possibility that light coloured asphalt pavements and roofs can actually cause an increase in the UHI effect. A field experiment conducted in Arizona shows that light coloured ground covers cause a decrease in surface temperature, but there was no significant temperature decrease found in the air temperatures 1.5m above the surface. This contradicts the work done by Yilmaz *et al.* (2008). There are also some negative effects on winter heating costs. The study assumed that the benefits and drawbacks from using white roofs are the same as those for light coloured asphalt pavements. A better comparison would be between light coloured asphalt pavements and rigid pavements made of portland cement concrete, a material which is lighter in colour and is commonly used for constructing roads in some areas, and light coloured asphalt pavements. A portland cement concrete pavement surface with the same albedo as a light coloured asphalt pavement surface should theoretically have an identical effect on the UHI. One part of the study that may be a cause for concern is that some of the solar radiation reflected off of the pavement surface may be absorbed into the surrounding tall buildings, which could increase their temperatures. However, this radiation is being trapped in the city regardless of the surface albedo. The paper also puts forward an assumption that there will be a very high albedo, as much as 0.5 which is comparable to that used for white roofs. This could cause problems with reflection and glare for pedestrians and drivers. In reality, the albedo for a light coloured asphalt pavement is much lower, in the range of 0.15 to 0.3, which is in the same range as portland cement concrete pavement (Levinson and Akbari, 2002).

In summary, there is probably a positive impact on the UHI effect through the use of light coloured asphalt pavement, but further study is required to quantify this.

2.5 Benefits of reducing pavement temperatures

Asphalt concrete is a temperature dependent material, so decreasing the maximum temperatures can have some significant benefits for the performance of the pavement.

Chen *et al.* (2010) discuss some of the problems caused by high asphalt concrete temperatures. There is a decline in the strength and structural stability of an asphalt concrete as the temperature increases due to the softening of the asphalt binder. As well, when the asphalt concrete temperature increases, the volume of the binder expands, which can lead to distresses such as bleeding. Stiffness and rutting resistance decrease with increasing temperatures. It is stated that at air temperatures less than 30°C, a conventional asphalt pavement will not experience significant rutting due to temperature. However, air temperatures above 38°C will cause rutting to increase rapidly and sustained air temperatures above 40°C will cause severe rutting in a matter of days. An example of this is that the landing gear of a parked Boeing 737 sunk 10-15cm into the pavement during a recent heatwave in Moscow (Russia Today, 2014).

A decrease in the maximum pavement temperatures will decrease these problems and increase the durability of the asphalt pavement.

Chapter 3

Testing program, materials and specimen fabrication

3.1 Materials

The hot-mix asphalt (HMA) used the testing program were a Superpave 19mm base course mix and a Superpave 12.5mm FC1 surface course mix. The materials were provided by AME. The mix designs involved are given in Appendix A

The Superpave 19mm base course mix is a standard hot mix asphalt. The asphalt binder incorporated was Superpave Performance Grade (PG) 70-28. The aggregates incorporated were 19mm stone, HL3 stone, high stability sand, and screenings. The 12.5mm FC1 surface course frictional mix is a polymer modified, warm mix asphalt. The term "warm mix" means that an additive was incorporated to decrease the required mixing, placement, and compaction temperatures. The polymer modification enhances (reduces) the temperature value susceptibility, increase the durability, and for the purpose of this research, makes the asphalt concrete surface "sticky," which increases the adhesion of surface coatings. The asphalt binder incorporated was PG 58-40P. The aggregates incorporated were 12.5mm stone, chip, screenings, and manufactured sand.

3.2 Preparation of asphalt concrete specimens

The plant prepared hot-mix asphalt mix was contained in 10kg boxes. The boxes were preheated in an oven at 110°C for a minimum of 2 hours in order to ”soften” the mix. The softened asphalt mix was then split into the required mass for each layer of the specimen. The asphalt mix was then heated to approximately 10°C higher than the specified (AME Mix Design) re-compaction temperature in a microwave. Heating times were approximately 10 minutes to reach the target temperature. The re-compaction temperatures of the SP19mm and SP12.5FC1 asphalt mixes were 150°C and 125°C, respectively.

3.3 Preparation of mould

Two moulds were used to fabricate the asphalt concrete specimens for this test. Both moulds consisted of a 305mm diameter steel pipe bolted to a steel base. The mould for preparing the base of the specimen was 350mm high, and the mould for preparing the surface of the specimen was 50mm high. The moulds were preheated in an oven to 60°C in order to decrease initial cooling of the asphalt mix. The sides of the moulds were lubricated with a safe food-grade lubricant (PAM) in order to facilitate removal of the completed specimen.

3.4 Compaction of specimens

A predetermined mass of asphalt mix was measured, then placed in the preheated mould. The temperature of the asphalt mix was measured using a probe thermometer, and compaction was started when the mix had cooled down to the re-compaction temperature. The asphalt mix was then rodded in order to distribute it evenly before compaction.

Thereafter, the asphalt mix was compacted using an impact hammer (Milwaukee SDS-Max Demolition Hammer, model number 5446-21) with a round 100mm diameter tamper attachment. The initial compaction was carried out by rocking the tamper back and forth while moving it around the surface. After the initial compaction, the tamper was held horizontal to the surface and slid around to smooth the surface. Lift thickness was pre-determined based on mass and expected density, so final compaction was reached when the thickness reached the required level. The height was taken at three symmetrical points around the mould in order to confirm if the compaction was proceeding in a uniform manner. The compaction time for each lift was approximately 8 to 10 minutes.

For the base course, lifts were added until the total height reached 260mm. Each lift was approximately 12kg, with a target density of 96% of the maximum relative density. Typical achieved density was 93 to 96%. The final lift mass was determined based on the remaining height to 260mm. Care was taken to ensure that the surface of the final lift was level. After the final lift was placed, a flat steel disk was placed on top and loaded with an approximately 30kg mass to improve the smoothness of the surface.

For the surface course, the specimen was compacted in one lift of 40mm. The

Figure 3.1: Compaction of surface course mix

thickness tolerance for surface deviation was 1mm. The mass of the lift was 6.9kg. As with the final layer for the base course, the surface of the specimen was made as smooth as possible, and load was applied after compaction to help smooth the surface. Some flushing was observed on the top surface of the specimen due to the compaction method. To use a more realistic surface for testing, the surface course specimens were used upside down. The compaction method for the surface course is shown in Figure 3.1. Typical density achieved was 94 to 96%

3.5 Removal of specimen from mould

The specimens were removed from the moulds approximately 30 minutes after compaction of the specimens was completed. For the base course, the bottom of the mould was removed and the mould was lifted approximately 50mm using a chain block. The sides of the mould were tapped with a hammer until the specimen started to slide out, at which time the mould was lifted clear of the specimen. This method worked best when the specimen was still at a temperature near 80°C. In cases where the specimen had cooled too much, it would not slide out, requiring the use of a hydraulic press.

For the surface course, the bottom of the mould was removed and the specimen pushed out be hand. For some specimens, the bottom had to be hammered off the mould.

3.6 Instrumentation

Thermocouples were installed at various depths aong the central axis of the specmines.

To install the thermocouples, the base course specimen was laid on its side and supported by a steel channel. A pilot hole was then drilled into the specimen using a 4.8mm bit in a drill press to the maximum extension of the drill press. The hole was then completed to the centre of the specimen (153mm) using a hand held hammer drill. A hole was placed at 30mm from the top surface and a further three more were installed at 50mm increments.

For the surface course specimen, the small thickness made drilling difficult. A steel channel was clamped to either side of the specimen in order to hold it vertical and prevent the drill from pushing out the sides. A level was used to insure that the hole was being drilled vertically. The hole was placed in the centre of the specimen, at 20mm depth.

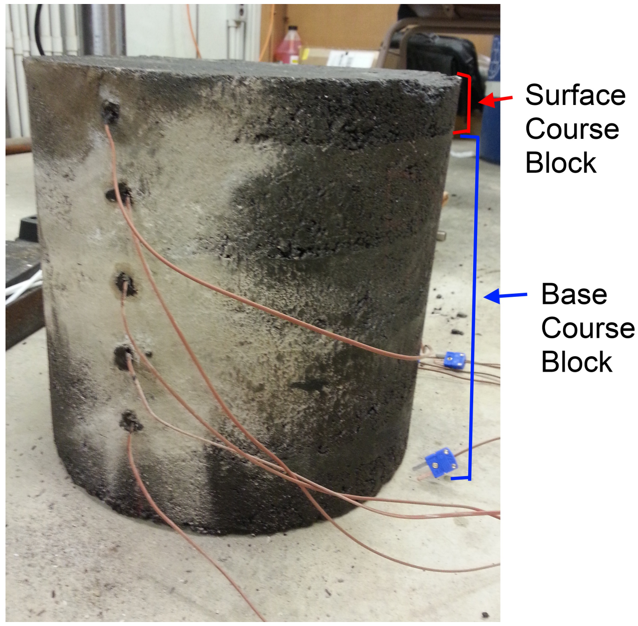

Figure 3.2: Instrumented specimen

Thermocouples were placed in the holes. In some cases, the holes had to be re-drilled in order to allow the thermocouple to reach full depth to the centre of the specimen. The holes were backfilled with a mixture of asphalt pavement sealer and sand which was pushed down the hole using a thin metal rod. A fully instrumented specimen is shown in Figure 3.2.

3.7 Joining surface course specimen to base course specimen

An emulsified asphalt tack coat was applied to the top of the base course block. The tack coat was mixed 1:1 with water and spread at a rate of 0.2kg/m^2.

The specimen was then dried under an infra-red heating panel for approximately 30 minutes. The tack coat is ready (cured) when it turns a brown colour and the surface is sticky to the touch.

The surface course block was next placed upside down on top of the base block (as noted previously). Heating was resumed until the surface temperature reached at least 45°C (60°C would be ideal, but it was difficult to achieve with the heater). Once the temperature was achieved, the heater was removed, and a steel plate was placed on top which was loaded with at least 30kg mass. This was left overnight for the specimen to set.

3.8 Applying the surface coating

Several materials were used as surface coatings to make light coloured surfaces in order to determine the effects of different surface albedos on the specimen temperature profile. The materials used are summarized in Table 3.1. In these surface coating materials, the black and white paints bracket the maximum and minimum albedo values in this study. The other coating materials are expected to produce grey colours at the asphalt concrete specimen surfaces.

Before a coating was applied, a thermocouple was glued to the surface of the specimen. This was done before application of the coating for two reasons. First, the surface must be clean to allow good cohesion. Second, the thermocouple itself should be coated so that it does not affect the surface temperature or temperature profile.

Paints were simply applied to the cold specimen surface with a roller. The various powdered coatings were spread while the surface was warm in order to simulate field application on a fresh compacted asphalt concrete surface. Heating was accomplished with the heating panel, to a temperature of at least 45°C. The coating was then applied with a brush. A piece of wax paper was then placed over the top and the

Table 3.1: List of surface coatings

Material
Natural untreated asphalt concrete
Hydrated lime
Limestone screenings
Baghouse dust
Portland cement
White Paint
Black Paint

powder was pressed into the surface using a steel cylinder as a "rolling pin". It should be noted that a polymer modified HMA surface course was used throughout to aid in coating cohesion.

The amount of coating to use was measured out before application. Based on the work by Abu-Halimeh (2007), the optimal mass of hydrated lime is 150g/m^2, so this was used for all coatings except limestone dust. The limestone dust failed to spread well, and 300g/m^2 had to be used to cover the surface.

Chapter 4

Determination of albedo

The conventional methods for determining albedo, as mentioned in Section 2.3, require a complex testing procedure and/or very expensive equipment. In order to readily determine the albedo of a surface, a simple, inexpensive method was developed. This method was calibrated by comparing its results with those obtained from the standard method ASTM E1918 (ASTM, 2006b)

4.1 Equipment used

The standard method for determining Albedo, ASTM E1918 (ASTM, 2006b), makes use of a pyranometer. In this study, the pyranometer that was used was made of a pair of Kipp & Zonen PAR LITE sensors mounted back to back. One sensor was oriented upwards to collect incident light, and the other was oriented downwards to collect reflected light. Data was recorded using a Campbell Scientific CR5000 datalogger.

The proposed simplified method used a Sekonic L-758DR light meter. Incident light was recorded using the illuminance meter function and reflected light was recorded using the luminance meter.

4.2 Testing procedure

Albedo was first measured using the pyranometer in accordance with ASTM E1918.

Next, the albedo was measured using the light meter. The Sekonic L-758RD is technically suitable for this purpose. The light meter was first placed level on the ground surface in order to record the incident light (Illuminance in lux). For reflected light (Luminance in cd/m^2), the light meter was held perpendicular to the surface at a height of approximately 1 metre above the surface. Incident and reflected light readings were taken less than 30 seconds apart in order to limit errors resulting from brightness variations. A minimum of three manual readings were taken to allow result averaging.

The light meter was also calibrated against a standardized Sekonic Exposure Profile Target II card, which has grey patches of known reflectivity (albedo) which vary from pure white to pure black.

4.3 Determination of albedo from recorded data

The pyranometer data was recorded in millivolts. There is a linear relationship between the measured millivolts and the amount of light received by the PAR LITE sensor, so millivolts could be directly used to calculate albedo. Albedo is calculated as the ratio between the readings of millivolts for reflected and incident light:

$$Albedo = \frac{Reflected\ light}{Incident\ light} \tag{4.1}$$

For the Sekonic light meter, the incident and reflected lights are recorded in different units. The following formula, based on Tatum (2011), was used to convert between reflected (Luminance in cd/m^2) and incident (Illuminance in lux) light:

$$Illuminance = Luminance \cdot \pi \tag{4.2}$$

This equation is applicable for a Lambertian surface, which is a non-glossy surface under diffuse lighting conditions. Under direct sunlight, a correction factor may be required. As a result, the albedo is calculated from the light meter readings as:

$$Albedo\ \beta = \pi \frac{Luminance\ (cd/m^2,\ Reflected)}{Illuminance\ (lux,\ Incident)} \tag{4.3}$$

4.4 Results

The albedos were determined for different surfaces using both the standard and the simplified methods. The surfaces considered ranged from fresh white snow to new black asphalt concrete. Figure 4.1 compares the albedo results obtained from both methods.

Albedo is recorded as a value between 0 and 1, where 0 means no light is reflected and 1 means 100% of the light is reflected. Black asphalt concrete surface is expected to have an albedo in the range of 0.04 and 0.16 (Pomerantz *et al.*, 2000), and fresh snow in the range of 0.8 and 0.95 (Yuri, 1998).

As shown in Figure 4.1, the correlation between the results of both methods is very good. The R^2 value was found to be 99.5% and the root mean square error (RMSE) was 4.4%. The maximum difference between the albedo measured from the pyranometer and light meter data was 0.05.

When analysing the data, it was determined that the accuracy with which the light meter could repeat readings was less than that of the pyranometer. The pyranometer conformed to the required accuracy in ASTM E1918 of no larger than 0.01 on a scale of 0 to 1. The light meter readings fluctuated up to 0.05 for a uniformly coloured surface. This can be attributed to the accuracy of manual readings and also the nature of the sensor. Readings cover a single point, so a non-uniform surface colour will yield different results. The minimum requirement for getting an accurate measurement with this method is 3 readings taken with a difference in albedo of less than 0.05. If the 3 readings are outside this range, then a minimum of 6 readings must be made. The maximum and minimum outliers are then removed before averaging. Taking the average of 6 to 10 readings will significantly improve the accuracy for a non-uniform surface.

Comparing the light meter results to the Sekonic Exposure Profile Target II card, the correlation is also very good. The R^2 value was found to be 99.9% and the root mean square error (RMSE) was 3.2%. The differences between the expected value and recorded value are displayed in Figure 4.2.

4.5 Limitations

As mentioned previously, measuring albedo using a technically light meter works best on non-glossy surfaces under diffuse lighting. Measurements are best taken inside, on an overcast day, or in the shade. If inside light is used, error may increase due to the accuracy of the meter. It should be noted that the albedo recorded may vary based on the light source used, so all measurements should be taken under the same

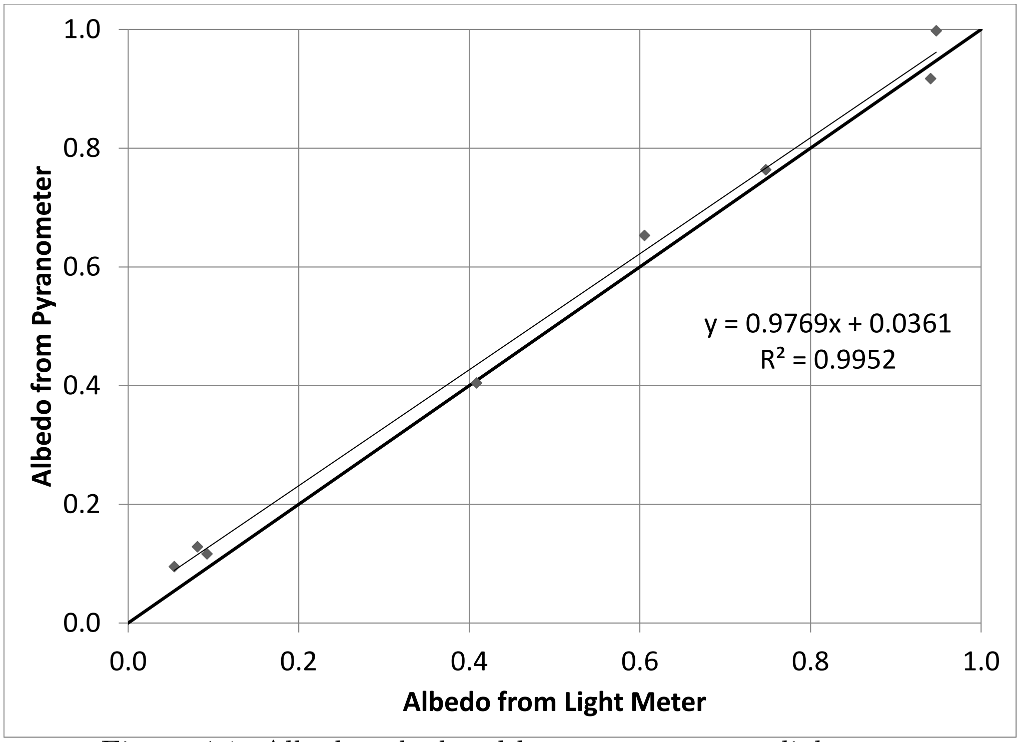

Figure 4.1: Albedo calculated by pyranometer vs light meter

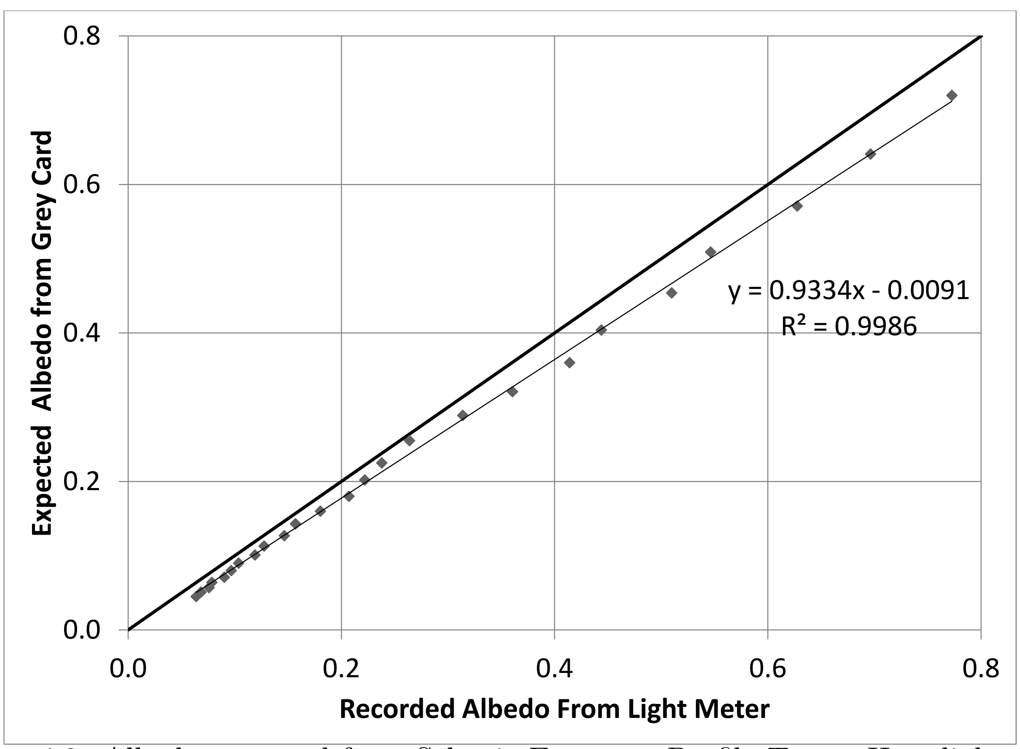

Figure 4.2: Albedo expected from Sekonic Exposure Profile Target II vs light meter albedo

Table 4.1: Albedo of asphalt concrete surfaces treated with different surface coatings

Material	Concentration	Albedo
Natural	–	0.044
Hydrated lime	$150g/m^2$	0.703
Limestone screenings	$300g/m^2$	0.537
Baghouse dust	$150g/m^2$	0.333
Portland cement	$150g/m^2$	0.373
White Paint	–	0.808
Black Paint	–	0.059

lighting conditions.

This simple light meter method has only been tested on grey scale surface. For differently coloured surfaces, the difference in wavelengths of reflected light as compared to grey surfaces may inhibit the accuracy of the albedo measurements.

The accuracy of this method for albedo measurement can be expected to be ± 0.025 for a surface of non-uniform colour when sufficient data points are taken for averaging. For a fully uniform surface the accuracy will be better.

4.6 Conclusions

The albedo of various grey coloured surfaces were determined by following ASTM E1918 and by the use of a technically suitable light meter. The light meter was also tested against a calibrated exposure profile target. Based on a good correlation between the results of both methods, the simple light meter method has been determined to be accurate.

The light meter was used to determine the albedos for all of the surface treatments used in this research. The results are summarized in Table 4.1

Chapter 5

Field testing

A number of different surface coatings were tested under field exposure conditions to determine their impact on the temperature of asphalt concrete specimens. A "natural" untreated asphalt concrete surface was used as the control, and black and white paints were used to bracket the maximum and minimum temperatures that could be expected.

5.1 Test setup

The test specimens were placed on a gravel bed approximately 300mm thick. The test location was in an open area outside the Applied Dynamics Laboratory (ADL), with direct sunlight (no shadow) for most of the day. The asphalt concrete specimens (cylinders) were insulated around the sides using 50mm thick expanded polystyrene cylindrical half shells, as shown in Figure 5.1. Four specimens were tested at the same time in order to compare the effect of different surfaces under identical exposure conditions.

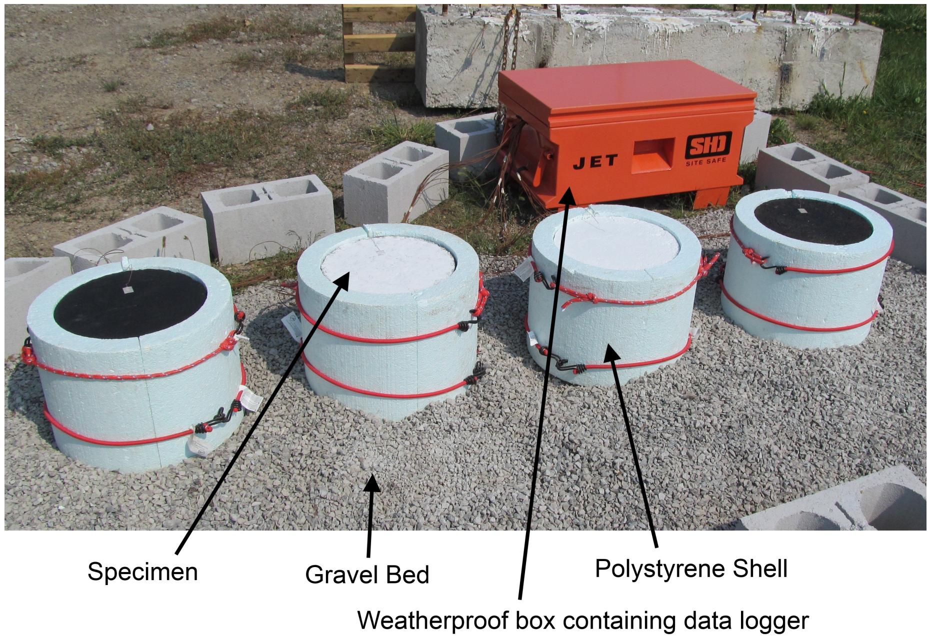

Figure 5.1: Test setup

The thermocouples were connected to a data logger and laptop. Temperatures were recorded every 10 minutes for the duration of the test. The data logger and laptop were secured in a locked weatherproof box.

5.2 Instrumentation

Thermocouples were installed in the specimens as described in Section 3.6. They were type T, 24 gauge wire, with special limits of error. The wire was cut to length (approximately 1m) and the sensor end connection was soldered. The thermocouples were installed into the centre of the specimen at depths from the surface of 20, 50, 120, 170, and 220mm. As well, a thermocouple was attached to the surface to measure the surface temperature and a probe thermocouple was placed in the gravel bed approximately 30mm below the specimen (depth from specimen surface of 330mm)

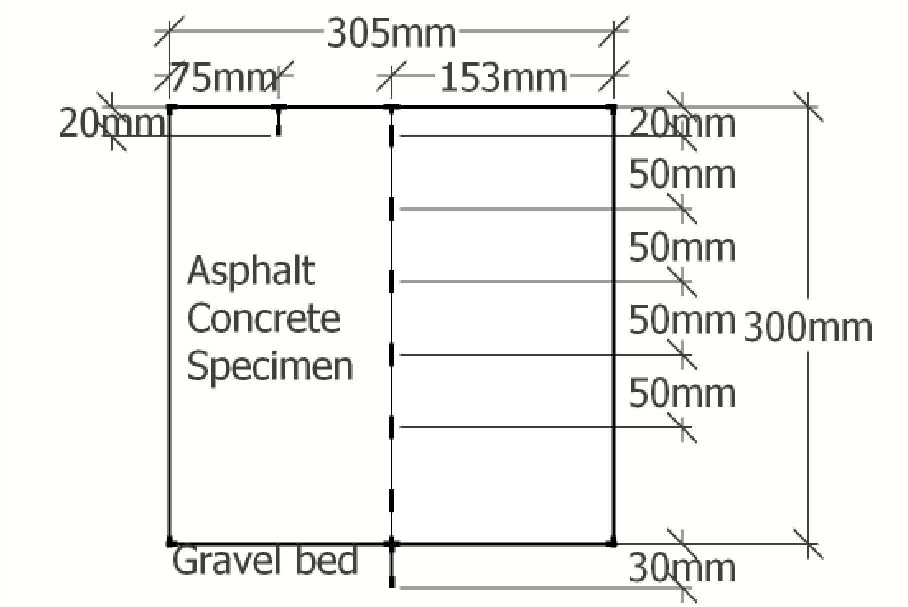

Figure 5.2: Thermocouple locations

to quantify the boundary condition at the bottom of the specimen. A control thermocouple was installed at 20mm depth from the specimen surface but only half the distance from the side (75mm) in order to check whether there was any significant deviation in horizontal temperature distribution. The locations of the thermocouples are shown in Figure 5.2.

5.3 Weather data

The weather data used for this study were wind speed, longwave downward radiation, shortwave downward radiation, and air temperature. The data was acquired from the McMaster Weather Station, which was located approximately 600m from the test site on the roof of the General Sciences Building. Weather data was recorded continuously at 15 minute intervals.

Table 5.1: Summary of testing program

Test #	Date	Surface Coatings
1	August 8-12, 2013	Natural untreated
		Black paint
		White paint
		Hydrated lime
2	August 13-19, 2013	Black paint
		Baghouse dust
		Portland cement
		Limestone screenings
3	August 19-22, 2013	Natural untreated
		Black paint
		White paint
		Hydrated lime

5.4 Results of the field tests

Three series of outdoor tests were completed at the test site outside of the ADL. Each test measured the temperature profile within the asphalt concrete specimens. Four specimens were tested for each testing period. Table 5.1 summarizes the different specimens tested in each series. The requirements for weather conditions were rain free days with mostly clear skies. Higher ambient temperatures would have been ideal, but within the allowable time frame the daily high temperatures did not exceed 30°C. A minimum of 48 hours from midnight to midnight were required for each testing phase to establish the temperature regime and the daily temperature variation, and to eliminate any initial temperature effects present at the beginning of the test.

5.4.1 Surface temperatures

The first outdoor test took place during the period of August 8 to 12, 2013. Four specimens were tested: natural control (no surface treatment), surfaces painted with white and black paints respectively, and a surface treated with hydrated lime (Table 5.1). The surface temperature histories of these four specimens are compared in Figure 5.3 at the end of this section. It can be seen that the white paint and hydrated lime have very similar surface temperature histories; the same can be said about the black paint and natural asphalt concrete black surface. This can be directly related to the albedo values, which are similar for each pair. The surface temperatures of white painted surfaces were approximately 40°C higher than the ambient air temperature. The temperature differences between black and white painted surfaces was as much as 18°C. This significant temperature difference was an ”extreme” result, as it compares the effects of the darkest and lightest colours available, with the albedos being 0.059 and 0.808, respectively. The weather conditions included some cloud cover, as indicated in some ”spiking” of the temperatures (Figures 5.3 to 5.8).

The second outdoor test took place under similar ambient conditions between August 13 and 19, 2013. As shown in Figure 5.4, the black paint again reached the highest surface temperatures. The baghouse dust and portland cement surfaces had similar performance, and the limestone screenings had the lowest temperatures. However, limestone screenings had very poor adhesion to the surface and would therefore probably be an unacceptable coating material. The baghouse dust and portland cement had albedo values of approximately 0.3, which is in the ”ideal” range for light coloured pavements. The two surface coatings yielded a temperature decrease of 7 to 10°C in comparison to the black surface of a natural asphalt concrete. Weather conditions for this test again included some cloud cover.

The third outdoor test took place between August 19 and 22, 2013. It was a replication of the first test series in order to confirm the repeatability of the test results. This period was warmer than the previous tests, so the asphalt concrete temperatures were correspondingly higher. The temperature difference between the black and white specimen surfaces was similar to that seen in the first test. The test results are plotted in Figure 5.5. Weather conditions were mostly clear skies and warm temperatures, resulting in the highest temperatures of the three tests.

In order to find a correlation between the surface temperature and albedo, a plot was made comparing the maximum surface temperature above ambient air temperature in relation to albedo. As shown in Figure 5.12, it can be seen that there is an approximately linear relationship between the albedo and maximum surface temperature above ambient.

5.4.2 Temperature profile with depth

The temperature distribution with depth in the specimen was also recorded for each specimen with a different surface coating. Examples of the full temperature record are shown in Figures 5.6 to 5.8 for a black painted specimen, a white painted specimen, and a lime treated specimen for test 1. It can be seen that the control thermocouple embedded only 75 mm into the specimen at a depth of 20 mm has values similar to the fully embedded thermocouple at the centre of the specimen. This indicates that horizontal heat flow within the specimen was negligible, which implied one-dimensional heat transfer.

The temperature plotted against depth is shown in Figures 5.9 to 5.11 for the hottest day of each test. The results of other days are shown in Appedix B Figures B.3 to B.9. Here, the temperature profile is plotted for when the specimen surface was hottest, which occurred between 14:00 and 16:00 depending on ambient weather conditions. It can be seen that the temperature differences are greatest within the top asphalt concrete layers, but at the ground level the temperatures are not significantly affected by the surface coatings.

The difference between the highest surface temperatures of the white and black specimen surfaces were quite large, while at depth the values converge to a value between 20 and 25°C. This value is the ground temperature, which does not change very much throughout the warm summer months. This is essentially in accord with typical asphalt pavement temperature monitoring of highway and airport pavements. (ref. Pomerantz *et al.*, 1999, 2000)

5.5 Observations and Conclusions

From the test results for the specimens with different surface coatings (treatments), a number of observations can be made:

- The natural surface of new asphalt concrete and the black painted surface have a similar albedo value, approximately 0.05. The black surface temperature could be 22°C higher than the ambient temperature for typical southern Ontario summer days.
- Lighter surface colour can significantly reduce the asphalt concrete surface temperature. Using the black painted surface as a the reference, the maximum temperature decrease for white paint and hydrated lime are in the range of

14 to 18°C. Portland cement and baghouse dust treated surfaces have similar albedos and can result in similar lower surface temperatures. Both surfaces experience a maximum decrease in the range of 6.5 to 8.5°C as compared to the black painted surface. The limestone screenings can reduce the pavement surface temperature by 9.5 to 12.5°C as compared to the black painted surface.

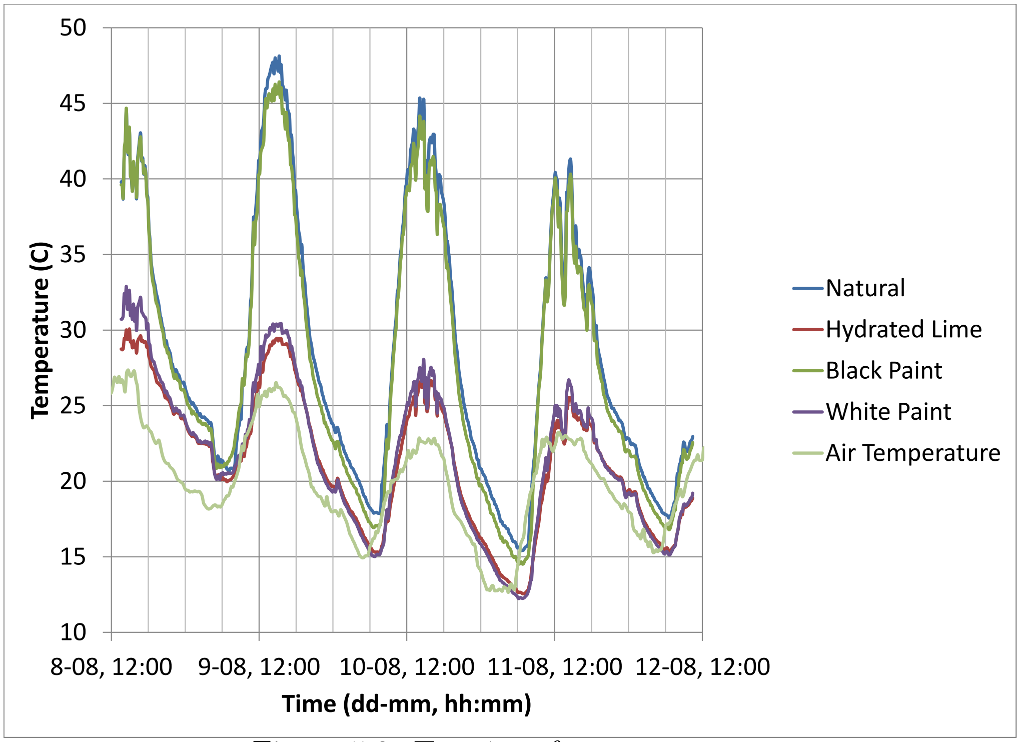

Figure 5.3: Test 1 surface temperature

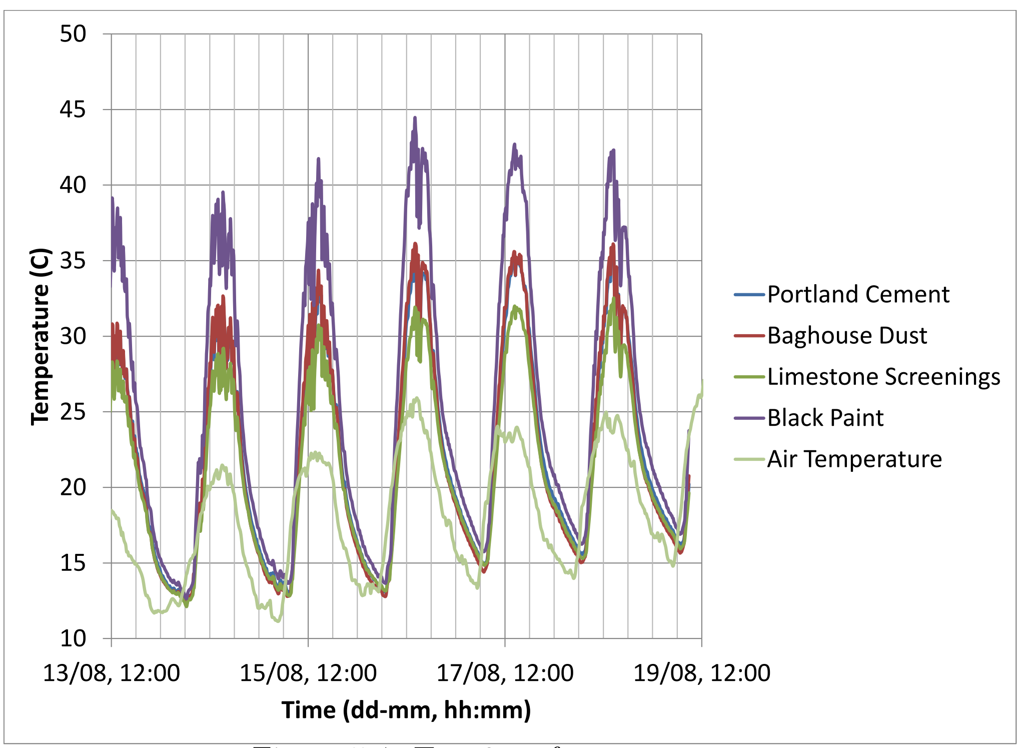

Figure 5.4: Test 2 surface temperature

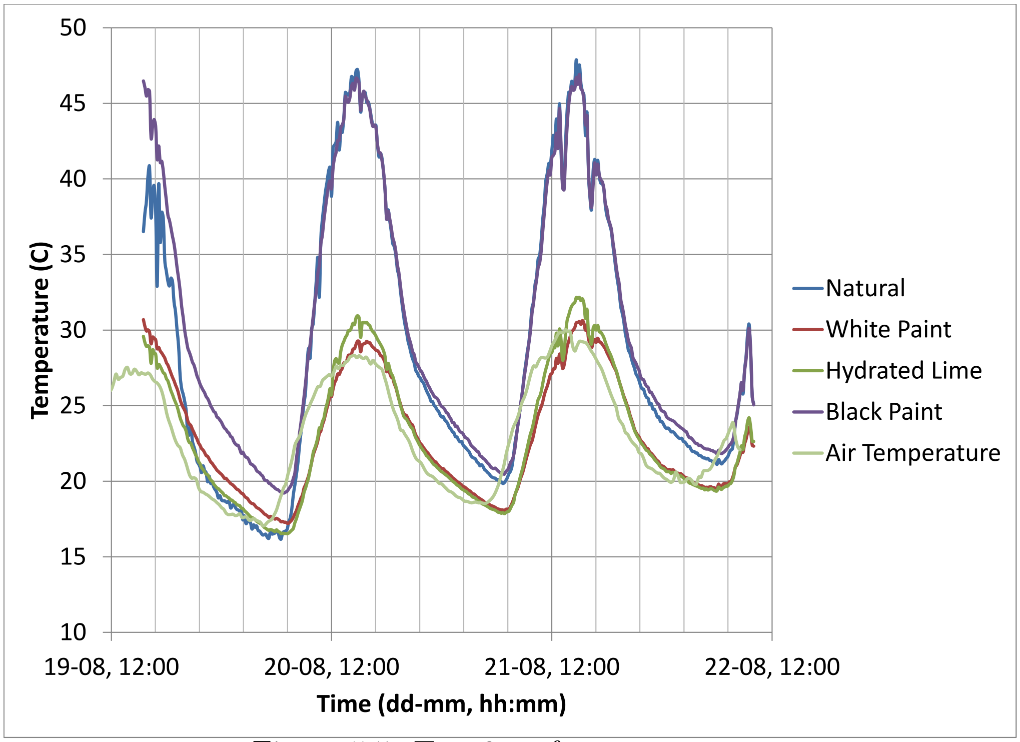

Figure 5.5: Test 3 surface temperature

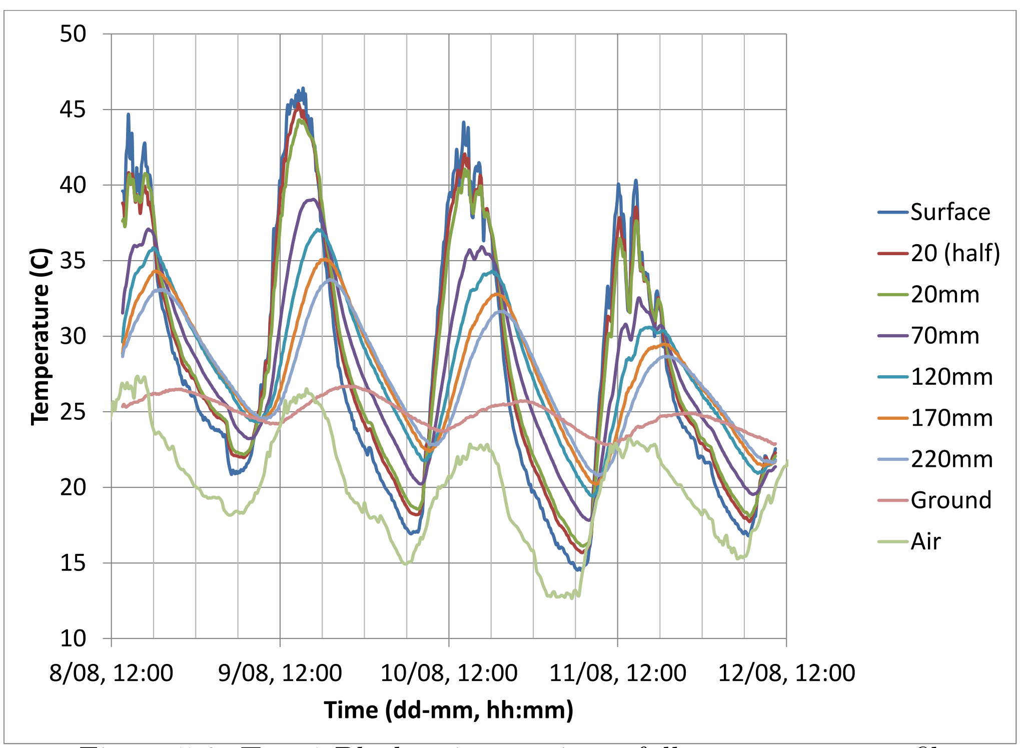

Figure 5.6: Test 1 Black paint specimen full temperature profile

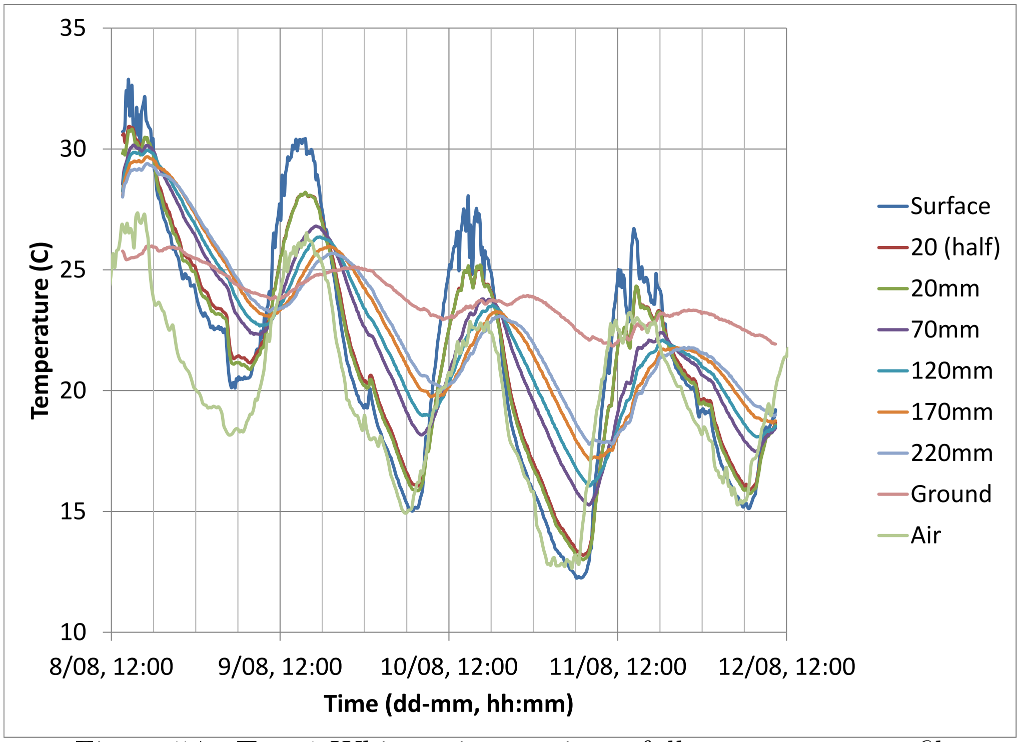

Figure 5.7: Test 1 White paint specimen full temperature profile

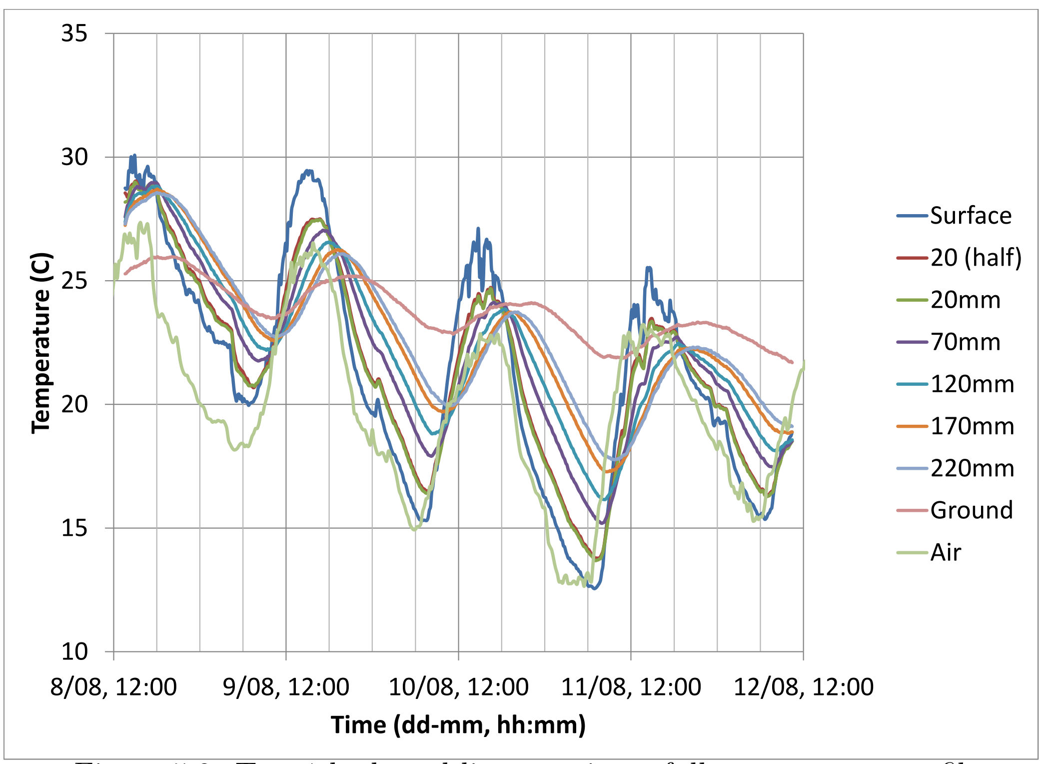

Figure 5.8: Test 1 hydrated lime specimen full temperature profile

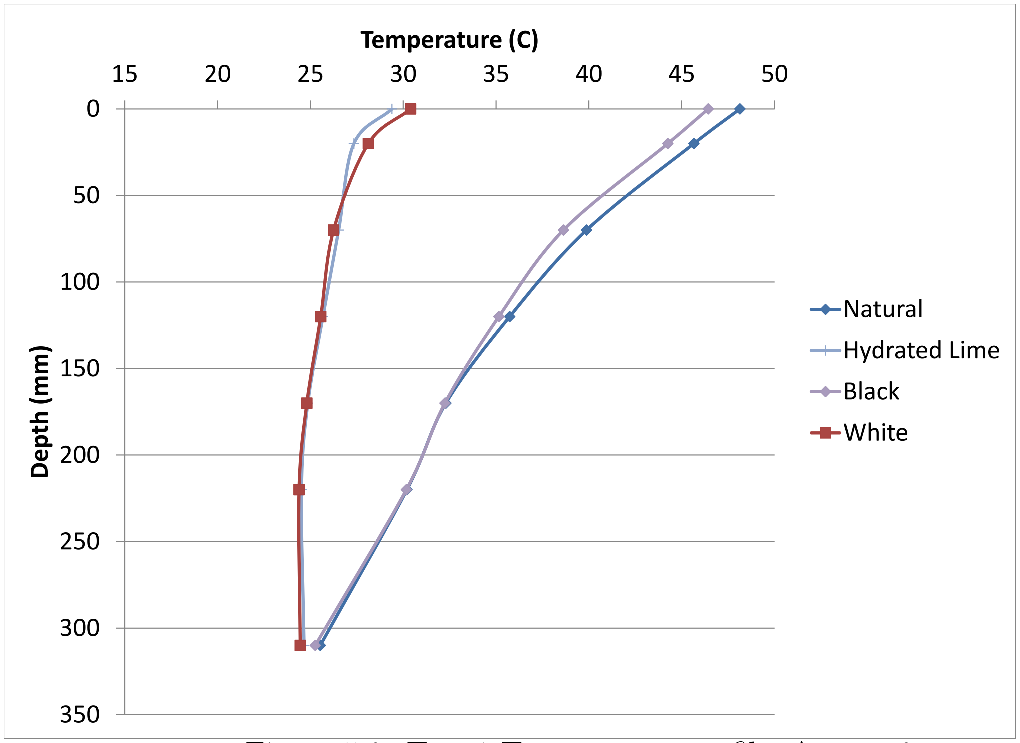

Figure 5.9: Test 1 Temperature profile, August 9

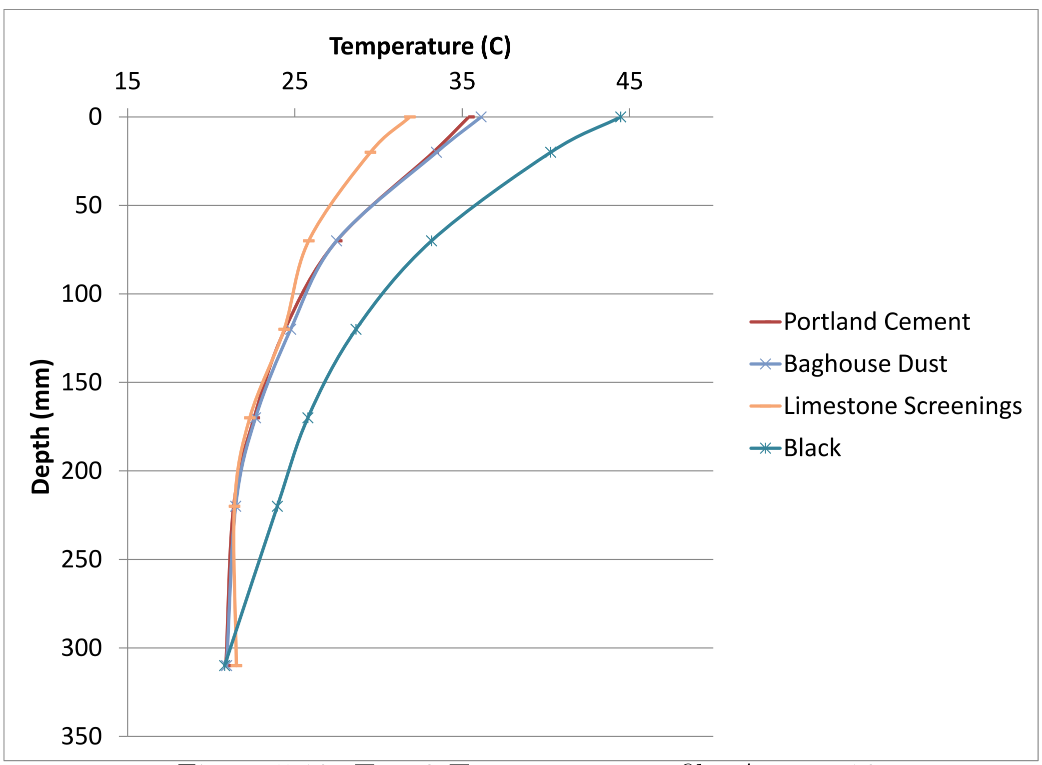

Figure 5.10: Test 2 Temperature profile, August 16

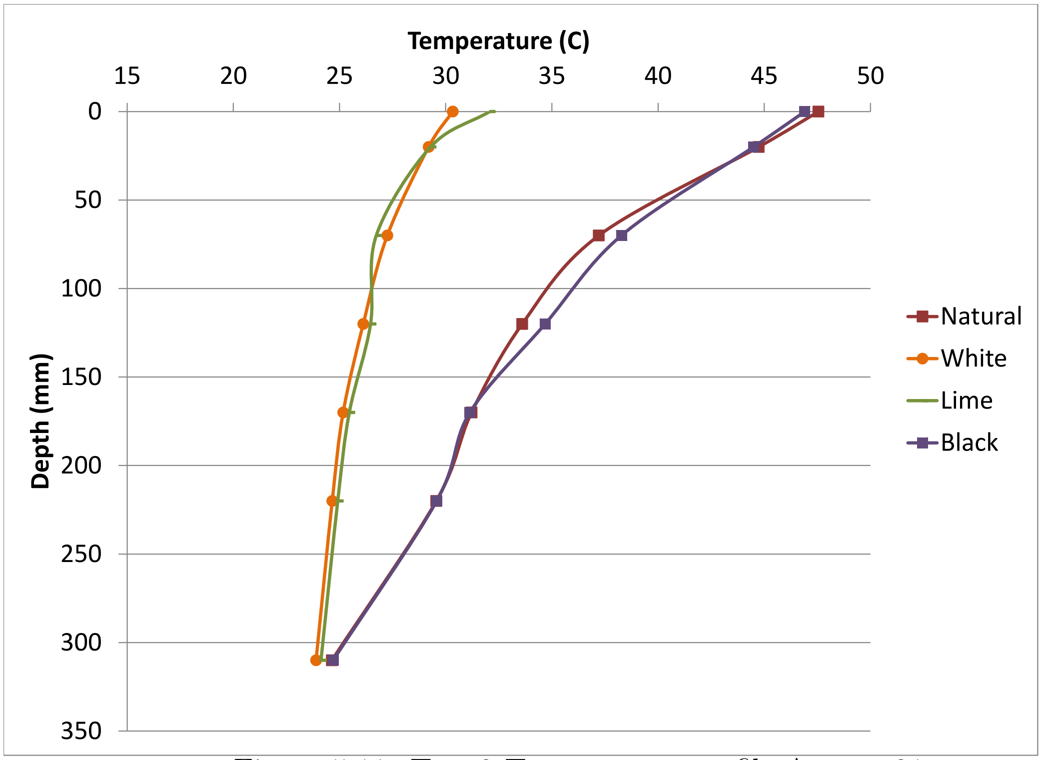

Figure 5.11: Test 3 Temperature profile August 21

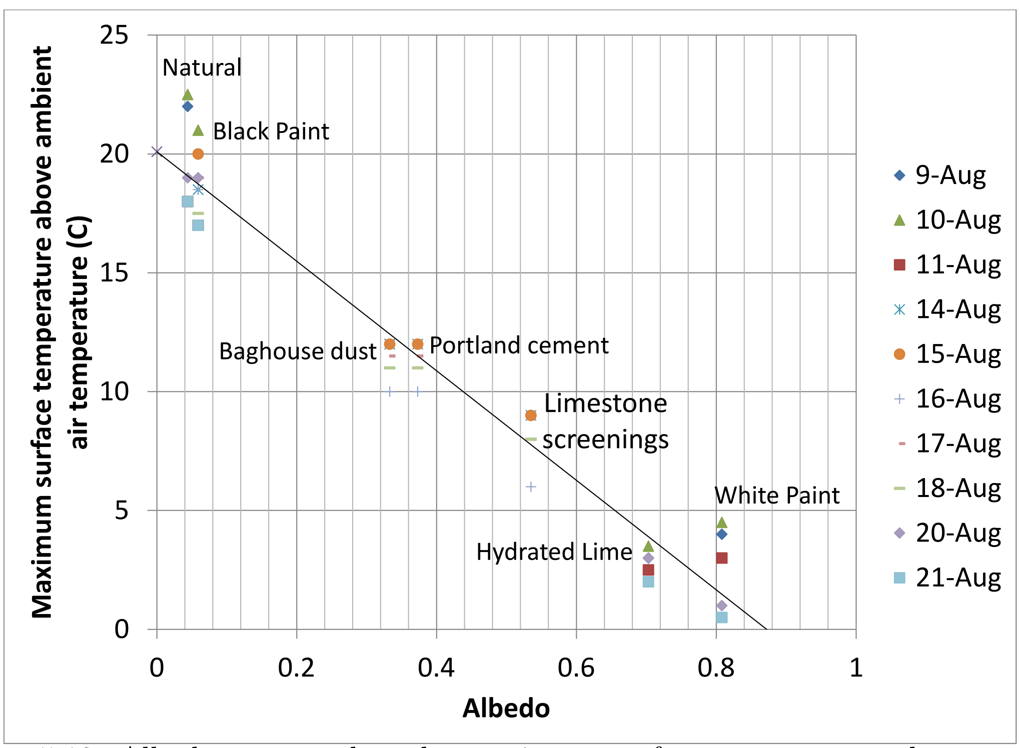

Figure 5.12: Albedo compared to the maximum surface temperature above ambient air temperature

Chapter 6

Durability analysis

The durability of any coating used to lighten asphalt concrete is very important. At the very least, the coating must last until the asphalt concrete surface has naturally aged to a lighter colour. This means that the material must last for several years.

6.1 Wet Track Abrasion Test

In order to test the durability of coatings, a modified version of the Wet Track Abrasion Test (ASTM, 2011) was used. The standard version of this test was used to determine the wear of a slurry seal through abrasion by a rubber hose. In the Wet Track Abrasion Test, a piece of standard rubber hose is weighted with 5lb (2.26kg) and "rubbed" over the submerged surface in a circular pattern by a planetary type mechanical mixer for 5 minutes. The change in weight of the slurry seal during the test indicates the amount of potential damage (wear and tear) as compared to a specification for slurry seal design. The procedure for the modified method used herein is outlined in Appendix C.

6.1.1 Wear analysis using albedo

For the testing of the durability of light coloured asphalt concrete surface coatings, the quantity of material removed is difficult to measure, but fortunately it is not important as compared to the longevity of the of increased albedo. In this research, the change in albedo was used as a measure of the durability. As wear is experienced during the test, some of the surface coating is removed along with some of the asphalt binder, while some of the surface coating is forced further into the "pores" of the asphalt concrete. The albedo was measured by using the light meter as described in Chapter 4 before and after the Wet Track Abrasion Test to determine whether the surface coating (colour) is still acceptable after wear.

A further modification to the test is to increase the time of abrasion. The standard test requires only 5 minutes of abrasion. It was found that this was not enough time for the surface coating to wear down significantly, so albedo was also recorded after testing for a total of 50 minutes and 150 minutes.

6.1.2 Preparation of surfaces

When applying the surface coatings in the laboratory, more ideal conditions could be implemented than in the field (Section 3.8). The application of a coating material in the real field situation would occur when the freshly laid asphalt concrete is still warm. In order to simulate this in the durability test, the asphalt concrete specimens were pre-heated in an oven to 60°C before the surface coating was applied as described in Section 3.8. This yielded a much better adhesion of the material to the surface.

The test was carried out on white paint, hydrated lime, baghouse dust, and on an untreated specimen. A specimen left over from the field testing (see Chapter 5) which had a surface coating of hydrated lime was also used. This specimen had poor cohesion due to the relatively low temperatures of application and most importantly, the surface conditions due to release agent use, richness, and smoothness, and as a result already showed significant wear. The limestone screenings were not tested, as the cohesion was so poor that the material could be simply brushed off. For these reasons, the Wet Track Abrasion Test is a questionable approach for the laboratory determination of the durability of asphalt concrete surfrace coatings, particularily if the coating condition issues are not resolved.

6.2 Test results

The results of the limited durability testing, with the outlined bonding concerns are shown in Figure 6.1. The test on the white paint was terminated after the initial 5 minute test, as the low surface friction caused little wear except in patches where the paint flaked off. The test had the effect of cleaning the surface, actually increasing the albedo. Low surface friction (safety) problem also eliminated the paint from being an acceptable surface coating. The natural surface showed a trend of marginal increase of albedo as the dark coloured binder was removed, exposing the lighter coloured aggregate. The baghouse dust showed a large decrease in albedo after the first 5 minutes (essentially removed), and after 50 minutes it was identical to an untreated natural asphalt concrete surface. A slight increase was noted after 150 minutes, which would indicate that the asphalt concrete surface was wearing, causing the aggregate to become exposed.

The focus of this testing was the hydrated lime coating. The initial albedo of 0.81 for the hydrated lime treated surface decreased to 0.38 after the initial 5 minutes and

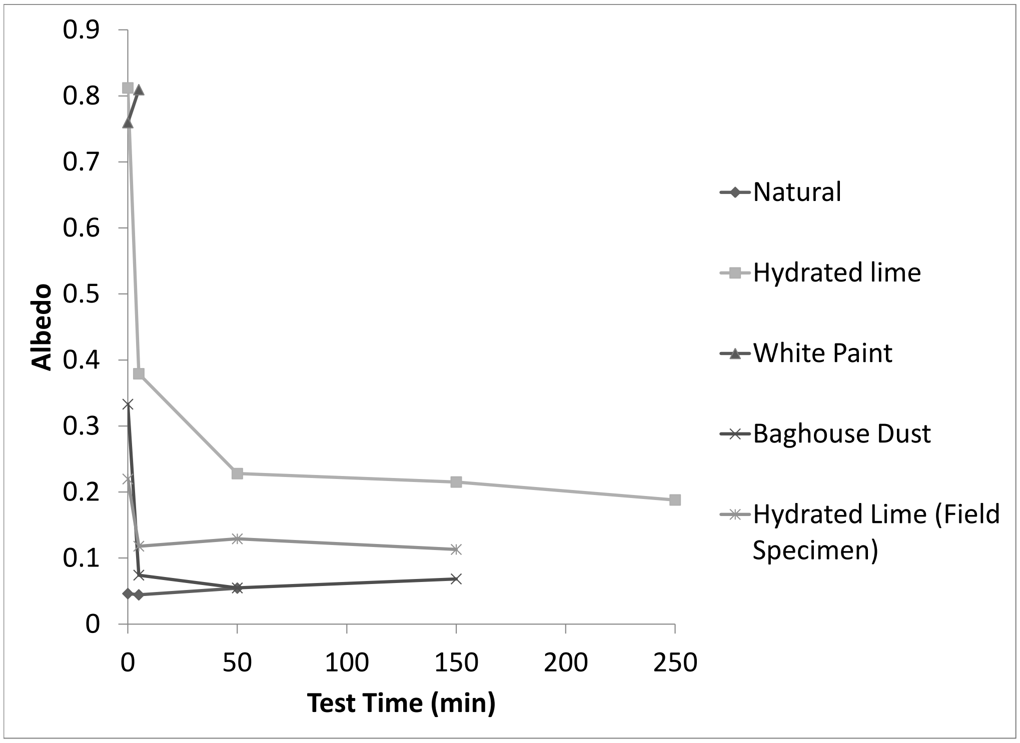

Figure 6.1: Results of durability test

decreased further to 0.23 after 50 minutes. If 0.23 can be assumed to be the albedo after several years, it would be deemed acceptable. After further testing for 150 minutes and 250 minutes, the albedos were 0.22 and 0.19, respectively. The results show that there was not any more significant drop of albedo over long periods. If 0.19 can be assumed to be the terminal albedo, it would still not be acceptable for use as a coating. The duration of abrasion has not been compared to the wear of a surface in a field condition, so a field test is required to provide more reliable long term results.

6.3 Proposed field testing for durability

Because of the limited nature of the Wet Track Abrasion Test and issues with the surface coating bond, a field test was proposed instead. This method would test the surface coatings as well as line marking paint using a modified version of ASTM D559-03 (ASTM, 2003). The surface coatings would be applied to an asphalt pavement road surface, which would eliminate any of the problems that were a result of using lab compacted asphalt. The abrasion mechanism would be a standard wire brush.

The friction of surfaces should be examined as well, including adding "grit" to the surface coatings to improve frictional values.

Chapter 7

Numerical model

This chapter presents a pavement temperature prediction model, by simplifying the asphalt concrete layer as an one-dimensional system. The goal of this model is to determine the maximum surface temperatures of the asphalt pavement by taking into account heat transfer in the pavement and proper boundary conditions. This model was implemented through FEM to simulate the tests described in Chapter 5.

7.1 Thermal model

When analysing the transient heat transfer process in an isotropic medium and for constant thermal conductivity, both the first law of thermodynamics, which states that thermal energy is conserved, and Fourier's law, that relates the heat flux with the thermal gradient, must be satisfied. The applicable heat transient two-dimensional transfer equation is expressed as (Incropera and Dewitt, 1996; Ozisik, 1985):

$$\frac{\partial T}{\partial t} = \alpha \bigtriangledown^2 T \tag{7.1}$$

or:

$$\frac{\partial^2 T}{\partial x^2} + \frac{\partial^2 T}{\partial z^2} = \frac{1}{\alpha}\frac{\partial T}{\partial t} \tag{7.2}$$

where $\alpha = k/(\rho C)$ is the thermal diffusivity, k is the thermal conductivity, and ρ and C stand for the density and the specific heat, respectively.

7.1.1 Energy balance in asphalt concrete pavements

As illustrated in Figure 7.1, which shows a schematic pavement cross-section and the heat-related processes that affect the pavement structure, the pavement temperature greatly depends on how the solar energy heats the pavement and how the pavement influences the air above it. In general, the temperature of the pavement is affected by many factors, such as solar energy, solar reflectance, material heat capacities, surface roughness, heat transfer rates, thermal emittance, wind speed. Rainfall, water migration and evaporation in the pavement are also part of the heat transfer process, which implies that permeability has an effect on the heat transfer process in pavements. Table 7.1 lists all of the energy transfer mechanisms at the pavement surface.

The pavement temperatures prediction model is established based on the basic principles of physics, including thermal dynamics and the theory of heat transfer. The first law of thermodynamics requires energy balance in the asphalt concrete pavement such that the net surface flux is zero:

$$q_{solar} + q_{convection} + q_{conduction} + q_{rain} + q_{IR} + ... = 0 \tag{7.3}$$

The factors that are most important for simulating an asphalt pavement surface

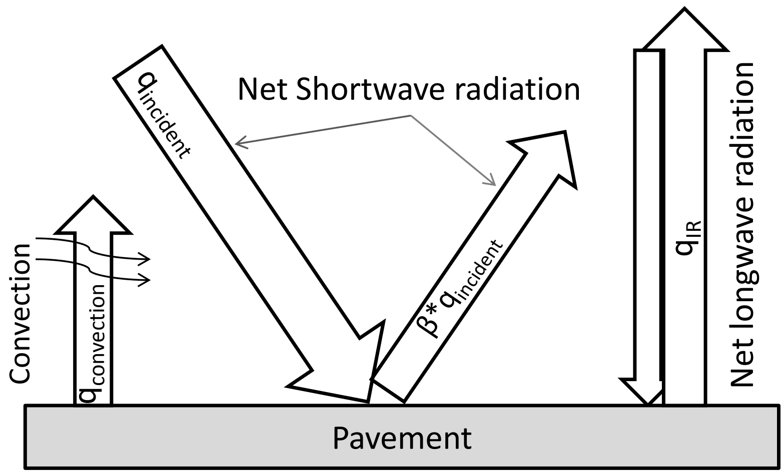

Figure 7.1: Thermal energy balance in pavement on a sunny day

Table 7.1: Energy balance at pavement surface

Heat Flux	Symbol
Incident Shortwave Radiation	$q_{incident}$
Reflected Shortwave Radiation	$\beta \cdot q_{incident}$
Net Shortwave Radiation	q_{solar}
Net Longwave Thermal (IR) Radiation	q_{IR}
Convective heat transfer to air	$q_{convection}$
Heat transfer due to evaporation	q_{rain}
Heat flow into/out of pavement	$q_{conduction}$

under maximum temperature conditions are the net shortwave solar radiation, q_{solar}, the net longwave thermal (infra-red) radiation, q_{IR}, and convection, $q_{convection}$. The conduction of heat through the pavement, $q_{conduction}$, is accounted for in the materials parameters. Rain, q_{rain}, has a cooling effect on the asphalt surface and as such is not necessary when estimating maximum temperatures (sunny days).

7.1.2 Solar radiation

The solar radiation that affects the surface temperatures is short wave energy, mostly falling within the visible spectrum. Some of the solar radiation is transferred to the pavement, while a percentage of it is reflected away. The reflected value is based on the albedo, β. The net solar radiation can be expressed as

$$q_{solar} = (1 - \beta) \cdot q_{incident} \tag{7.4}$$

where $q_{incident}$ is the recorded hourly solar radiation if available, or determined based on a model as described below.

Although a single figure for the albedo of a surface is useful in estimating radiation fluxes, the reflectivity actually depends strongly on the wavelength of the electromagnetic radiation (McGuffie and Henderson-Sellers, 2014; Akbari and Matthews, 2012). The solar radiation includes shortwave radiation (visible light, with wavelength of 400 to 700 nm) and longwave radiation (near infrared, wavelength 700 to 2500 nm). A large fraction of the sun's energy is in the visible (~43%) and near infrared (~52%) spectrum. Since the albedo varies with the wavelength, one may alternatively determine the contribution of these two types of radiation separately.

Shortwave radiation model (visible light)

The shortwave radiation is available for use directly in this model. However, for simulations at other locations, this data may not be available. It is then necessary to "create" an estimate for the shortwave radiation.

It is possible to simulate the shortwave radiation received at any location based solely on its latitude and longitude. This is because the energy output of the sun, the orbital path and rotation of the earth, as well as the composition of the atmosphere are known. A shortwave radiation model, explained by Stull (2000), has been developed and can be used to determine the hourly radiation for any location. The model requires the following input parameters:

- The solar declination angle, δ_s.
- The Julian Day, d, which is the day of the year.
- The summer solstice June 22, d_r, which is 173 or for a leap year 174.
- The number of days in the year, d_y is 365 or for a leap year 366.
- ϕ_r is the tilt of the earth's axis, which is 23.49°.
- The local elevation angle of the sun, ψ.
- Latitude ϕ and longitude λ_e.
- Time of day t_{UTC}, which is reported in Coordinated Universal Time.
- The constant C, which is 360°. Length of the day t_d, which is 24h.
- The solar constant S, which is 1368 W/m^2.
- Net sky transmissivity T_r.
- Cloud cover fractions σ_H, σ_M, and σ_L, which for the purposes of this model are assumed to be 0 indicating no cloud cover.
- The incident solar radiation $q_{incident}$.

The solar declination angle δ_s is first calculated as:

$$\delta_s = \phi_r cos\left(\frac{C(d-d_r)}{d_y}\right) \tag{7.5}$$

The local elevation angle ψ of the sun depends on δ_s as well as the lattitude ϕ and longitude λ_e of the locations, such that

$$sin(\psi) = sin(\phi)sin(\delta_s) - cos(\phi)cos(\delta_s)cos\left(\frac{C \cdot t_{UTC}}{t_d} - \lambda_e\right) \tag{7.6}$$

The net sky transmissivity is determined as

$$T_r = (0.6 + 0.2sin\psi)(1 - 0.4\sigma_H)(1 - 0.7\sigma_M)(1 - 0.4\sigma_L) \tag{7.7}$$

which leads to

$$q_{incident} = S \cdot T_r \cdot sin\psi \tag{7.8}$$

The values may be higher than the actual recorded data because this model does not account for cloud cover.

7.1.3 Longwave radiation (infrared light)

The net Infrared radiation (i.e., thermal or long-wave radiation) at the pavement surface is described as follows (Yavuzturk *et al.*, 2005):

$$q_{IR} = h_r \cdot (T_{sky} - T_{surface}) \tag{7.9}$$

where h_r is a linearised radiation coefficient

$$h_r = 4\epsilon\sigma \left(\frac{T_{surface} + T_{sky}}{2}\right)^3 \tag{7.10}$$

where ϵ is the emissivity coefficient of the pavement material, σ is the Stefan-Boltzmann constant, $T_{surface}$ is the surface temperature of the asphalt concrete, T_{sky} is the temperature in the upper atmosphere. T_{sky} can be determined based on recorded IR downward radiation (E) if available by (Bliss Jr, 1961):

$$T_{sky} = \sqrt[4]{\frac{E}{\sigma}} \tag{7.11}$$

For most locations, longwave radiation data is not available. As a result, an estimate for the longwave radiation must be made. According to Alavi *et al.* (2013), T_{air} may be used to substitute for T_{sky}, but there is a significant loss in accuracy. Unlike shortwave radiation, the longwave radiation is not a value that can be modelled. Instead, an average value may be used. Based on data from the McMaster Weather Station, the nominal average of longwave radiation during the summer months is 400W/m^2, which corresponds to a T_{sky} value of 16.7°C. The accuracy of this estimate is considered in Section 8.2.

In this research, the longwave radiation used was recorded using a radiometer. This value is then used to estimate the upper atmosphere temperature, T_{sky}

7.1.4 Convection

The convection heat transfer between the pavement surface and the air immediately above may be induced by both free and forced convection.

Convection is the mechanism of heat transfer through a fluid in the presence of bulk fluid motion. In general, convection is affected by surface characteristics, thermal conductivity of air, and flow characteristics of the fluid (e.g.,turbulence and the speed, etc.). Convection is classified as natural (or free) and forced depending on how the fluid motion is initiated. In natural convection, any fluid motion is caused by natural means such as the buoyancy effect, i.e. the rise of warmer fluid and fall of cooler fluid. Whereas in forced convection, the fluid is forced to flow over a surface or in a tube by external means such as wind.

The convection flux is described as

$$q_{convection} = h_c(T_{air} - T_{surface}) \tag{7.12}$$

where h_c is the convection coefficient. Various empirical formulations have been proposed for determining the convection coefficient for different geometries. For a pavement surface, correlations for a horizontal flat plate are the most applicable.

In convection heat transfer, a non-dimensional heat transfer coefficient, the Nusselt number N_u, is generally used to represent the enhancement of heat transfer through a fluid as a result of convection relative to conduction across the same fluid layer:

$$N_u = \frac{\delta h_c}{k} = \frac{q^*_{conv}}{q^*_{cond}} \tag{7.13}$$

where k is the thermal conductivity of air and δ is the characteristic length, i.e. D for a tube and L for a flat plate.

For free convection heat transfer, N_u is a function of the Rayleigh Number (R_e), which is defined as the ratio of inertia forces to viscous forces in the fluid:

$$R_e = \frac{\text{inertia forces}}{\text{viscous forces}} = \frac{\rho V \delta}{\mu} = \frac{V\delta}{\nu} \tag{7.14}$$

where ρ = mass density (kg/m^3), Cp = specific heat capacity ($J/kg \cdot K$), μ = dynamic viscosity ($N \cdot s/m^2$), ν =kinematic viscosity and $\nu = \mu/\rho$ (m^2/s). In external free convection flows over a horizontal flat plate, the critical Rayleigh Number is about 10^7. Incropera and Dewitt (1996) proposed the following relations for free convection from the upper surface of a heated or cooled plate:

$$\nu = 0.54R_e^{1/4}, \quad 10^4 < R_e < 10^7; \text{laminar flow} \tag{7.15}$$

$$\nu = 0.15R_e^{1/3}, \quad 10^7 < R_e < 10^{11}; \text{turbulent flow} \tag{7.16}$$

While several empirical relationships to estimate convection coefficients for pavement analysis are available in the literature, for this study, the convection coefficient was determined based on the wind speed available in the weather data using the following equation (Earle, 2004):

$$h_c = 5.7 + 3.9v \quad \text{for} \;\; v < 5m/s \tag{7.17}$$

$$h_c = 7.4v^{0.8} \quad \text{for} \;\; 5 < v < 30m/s \tag{7.18}$$

The above equations can be applied to smooth large plane surfaces. The rough nature of an asphalt surface will result in a slightly higher value for h_c, but it is insignificant within the accuracy of measured wind speed.

7.1.5 Air temperature

The hourly air temperature is often readily available, but if it is not, it should still be possible to obtain daily maximum and minimum air temperatures. By assuming that the minimum temperature will occur at 03:00 and the maximum temperature will occur at 15:00, a smoothed curve can be used to simulate the hourly temperature variations. A sine curve may be used, but in this case the curve is automatically generated in Abaqus.

7.1.6 Windspeed

The windspeed is used to determine the coefficient h_c. Windspeed data is not generally available in weather databases, so some estimate is generally necessary.

A reasonable estimate for windspeed must be made for the hottest day of the year. Zero windspeed is not realistic in most situations and will vastly overestimate the temperatures even compared to a low windspeed. If there is some traffic flow over then road, then it could be assumed that there is at least some air movement.

For the purposes of this research, an average windspeed was assumed to be 2.4m/s, which is the average windspeed for August as recorded at the Hamilton RBG weather station (Environment Canada, 2010).

7.2 Summary of material properties and model parameters

When modelling in Abaqus (Section 7.3, the program used herein, the program does not use any units or unit conversions between calculations, so all units have to be consistent. For this purpose, all values were defined using the base units kg, m, °C, and s for mass, length, temperature, and time, respectively.

The various parameters and constants required for defining the material properties are outlined in Tables 7.2 and 7.3.

Table 7.2: Material parameters

Material	Conductivity ($W/m°$C)	Density (kg/m^3)	Specific Heat ($J/kg°$C)
SP12.5FC2	1.3	2400	950
SP19	1.3	2500	950
3/4” gravel	1.7	2200	1100

Sources: Doré and Zubeck (2009), Gui *et al.* (2007), Yavuzturk *et al.* (2005)

Table 7.3: Constant and initial values

Name	Value
Absolute Zero	-273.15°C
Stefan-Boltzmann	5.6704e-8$W/$m^2°C^4
Emissivity	0.85
Initial temperature	30°C
Incident longwave radiation (If data not available)	400W/m^2

7.3 Finite element model

7.3.1 Discretization and finite element mesh

A series of finite element simulations using an established model were performed to simulate the field tests. As described in Chapter 5, the field test can be considered as a 1D transient thermal flow problem. The software package ABAQUS (Appendix D) was used for all simulations. The finite element model consists of a 300mm diameter cylinder with a top 40mm asphalt concrete layer (SP12.5 FC2), a middle 260mm thick asphalt concrete layer (SP19), and a 1000mm thick gravel base/subgrade layer, as illustrated in Figure 7.2.

The cylinder of the asphalt concrete specimen and the base/subgrade are discretized by 8 noded-brick elements (152 elements) of different sizes to consider the thickness of different material layers and the temperature variation in the system. Mesh sensitivity was examined by using a number of mesh sizes, varying from 10mm spacing to 100mm spacing (in the vertical direction). It was determined that a very fine mesh did not significantly improve the accuracy of the results while greatly increasing the simulation time. Also, it was not necessary to have a fine mesh in the base/subgrade section, as it was only used as a heat sink/source and not as part of the pavement profile. As a result, the mesh spacing was as follows: 20mm spacing within the top 40mm, 37mm spacing within the middle 300mm, and 100mm spacing within the base/subgrade 1000mm as shown in Figure 7.2.

7.3.2 Numerical algorithm and maximum time step increment

This model uses a transient time thermal model programmed in Abaqus. A backwards difference algorithm is used for time integration (Simulia, 2011):

$$\dot{U}_{t+\Delta t} = (U_{t+\Delta t} - U_t)(1/\Delta t) \tag{7.19}$$

Where t is the initial time, Δt is the time step, and U is the internal energy in the model. This is then solved using the Newton-Raphson method. The full algorithm from the Abaqus 6.11 Theory Manual is included in Appendix D (Simulia, 2011).

While ABAQUS can automatically determine the step size in the simulations, choosing a reasonable maximum time step was vital to achieving reasonable results describing the time history of temperature variation. In this research, the chosen maximum time step increment was 0.75 hour after several trial simulations. It was found that shorter time steps significantly increased computation time but did not yield meaningfully more accurate results.

7.3.3 Boundary conditions

The boundary conditions for the surface were described in the above Sections. The side boundary conditions were taken as fully insulated in order for the model to exhibit one dimensional behaviour. The bottom boundary condition was more complex to determine. Gui *et al.* (2007) used some nominal or measured value as the bottom boundary condition, while (Yavuzturk *et al.*, 2005) has taken the bottom boundary of the pavement as fully insulated.

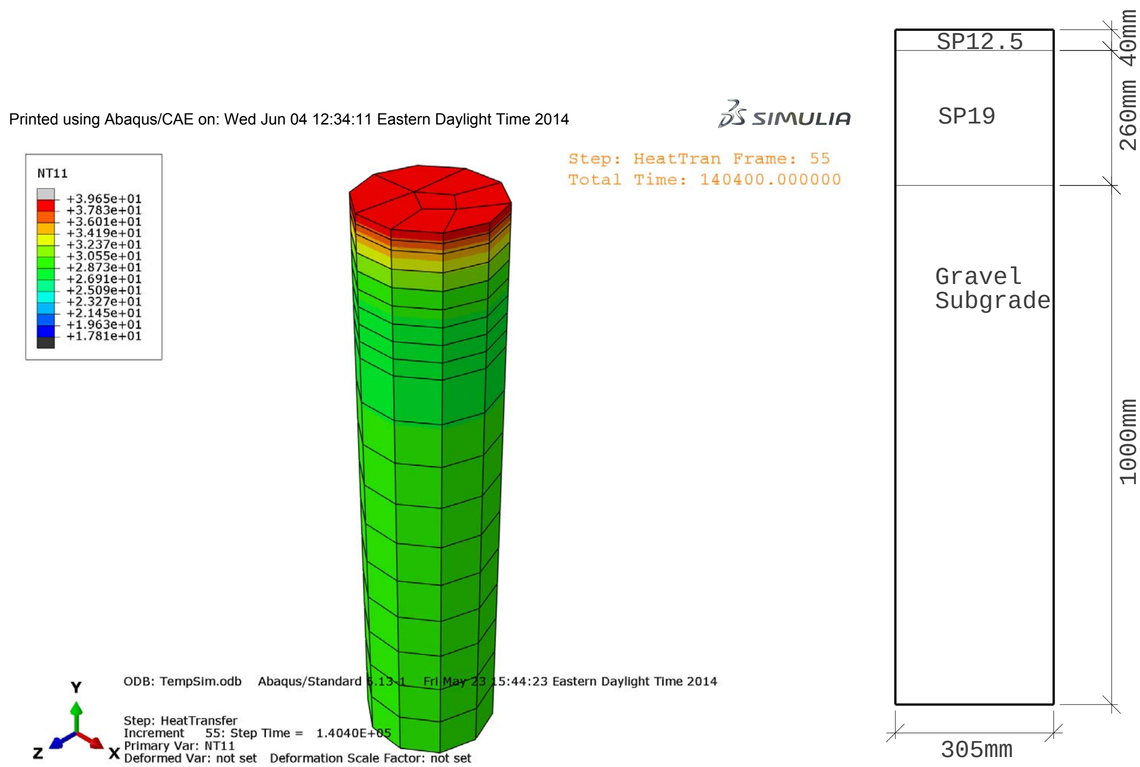

Figure 7.2: Model layout and mesh

Through the trial of several different scenarios, it was determined that the best method without requiring recorded data would be to place 1m of simulated gravel base/subgrade material below the asphalt with an initialised temperature of 30°C and a fully insulated bottom boundary.

7.3.4 Summary of the FEM model

1. Field equation:

$$\frac{\partial T}{\partial t} = \alpha \bigtriangledown^2 T$$

2. Boundary conditions:

   (a) Top boundary: Various flux values

      i. Initial model: All values calculated from local weather data

         - Shortwave solar radiation from recorded data, net value calculated using Eq. 7.4
         - Incident longwave radiation from recorded data, T_{sky} estimated from data using Eq. 7.11. Net longwave calculated using Eq. 7.9, coefficient h_r calculated using Eq. 7.10.
         - Windspeed from recorded data, coefficient h_c calculated using Eq. 7.17 or 7.18. Convection flux calculated using Eq. 7.12.
         - Air temperature from recorded data

      ii. Simplified model: All value estimated based on commonly available weather data from sources such as Environment Canada

         - Shortwave solar radiation calculated using Eqs. 7.5-7.8, net value calculated using Eq. 7.4

- Incident longwave radiation estimated to be $400W/m^2$, T_{sky} estimated from data using Eq. 7.11. Net longwave calculated using Eq. 7.9, coefficient h_r calculated using Eq. 7.10.
- Windspeed estimated from average monthly value from the Canadian Climate Normals (Environment Canada, 2010), 2.4m/s used, coefficient h_c calculated using Eq. 7.17 or 7.18. Convection flux calculated using Eq. 7.12.
- Maximum and minimum daily air temperatures as recorded by a local weather station. Hourly temperature estimated with a smooth curve as described in Section 7.1.5.

(b) Bottom boundary: Fully insulated

3. Time-integration algorithm: Implicit backwards difference method, Eq. 7.19.

Chapter 8

Model results and analysis

All simulations were performed using both the complete model and the simplified model. The complete model uses all available recorded data, while the simplified model uses estimates for all data based on readily available information.

8.1 Complete model results

8.1.1 Test 3

The complete model, as it is defined using only recorded data, was used to determine the accuracy of the overall modelling approach. The third test (Test 3), which took place on August 19 to 22, 2013, was used as the baseline for modelling. The weather on these days was good, with warm temperatures and mostly clear skies.

Figures 8.1 to 8.4 show the surface temperature time histories obtained from numerical simulations and measurements for various surface conditions. The results from both the complete model and the simplified model are shown in these figures. In this Section, only the results from the complete model are discussed. The temperature history of the surface profiles for all four specimens in Test 3 showed results very close to the recorded data. With the exception of the jagged shape of the recorded time history which is a result of local weather variations (clouds for instance), the model closely follows the time history.

Figures 8.5 to 8.8 show the temperature profiles with depth in the asphalt concrete specimens under different surface conditions in Test 3. Only the results at the time of highest daily surface temperature are presented. The temperatures at the surface closely followed the recorded data for Test 3, while at the ground surface the calculated values are generally higher than the measured values. This may be due to the boundary conditions in the testing setup. The ground surrounding the specimens is not insulated, which may allow more heat flow in or out of the base of the specimen. This has resulted in the recorded temperatures in the ground below the specimen remaining at approximately 25°C.

8.1.2 Test 1

The first test, Test 1, (Figure 8.9 to 8.12) involved the same surface coatings as the Test 3. In this test, the air temperatures were cooler than those in Test 3 and the sky was partially cloudy. In Test 1, the reason for running a two day simulation becomes apparent. The first day of simulation shows some inaccuracy in the estimation of the surface temperature history, most notably for the black and natural surfaces, while the second day shows more accurate values. This may be a result of the initial temperature used in the model being different from the field conditions; by the second day the influence of the initialization value has been greatly reduced. The temperature profiles with depth (Figures 8.13 to 8.16) again show a good correlation between the recorded and modelled values. The results of the first test day are less accurate, for the same reason as given above; for the second day the results are more accurate. Again, there is some deviation at depth which may be a result of the field conditions and the defined boundary conditions in the model.

8.1.3 Test 2

The second test, Test 2, (Figures 8.17 to 8.20) was used to compare surfaces with different albedo values to the main test group. A black paint specimen was used to compare the maximum temperatures to the other groups. As with Test 1, th weather conditions for testing were not ideal. Here, it is again seen that there are errors in estimation for the first day, which is significant for all specimens. As anticipated, the second day showed values much closer to those recorded. Owing to the poor weather conditions, the accuracy of prediction was slightly lower for Test 2 for all of the specimens, including the black specimen that had been tested before. Because of this, the less than ideal weather conditions can be considered as the likely cause for error. Still, the accuracy of estimation for maximum temperatures was between 4 to 6°C.

The temperature profiles for Test 2 (Figures 8.21 to 8.24) also showed lower accuracy, similar to that found for the surface temperatures. In the recorded data for day 1, the temperature profiles show a sharp drop in temperature in the top 20mm. The surface temperatures also show a significant decrease between 13:00 and 16:00. This is a result of cloud cover and/or increased windspeed during that period, which can have a significant cooling effect. This cooling effect is not taken into account in the proposed general model, but it can be considered by further improvement of the model input.

In Test 2, the albedo values of the surface were closer to what could be expected for a surface coating that has been worn down over time. The very high albedo of fresh white paint and hydrated lime are unrealistic for use in a road, because the albedo will decrease with wear and the high albedo values could, perhaps, cause reflection and line marking visibility problems for drivers. This should be considered in the future coating research. The relatively lower albedo values for the baghouse dust and portland cement, approximately 0.35, are much closer to the desired value (light coloured) for an aged asphalt concrete surface. These surfaces showed a decrease in temperature of 7 to 9°C as compared to the black painted and new asphalt concrete surfaces. This difference is not as large as the difference between white and black, but it is still a significant improvement. On a hot day, this difference would be expected to be much higher.

8.2 Simplified model results

The simplified model using estimated values, was designed to use only the minimum data that is readily available. As such, the results were not expected to be as accurate as the complete model.

For the darker coloured surfaces, such as the natural and black surfaces shown in Figures 8.1 and 8.3, the error in estimation is increased by 5 to 7°C as compared to the complete model. This observation was made for both Test 1 and Test 3. For the lighter coloured surfaces, such as the hydrated lime and white surfaces shown in Figures 8.2 and 8.4, the accuracy is much better, on the order of 1 to 5°C higher than

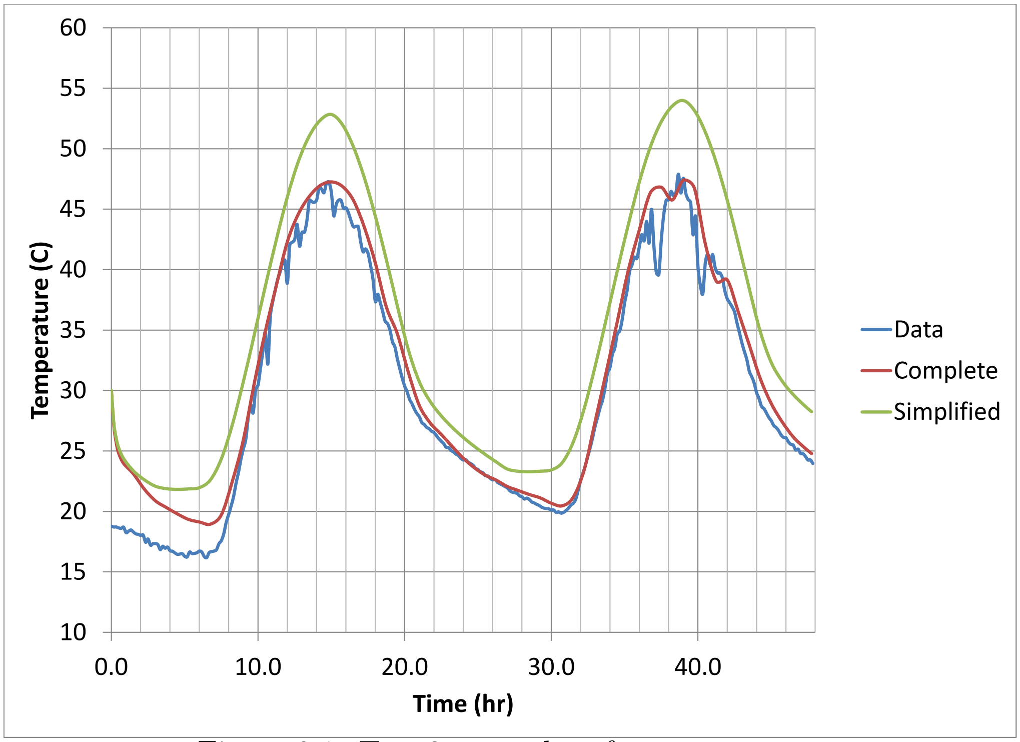

Figure 8.1: Test 3 natural surface temperature

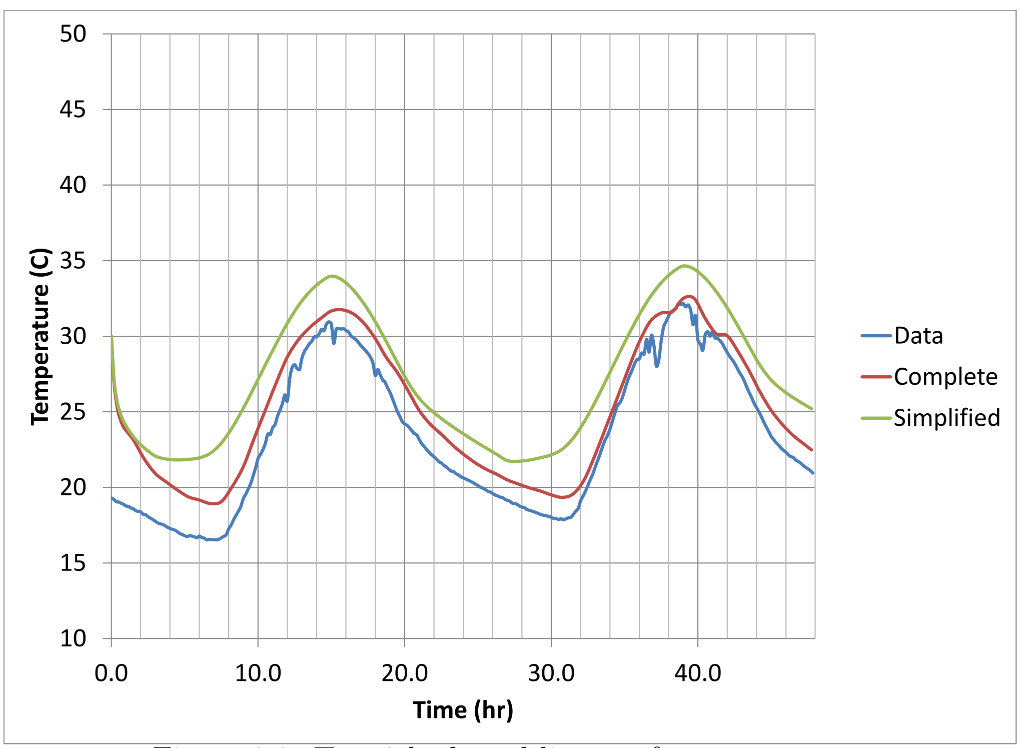

Figure 8.2: Test 3 hydrated lime surface temperature

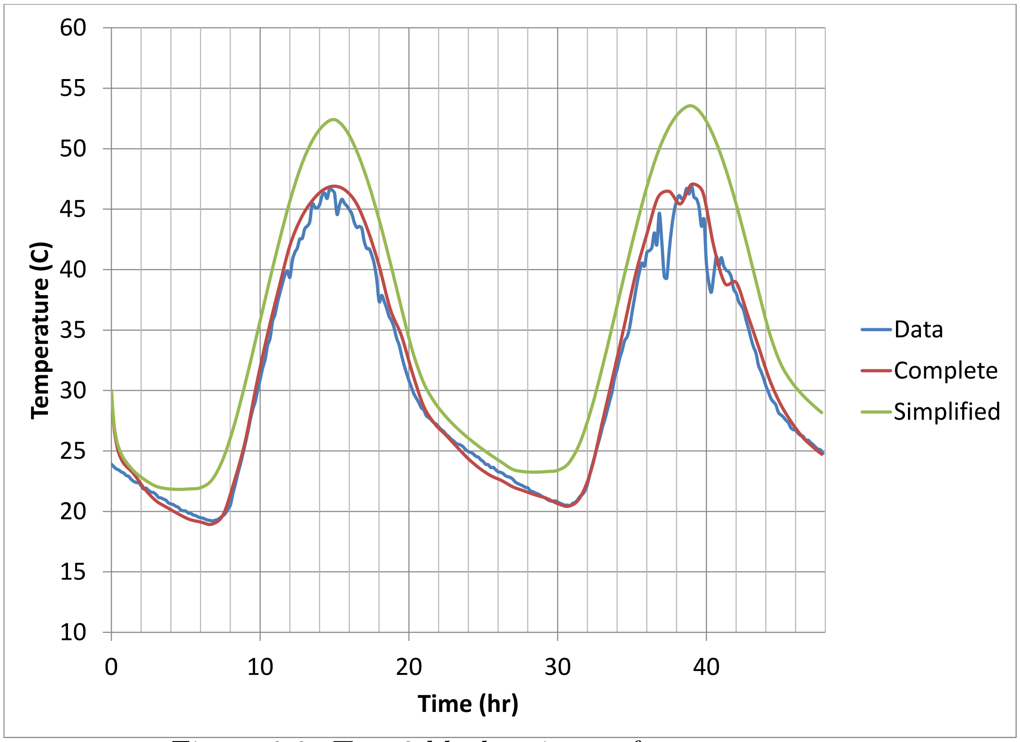

Figure 8.3: Test 3 black paint surface temperature

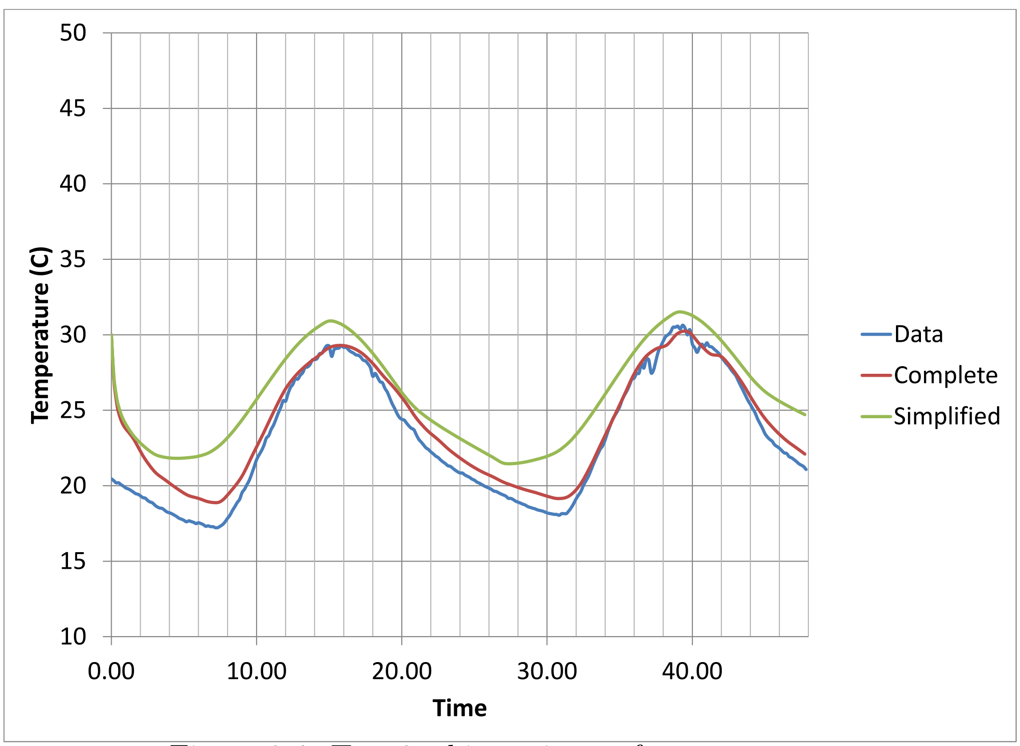

Figure 8.4: Test 3 white paint surface temperature

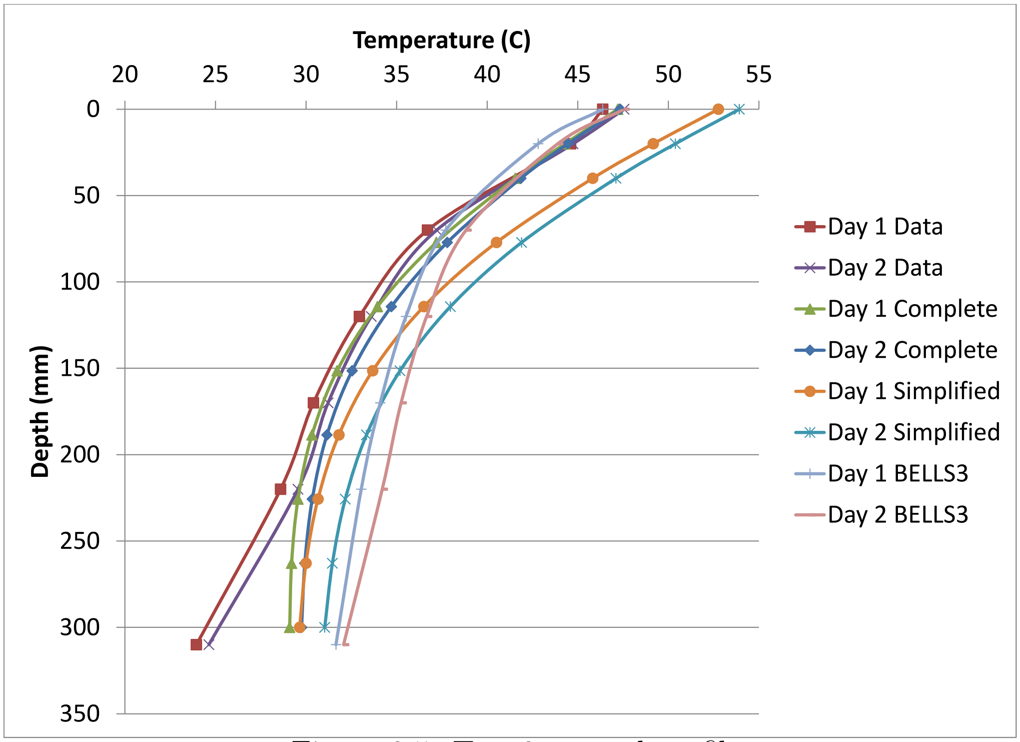

Figure 8.5: Test 3 natural profile

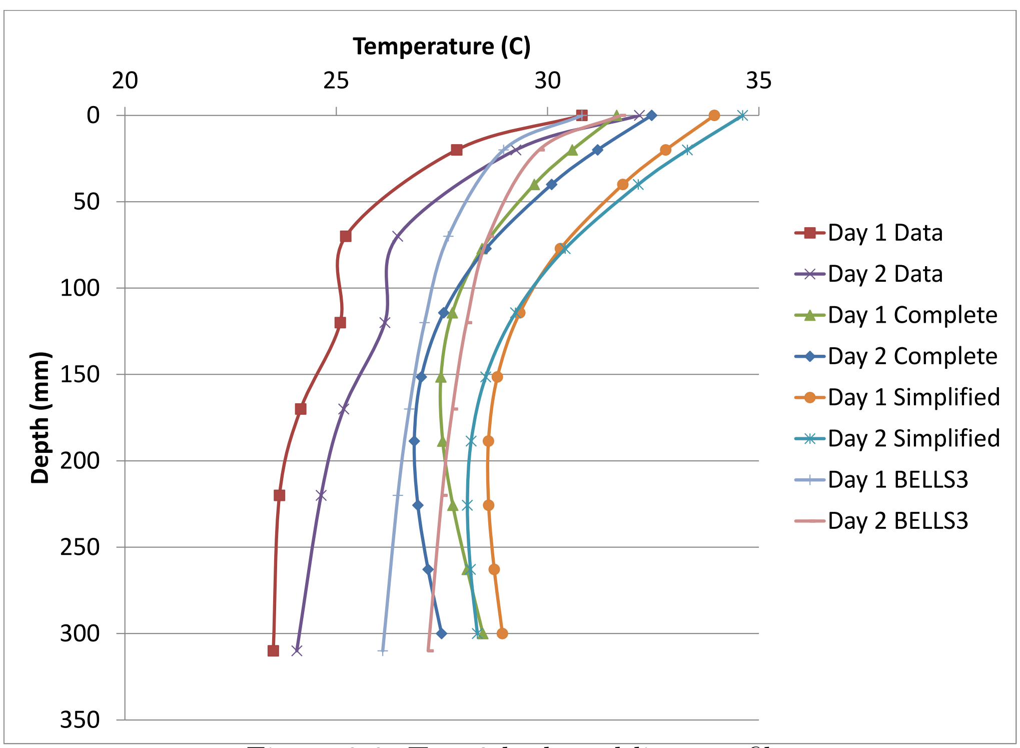

Figure 8.6: Test 3 hydrated lime profile

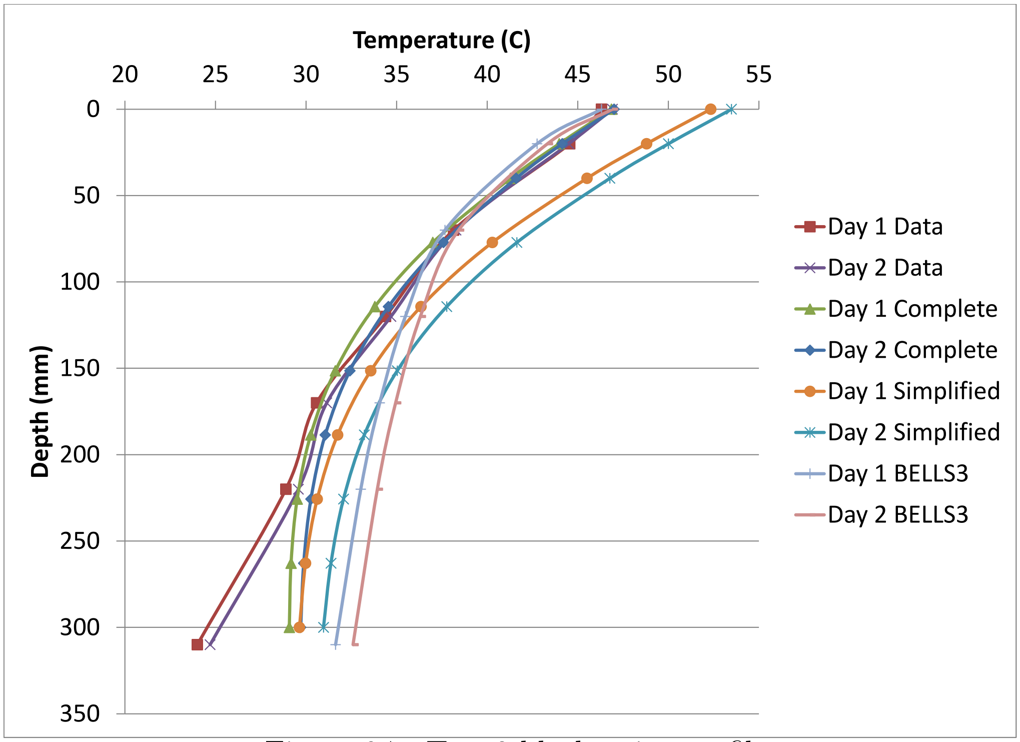

Figure 8.7: Test 3 black paint profile

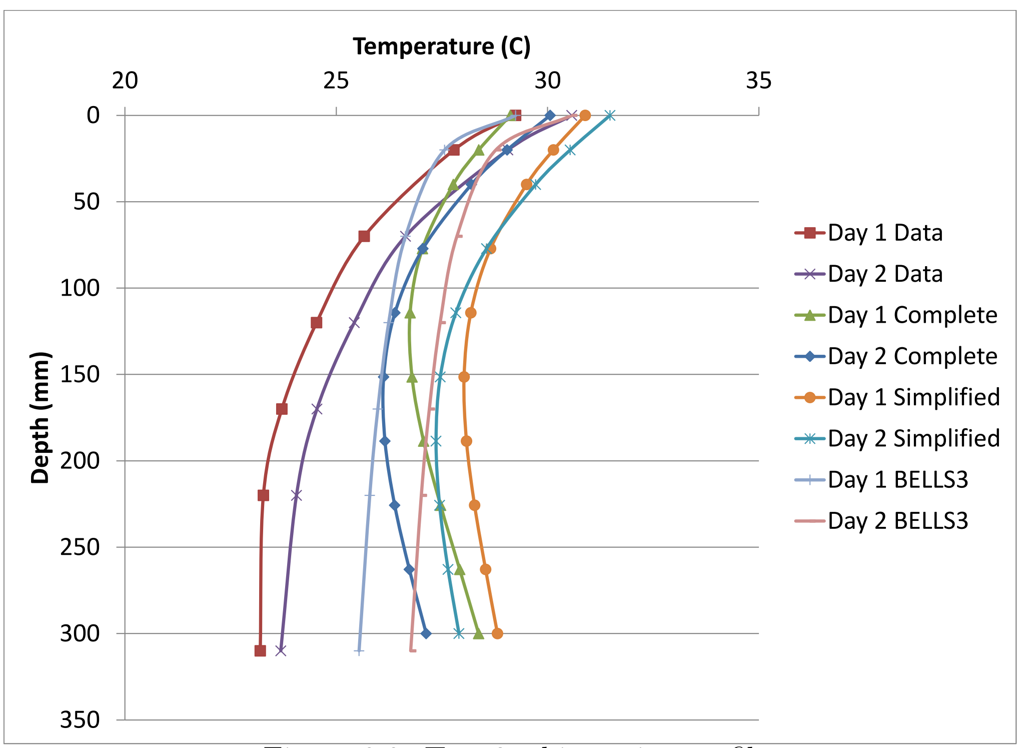

Figure 8.8: Test 3 white paint profile

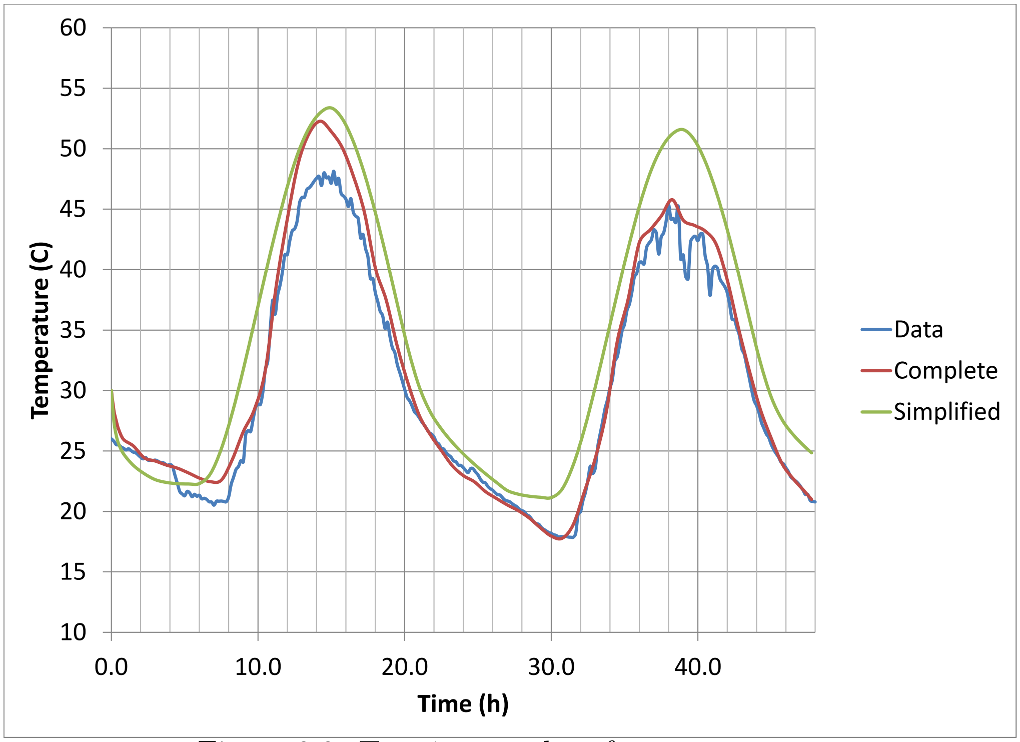

Figure 8.9: Test 1 natural surface temperature

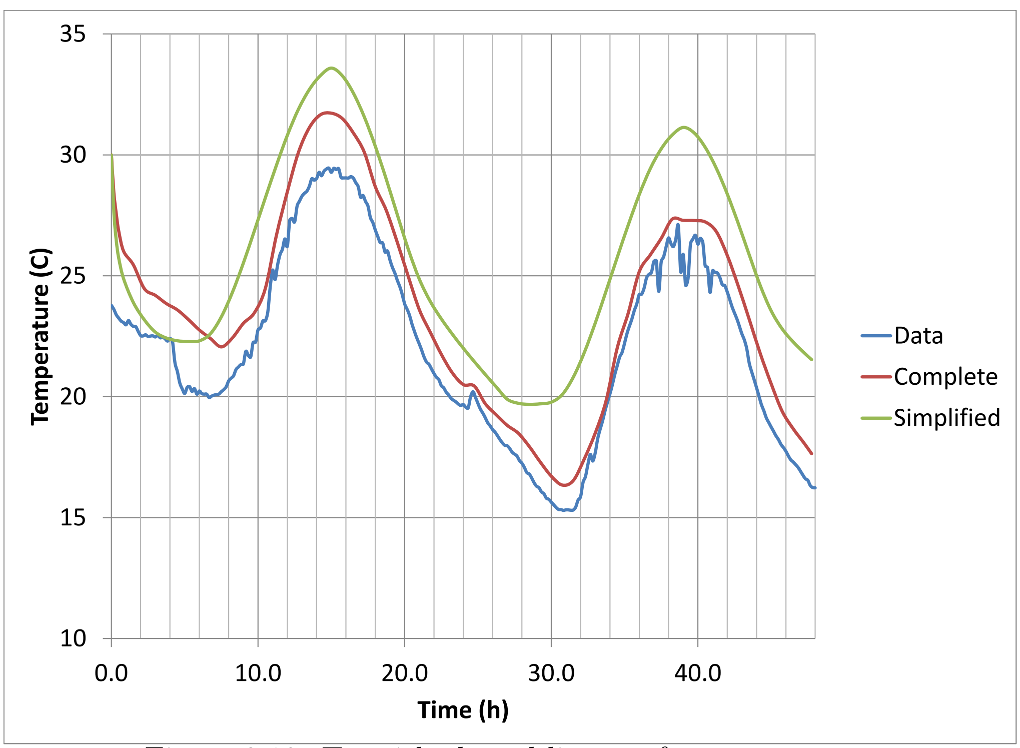

Figure 8.10: Test 1 hydrated lime surface temperature

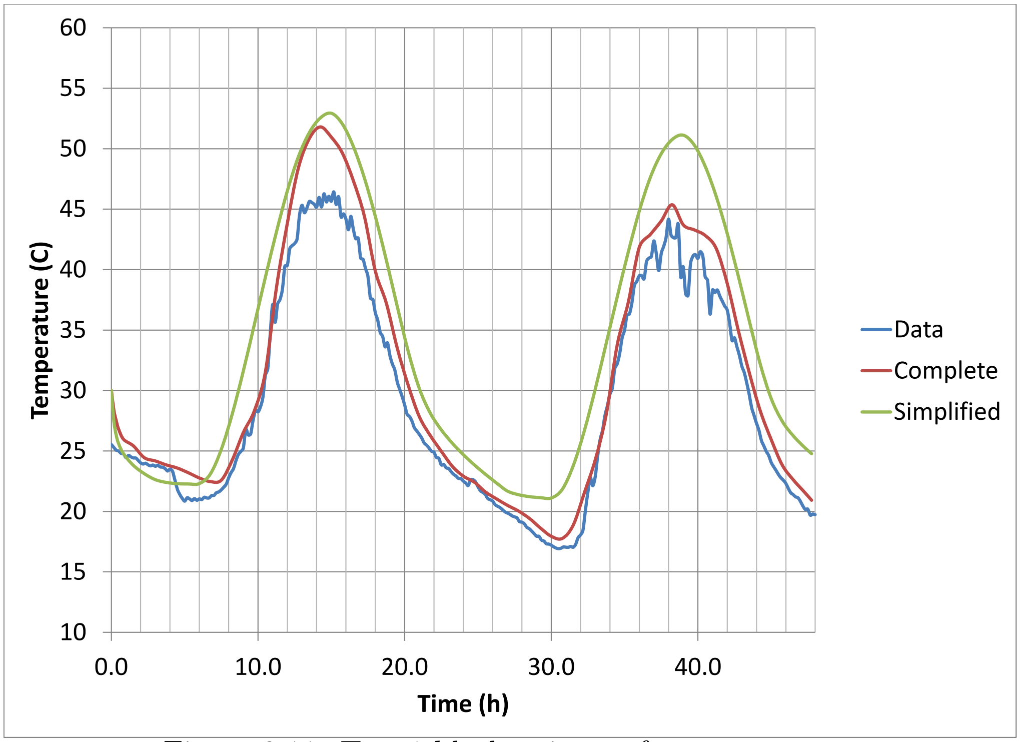

Figure 8.11: Test 1 black paint surface temperature

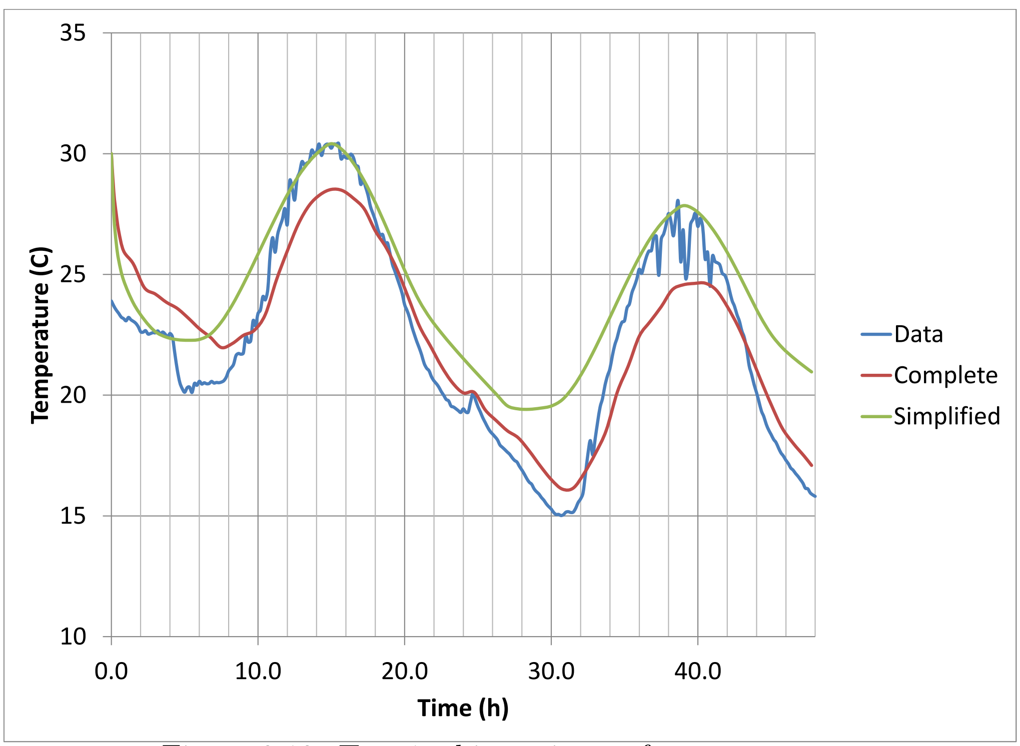

Figure 8.12: Test 1 white paint surface temperature

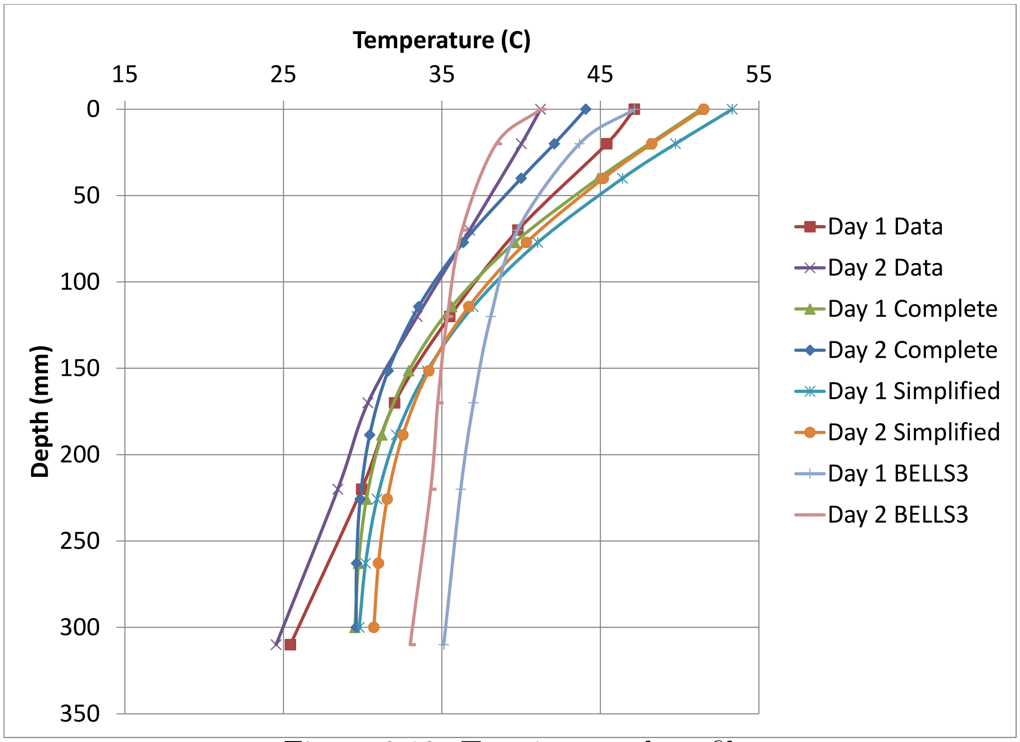

Figure 8.13: Test 1 natural profile

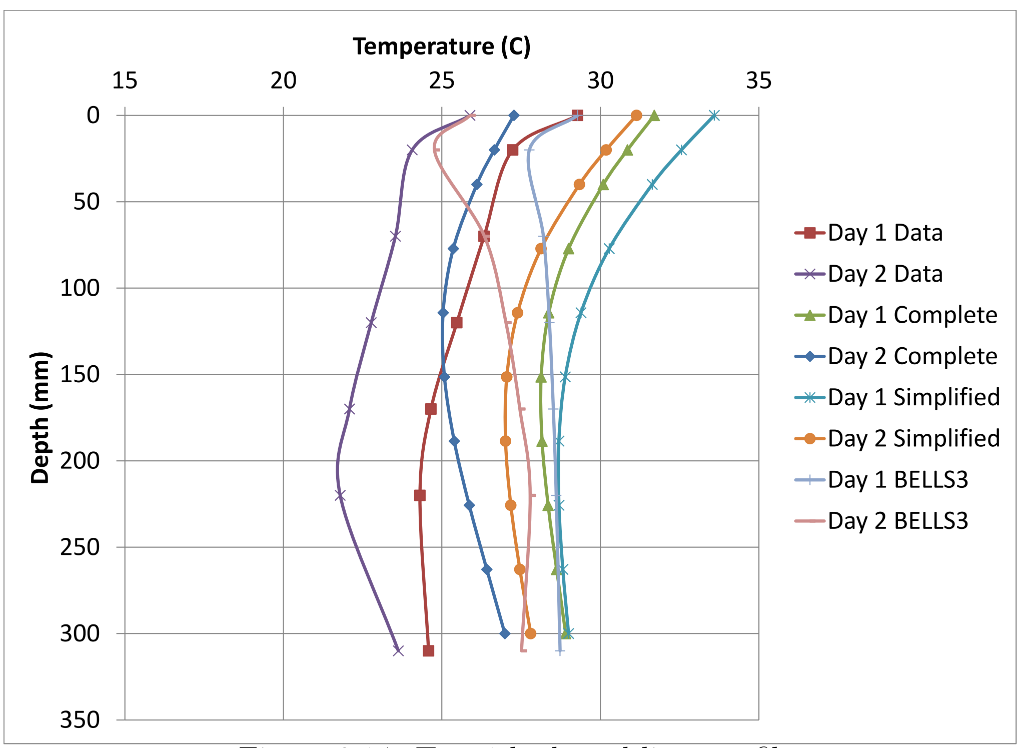

Figure 8.14: Test 1 hydrated lime profile

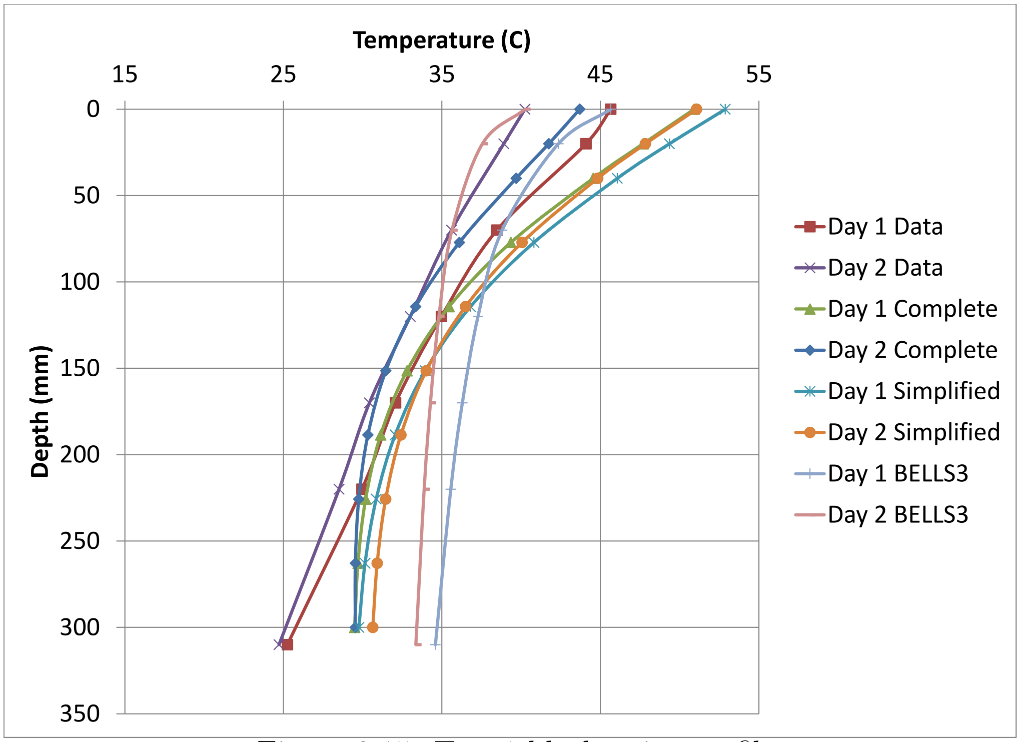

Figure 8.15: Test 1 black paint profile

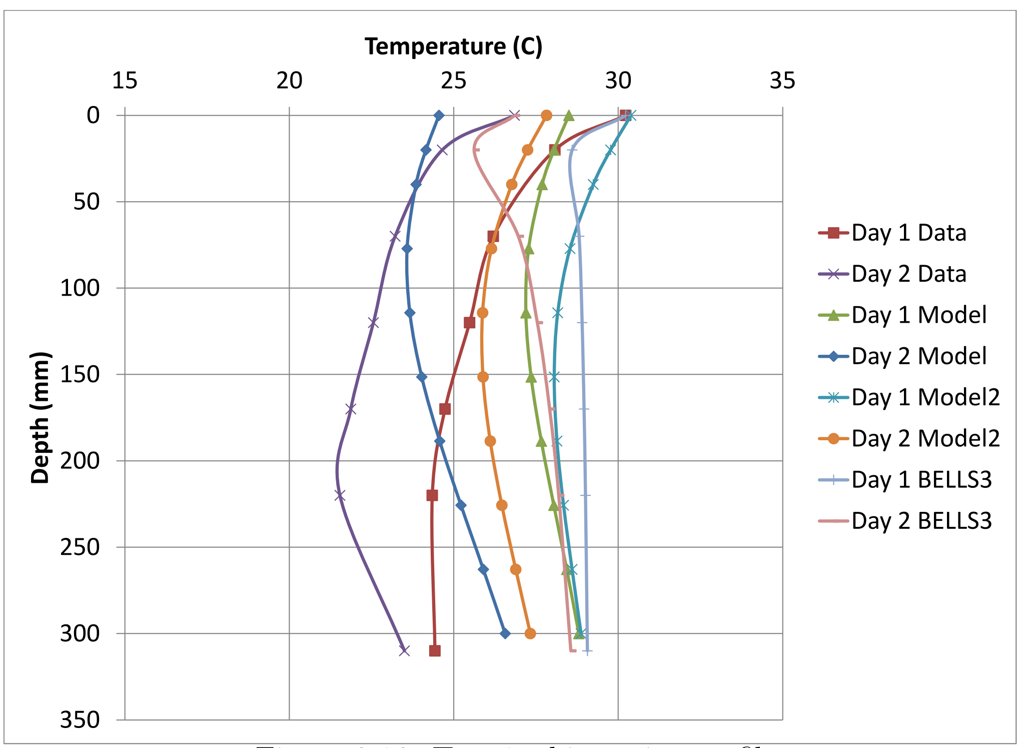

Figure 8.16: Test 1 white paint profile

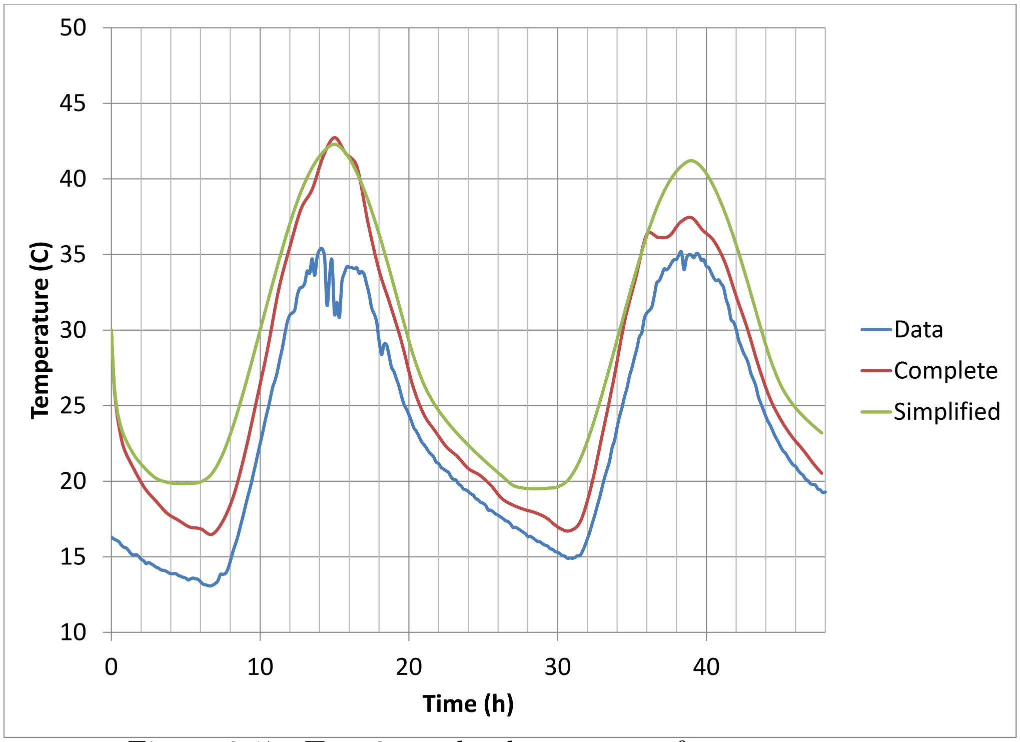

Figure 8.17: Test 2 portland cement surface temperature

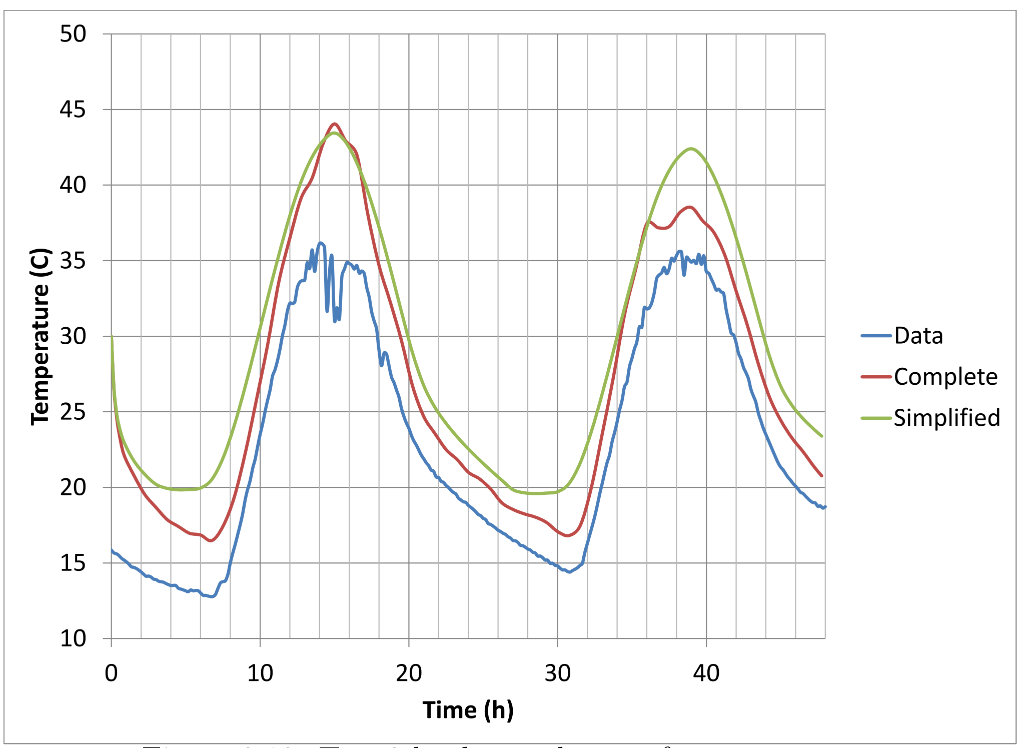

Figure 8.18: Test 2 baghouse dust surface temperature

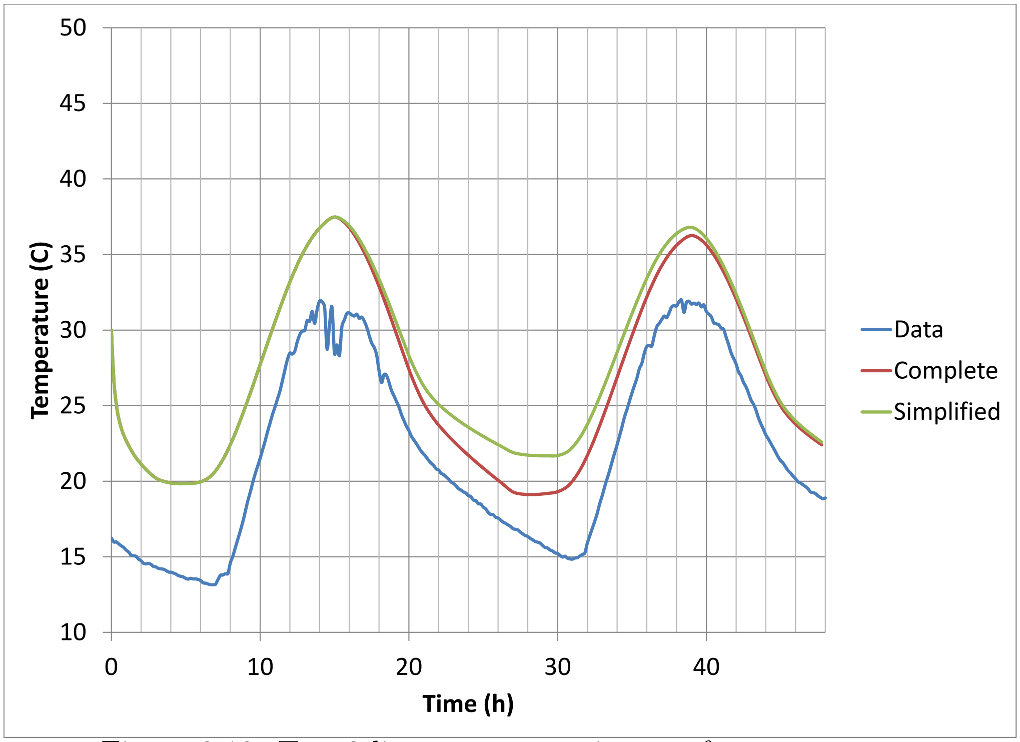

Figure 8.19: Test 2 limestone screenings surface temperature

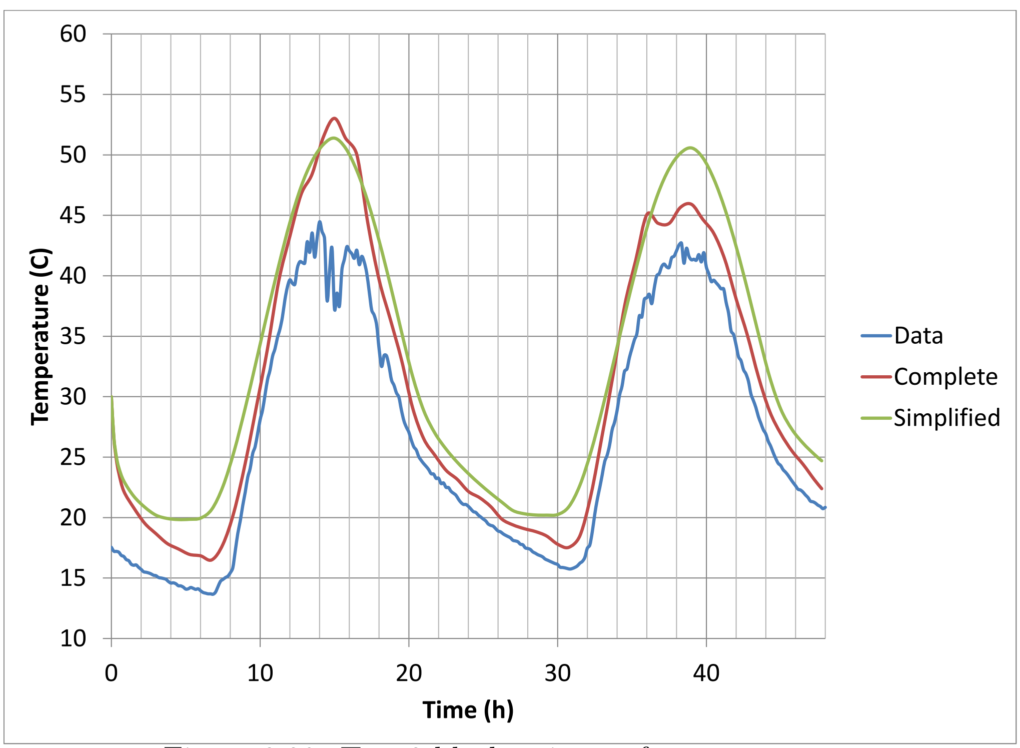

Figure 8.20: Test 2 black paint surface temperature

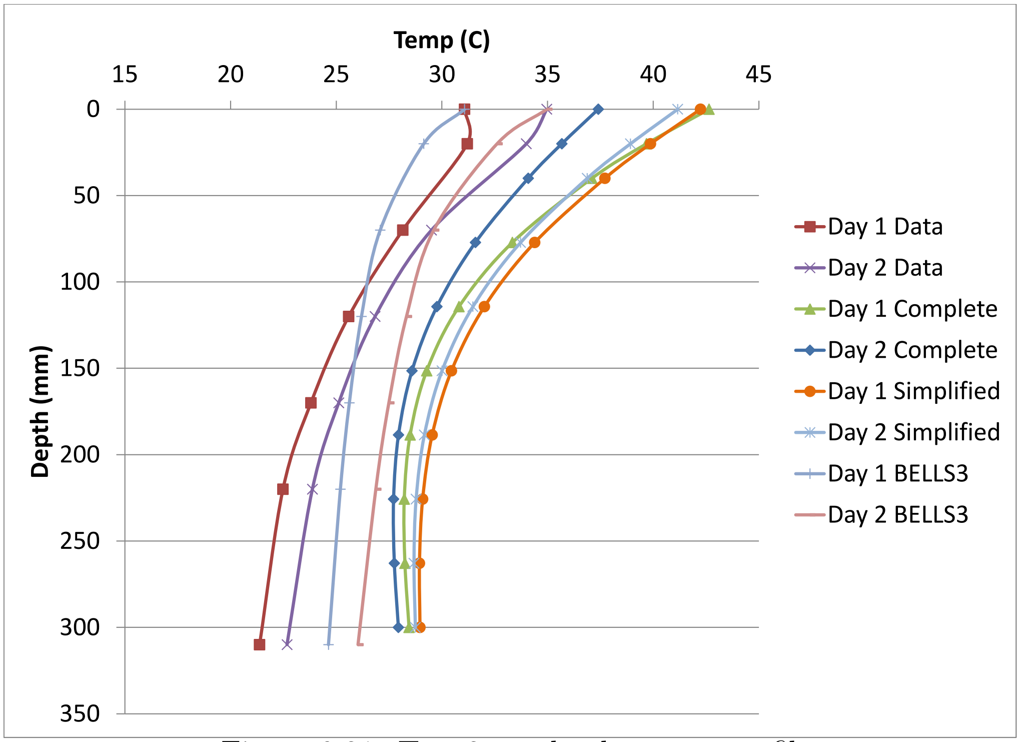

Figure 8.21: Test 2 portland cement profile

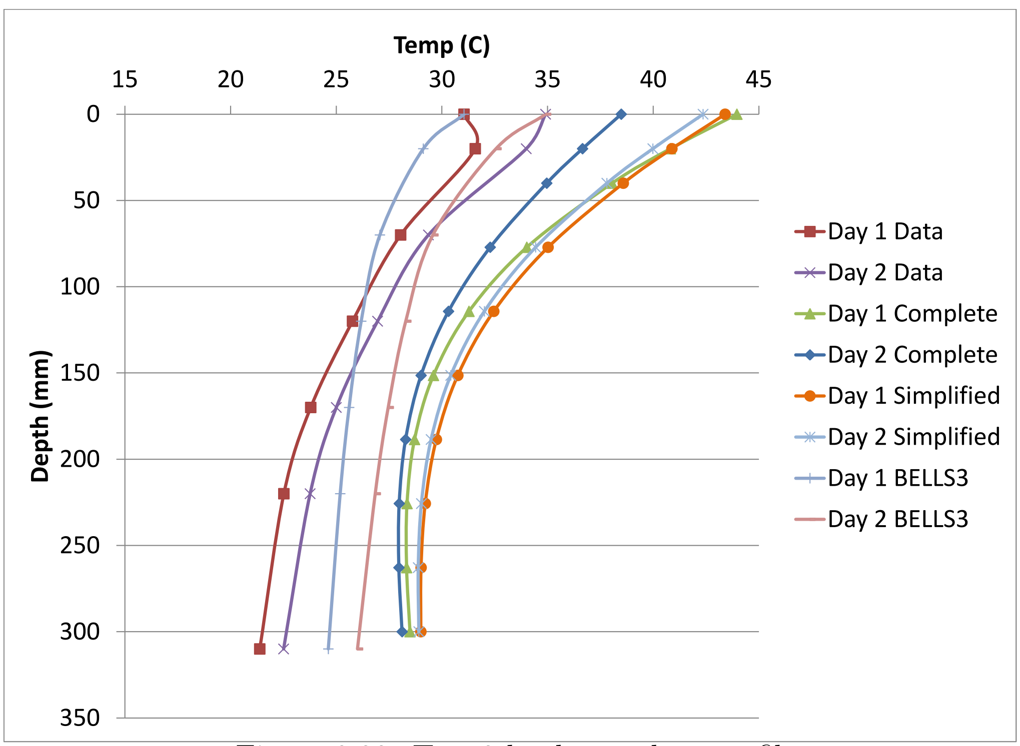

Figure 8.22: Test 2 baghouse dust profile

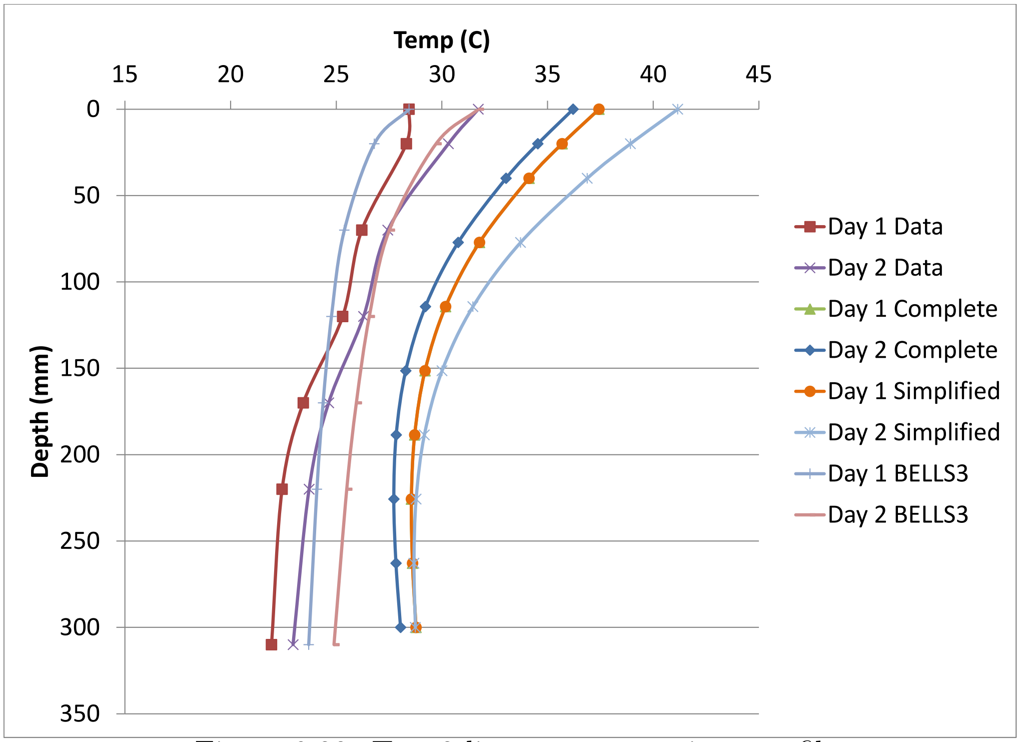

Figure 8.23: Test 2 limestone screenings profile

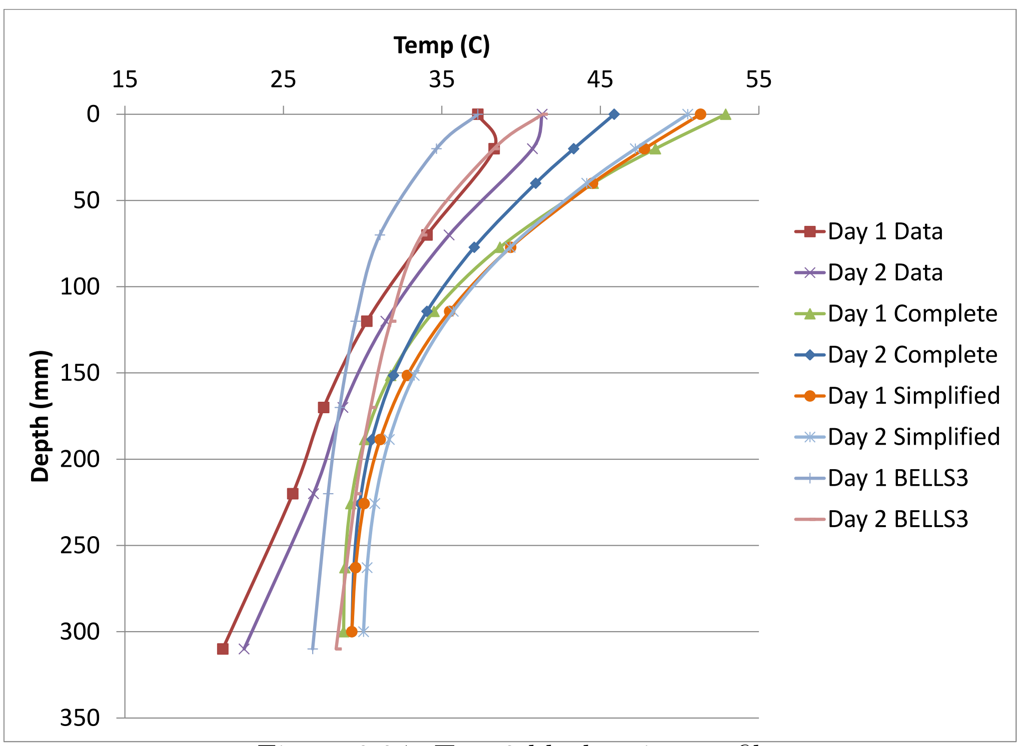

Figure 8.24: Test 2 black paint profile

the complete model. The baghouse dust and portland cement coated asphalt surfaces in Test 2 (Figures 8.17 and 8.18) showed an increase in temperature of 4 to 6 °C over the complete model.

When comparing the overall time history curves, the maximum temperatures for both models and the data reach their maximum at the same point for all simulations. For the minimum temperatures, the simplified model reaches a minimum before both the complete model and the data. If the model inputs can be adjusted to eliminate this difference, the overall accuracy of the model may improve.

This order of accuracy is reasonable, given the nature of the asphalt concrete materials and the uncertainty in weather conditions. When using this model, it is best to use all of the available recorded data before resorting to using the estimated values. In particular, the hourly air temperature is usually readily available. Hourly windspeed has a significant impact on the temperature. It is not readily available from most databases, but it is relatively easy to record if necessary. The longwave radiation (or sky temperature) is difficult to record, but was found to be the least significant of all the variables.

Shortwave solar radiation can be another large source of error. In Ontario, when there is often cloud cover, the accuracy of the estimates can be low and have a significant impact on the results. This is not as significant for hot weather conditions, which are of most concern for cool pavement technology. In a deserted region, there would normally be no cloud cover, which would result in an estimate very close to the actual value. To record the actual solar radiation requires expensive equipment and as such is rarely reported. It should be noted that for future Mechanistic Emperical pavement designs that require climatic data, that the weather data information can

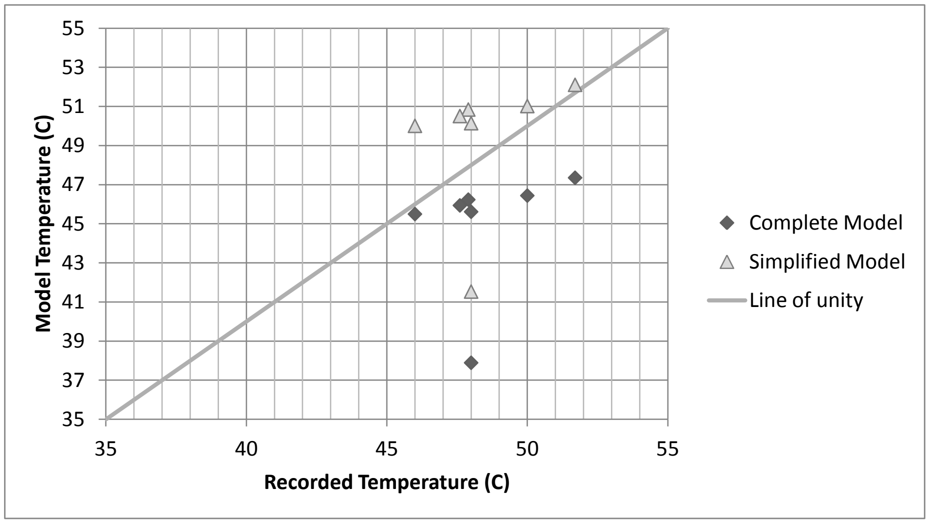

Figure 8.25: Local temperature predictions

be enhanced to include all of the information for the model through improved and/or increased weather monitoring stations in the agency's area.

8.3 Comparison to local temperatures

The temperatures and albedo values of asphalt concrete surfaces were recorded at various locations around the McMaster University campus on June 27, 2014 between 12:00 and 12:30 local time. The local climate data and albedo were then input into both models in order to determine whether this data would accurately predict the surface temperatures at the time of reading. The results of this test are shown in Figure 8.25.

It can be seen that the model can produce a reasonable estimate for the surface temperature. Using the complete model, the temperatures were underestimated by up to 4°C, and using the simplified model, values were overestimated by up to 4°C. The underestimation of the complete model is likely due to the local microclimate effects from the surrounding buildings. The buildings sheltered the surfaces from wind, which caused much lower windspeed than that recorded at the weather station and thus resulted in a higher recorded temperature than the estimate. There was one outlying value, which was a yellow painted surface. The low estimated temperatures can be attributed to the surrounding black asphalt transferring heat to the yellow area. The conditions for a road surface, which consist of large sections of uniformly coloured asphalt concrete that are not close to buildings, would likely yield a more accurate estimate. This should be considered in future research, particularly wind and/or vehicle aerodynamic influences.

8.4 Estimation of maximum asphalt temperatures

To use this model for the estimation of maximum asphalt temperatures, average conditions for the warmest part of the year were assumed. The simplified model version was used based on the estimated data. The data used for this simulation came from the database of the McMaster Weather Station. The maximum 7-day temperature was taken for the summer months in 2013. The daily minimum temperature was estimated by taking the average difference between daily maximum and minimum temperatures. Solar shortwave and longwave radiation were estimated based on the methods outlined in Chapter 7. Average windspeed was estimated from the Canadian Climate Normals database (Environment Canada, 2010). Simulations were conducted for both a fresh black asphalt concrete with an albedo of 0.059 and a worn lime coated asphalt concrete with an albedo of 0.19.

The inputs and results are shown in Table 8.1. There is a difference of 4.5°C between the black and worn hydrated lime surfaces. This difference is much less

Table 8.1: Temperature estimates

Name	Value
Maximum 7-day temperature	31.6°C
Average temperature difference	9.2°C
Minimum temperature	22.4°C
Average windspeed	2.4m/s
Longwave Radiation	400W/m^2
Estimated Max for black asphalt	58.5°C
Estimated Max for worn lime coated asphalt	54°C
Estimated Max from LTPPBIND software	49°C

extreme than the difference between black and freshly placed hydrated lime, which can be as much as 10°C, but can still be considered an improvement. The estimates are higher than that given by LTPPBind, which suggests a maximum surface temperature of 49°C and an asphalt binder high temperature performance grade of 52 in Hamilton. The asphalt binder specified for use in Hamilton is Performance Grade PG 58-28 (OPSS, 2013), which matches the temperature estimate from the simplified model. There is some error with this simulation, as the simplified model may yield an error of 5°C to 7°C. However, it would seem that the estimate provided by LTPPBind is rather low. In the field tests, temperatures of up to 48°C were recorded, despite the air temperatures remaining below 30°C. With several consecutive days of maximum air temperatures above 30°C, it would be expected that the surface temperatures could reach much higher than 49°C. In the local temperature investigation, temperatures were recorded up to 52°C at 12:00. The hot sunny conditions that day would cause surface temperatures to continue increasing until about 15:00.

8.5 Comparison to BELLS3 Model

The BELLS3 Model (ASTM, 2006a) is a method for estimating the temperature of an asphalt pavement with depth. This method is not calibrated for depths less than 25mm or greater than 150mm. Despite this, the BELLS model was used to compare the estimate with the models described in this paper at the same depths as the thermocouples.

The dark coloured specimens (Figures 8.5 and 8.7) show similar results between the BELLS3 method and the complete model for the first 70mm. Below 70mm, the BELLS3 method tends to overestimate the temperature by as much as 4°C.

For the lighter coloured specimens (Figures 8.5 and 8.8), the correlation between the BELLS3 and complete models are very good. The difference in estimates varies by approximately 1°C.

Comparing the results of Test 2 (Figures 8.21 to 8.24)shows a problem with the estimates. Here, some cloud cover had caused a significant decrease in the temperature of the asphalt concrete surface. The BELLS3 method uses the recorded surface temperature as the baseline for estimates, so an abrupt change in temperature can skew the results. This resulted in estimates lower than the actual pavement temperature. This drop in temperature had also caused errors in the complete and simplified models, which in this case over-estimated the temperatures, making the BELLS3 model appear to be more accurate for Test 2.

8.6 Microclimate

The effect of wind speed on a pavement's surface temperature is significant. In Figure 8.26, simulations with different wind speeds are compared. There is a temperature decrease of as much as 20°C when the wind speed changes from zero to 10m/s. Using an average wind speed for the day also yielded a different result than the recorded hourly wind speed.

Another effect of wind speed is that a change in wind speed can cause significant immediate decreases in the surface temperature. In Figure 8.27, a simulation is shown where a zero initial wind speed is changed to 5m/s. Here, the surface temperature drops 10°C over a period of 45 minutes, while the temperature at 20mm depth only changes by 5°C. A less drastic change was observed during Test 2 (Figures 8.21 to 8.24), where the surface temperate recorded for Day 1 is less than the temperature at 20mm. The change in surface temperature caused by changes in windspeed is the reason that the Superpave design method suggests using temperature recorded at a 20mm depth.

The cooling effect of air flow can be caused by natural weather patterns, but it may also be impacted by traffic flow. High speed traffic may cause higher airspeed at the road surface, allowing heat to dissipate to the air faster and decreasing temperatures. At the same time, slow moving traffic may impede air movement at the road surface, causing an increase in temperature. In a study by NASA (2008), it was stated that at highway speeds, as much as half of a trucks power is used in overcoming aerodynamic drag. This drag causes turbulence which moves huge volumes of air, which may effect the surface airspeed and temperature. Some aerodynamic modifications to modern trucks, such as those outlined by Patten *et al.* (2012), may decrease this turbulence,

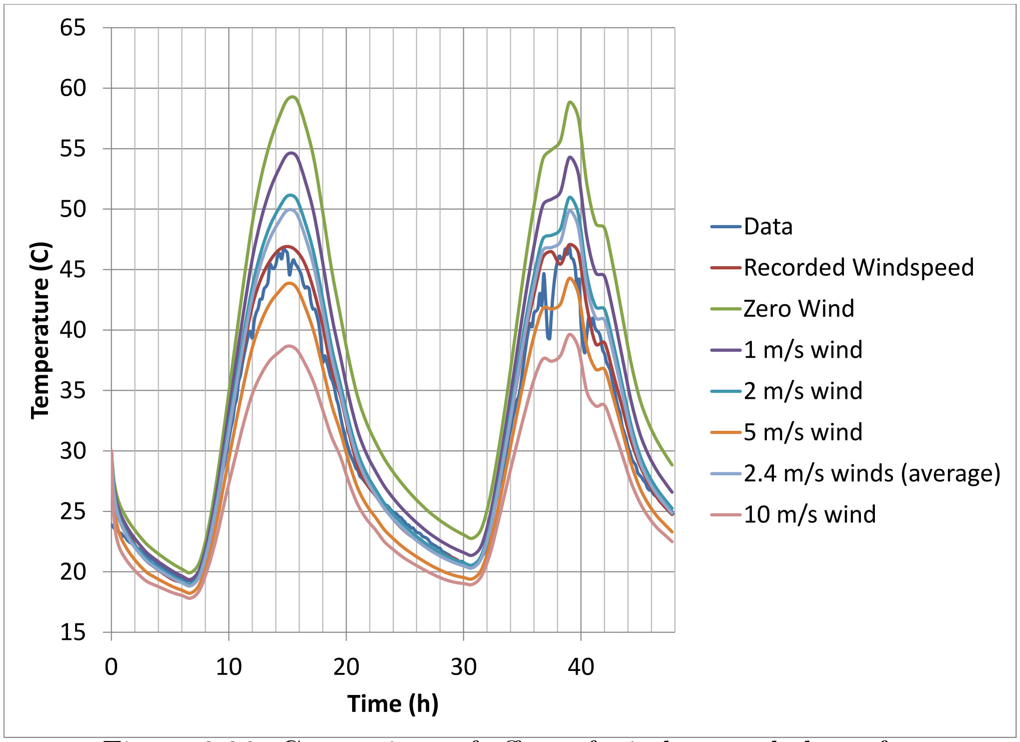

Figure 8.26: Comparison of effect of wind on asphalt surface

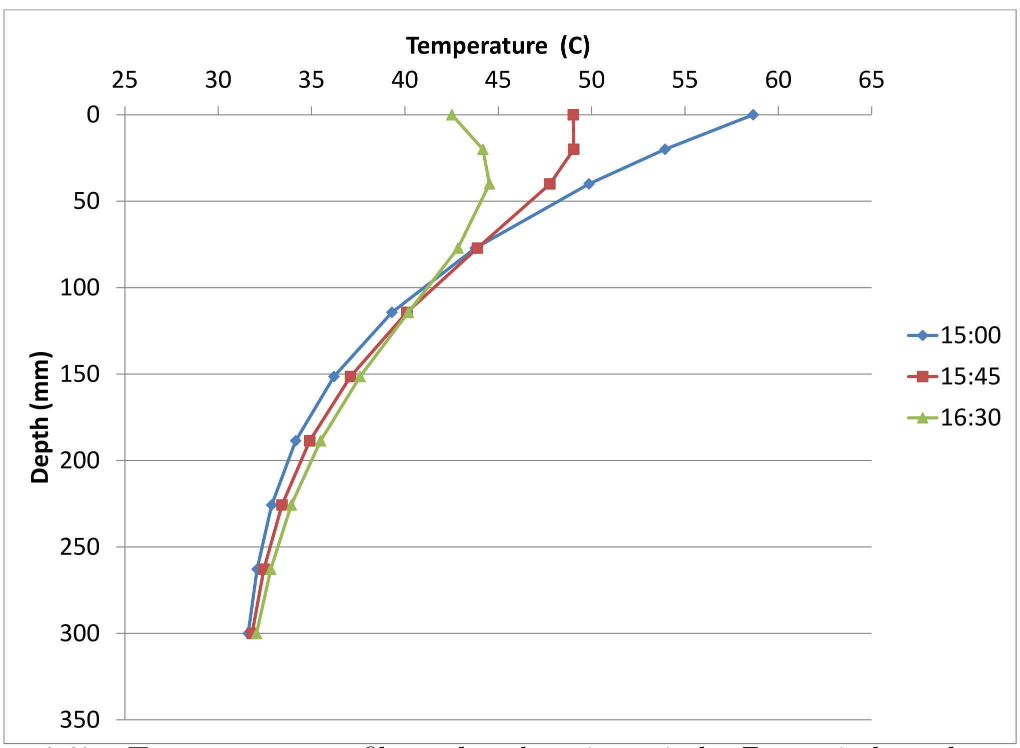

Figure 8.27: Temperature profile under changing wind. Zero windspeed to 15:00, then windspeed changes to 5m/s

which may alter the effect on surface air speed.

Another consideration to be made with microclimate models is the waste heat produced by automotive engines. This may have an impact on the road surface temperature, especially for slow moving traffic.

In conclusion, the overall effect of microclimate should be further studied for its impact on asphalt pavement temperatures.

8.7 Sensitivity analysis for simplified model

For the simplified model, the estimation parameters for all of the boundary conditions had to be determined and analysed. All of the values were compared to the results from Test 3 before being used to simulate Test 1 and Test 2.

In Figures 8.28 to 8.31, the various estimated parameters are individually tested against the Test 3 data. Here, the use of T_{air} in the place of T_{sky} yields an over-estimation of 2 to 3°C, while the use of a constant value of $T_{sky} = 16.7$°C yields a value within 1°C of the fully constrained simulation result. Thus the use of a constant value was chosen. The use of a model for determining the shortwave radiation yielded an accuracy of 1 to 3°C. This is considered reasonably accurate, as the cloud cover effects the temperature estimates. The use of only daily maximum and minimum air temperatures to estimate hourly air temperatures yields a simulation result with no significant deviation from the recorded values. The use of an average wind speed of 2.4m/s yields a level of accuracy of 1 to 3°C. The use of any of the individual estimated factors can yield a very accurate result, but when the factors are combined the accuracy diminishes to within 5°C.

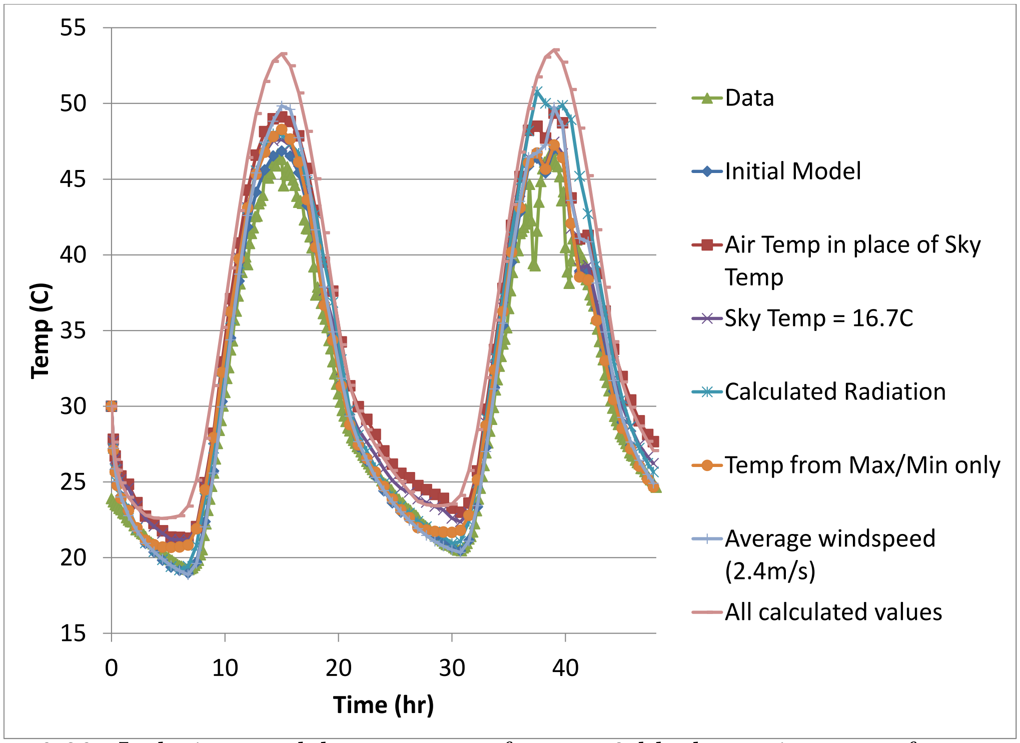

Figure 8.28: Isolating model parameters for test 3 black specimen, surface temperature

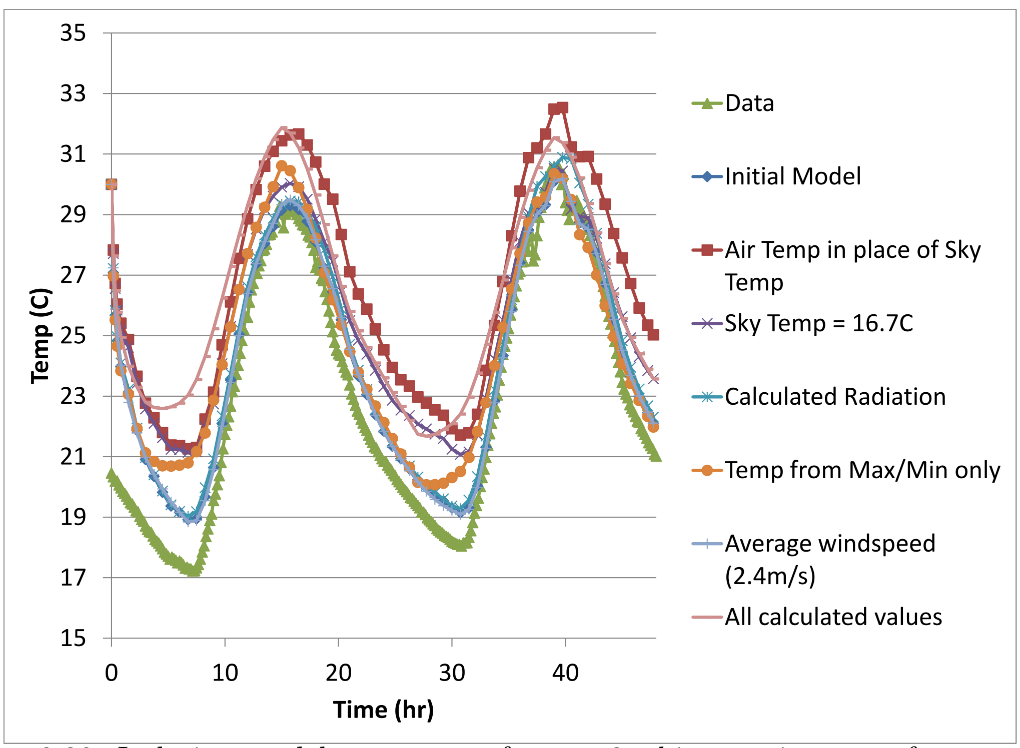

Figure 8.29: Isolating model parameters for test 3 white specimen, surface temperature

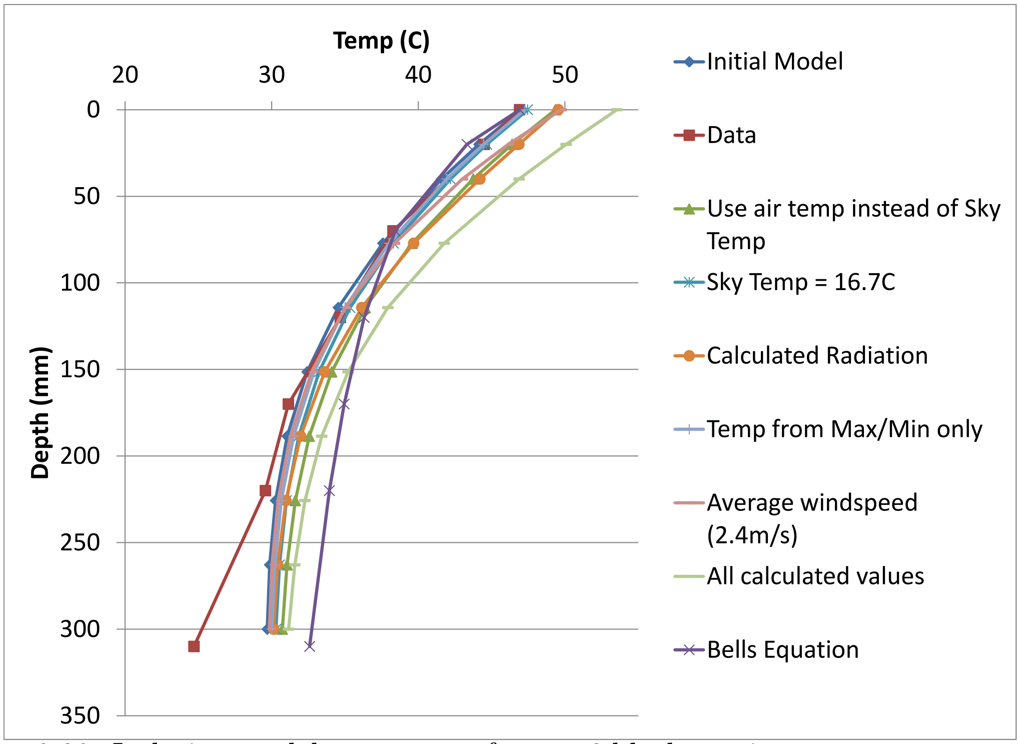

Figure 8.30: Isolating model parameters for test 3 black specimen, temperature profile

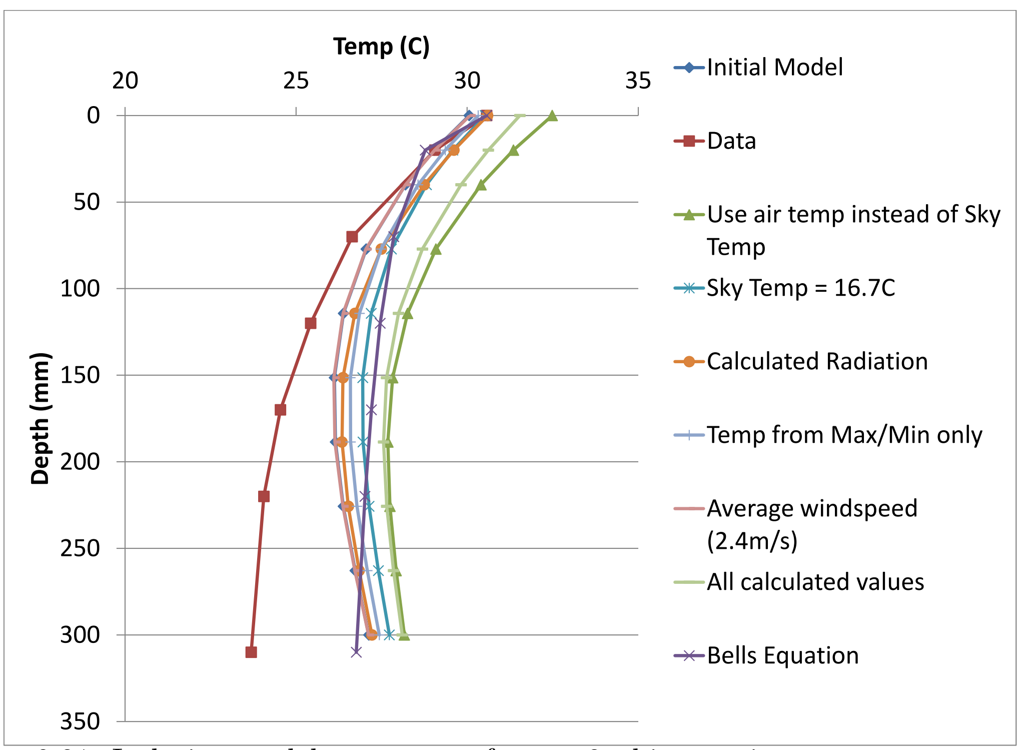

Figure 8.31: Isolating model parameters for test 3 white specimen, temperature profile

Chapter 9

Results and discussion

9.1 Applications of the model

The model developed can be used to predict the maximum temperature in an asphalt pavement at any specific day during the warmest part of the year, while taking into account the albedo of the surface. It can also be used to predict the temperature with depth at any time. To predict the maximum temperatures in an asphalt pavement, this model can be used by inputting the climate data for the warmest month of the year.

Microclimate effects on the pavement temperature can also be modelled when localised data is available.

9.2 Limitations

The field test and model results are based on one specific test at a single location and time. The model should be compared to test data from other locations for confirmation of accuracy. As well, this test has been carried out using a single asphalt pavement design. The accuracy may differ if other asphalt pavement designs are used.

The method used for the determination of albedo has only been confirmed for grey-scale surfaces. Accuracy for other coloured surfaces has not been confirmed. As well, values may vary by up to 0.05 depending on the light source used, so for comparative reasons it is best to take all readings under the same conditions.

9.3 Future work

The microclimate effects of wind and traffic movement may have a significant impact on the asphalt pavement temperature, so further microclimate development should be pursued.

The durability of hydrated lime as a coating, as well as other surface coating materials, should be considered. The macrotexture of a surface which has been coated with hydrated lime or some other material should be analysed to determine whether it maintains adequate frictional properties.

This model should be applied to temperatures in other regions to confirm whether it can accurately predict surface temperatures based on local conditions. Further refinements can be made to the inputs to increase the accuracy of the estimation.

9.4 Conclusion

The conclusions made through the course of this research are summarized below.

- Using a white coloured surface decreased the surface temperatures of asphalt concrete by as much as 17°C compared to the dark coloured surfaces.

- Using light coloured surfaces with albedo values in the range of 0.2 to 0.3 yielded a temperature decrease of approximately 7 to 10°C. This difference may become larger under warmer weather conditions.
- A simple method was developed to characterize the surface albedo using a technically suitable light meter.
- A method was developed, based on the Wet Track Abrasion Test, to determine the durability of a surface coating. There were significant problems with applying coatings to be tested that must be considered.
- The use of hydrated lime, applied to a polymer modified asphalt, yields a long term albedo of approximately 0.19 based on the Wet Track Abrasion Test, noting the significant test limitations. This is being checked by field durability tests by others.
- The complete model was able to accurately predict the surface and profile temperatures of an asphalt pavement when taking into consideration the surface albedo.
- When comparing the temperature profile results from the developed model to the BELLS3 method, it was found that the accuracy is within the same range.
- The simplified model was found to have a decreased accuracy as compared to the complete model due to limited input data, but it should be applicable to any location.
- Wind has a critical effect on the surface temperature of an asphalt pavement. A change in wind speed from 0m/s to 10m/s can decrease surface temperatures by 20°C.

Bibliography

Abu-Halimeh, I. (2007). *Surface Colour Effects on the Thermal Behaviour and Mechanical Properties of Hot Mix Asphalt*. Master's thesis, McMaster University.

Akbari, H. and Matthews, H. D. (2012). Global cooling updates: Reflective roofs and pavements. *Energy and Buildings*, **55**, 2–6.

Akbari, H., Levinson, R., and Stern, S. (2008). Procedure for measuring the solar reflectance of flat or curved roofing assemblies. *Solar Energy*, **82**(7), 648–655.

Alavi, M. Z., Pouranian, M. R., and Hajj, E. Y. (2013). Prediction of asphalt pavement temperture profile using the finite control volume method. In *93rd Annual Meeting of the Transportation Research Board*.

ASTM (2003). ASTM D559-03: Standard Test Methods for Wetting and Drying Compacted Soil-Cement Mixtures. ASTM International, West Conshohocken, PA.

ASTM (2006a). ASTM D7228-06a: Standard Test Method for Prediction of Asphalt-Bound Pavement Layer Temperatures. ASTM International, West Conshohocken, PA.

ASTM (2006b). ASTM E1918-06: Standard Test Method for Measuring Solar Reflectance of Horizontal and Low-Sloped Surfaces in the Field. ASTM International, West Conshohocken, PA.

ASTM (2009). ASTM C1549-09: Standard Test Method for Determination of Solar Reflectance Near Ambient Temperature Using a Portable Solar Reflectometer. ASTM International, West Conshohocken, PA.

ASTM (2011). ASTM D3910-11: Standard Practices for Design, Testing, and Construction of Slurry Seal. ASTM International, West Conshohocken, PA.

ASTM (2012). ASTM E903-12: Standard Test Method for Solar Absorptance, Reflectance, and Transmittance of Materials Using Integrating Spheres. ASTM International, West Conshohocken, PA.

Bliss Jr, R. W. (1961). Atmospheric radiation near the surface of the ground: a summary for engineers. *Solar Energy*, **5**(3), 103–120.

Chen, M., Xu, G., Wu, S., and Zheng, S. (2010). High-temperature hazards and prevention measurements for asphalt pavement. In *2010 International Conference on Mechanic Automation and Control Engineering (MACE)*, pages 1341–1344. IEEE.

Doré, G. and Zubeck, H. K. (2009). *Cold regions pavement engineering*. ASCE Press.

Earle, R. L. (2004). *Unit operations in food processing*. The New Zealand Institute of Food Science and Technology (Inc.), web edition. http://www.nzifst.org.nz/unitoperations/httrtheory6.htm.

Emery, J. J., Guo, P., Stolle, D. F., Hernandez, J., and Zhang, L. (2014). Light-coloured grey asphalt pavements: from theory to practice. *International Journal of Pavement Engineering*, **15**(1), 23–35.

Environment Canada (2010). *Canadian climate normals, 1981-2010.* Canadian Climate Program, Environment Canada, Atmospheric Environment Service Downsview, Ontario, Canada.

Feng, D. and Zhang, X. (2009). Heat reflection coating design and performance. In *ICCTP 2009@ Critical Issues In Transportation Systems Planning, Development, and Management*, pages 1–7. ASCE.

Gui, J., Phelan, P. E., Kaloush, K. E., and Golden, J. S. (2007). Impact of pavement thermophysical properties on surface temperatures. *Journal of Materials in Civil Engineering*, **19**(8), 683–690.

Incropera, F. P. and Dewitt, D. P. (1996). Introduction to heat transfer. *John Wiley & Sons. New York. NY.*

Kinouchi, T., Yoshinaka, T., Fukae, N., and Kanda, M. (2004). Development of cool pavement with dark colored high albedo coating. In *5th Symposium on the Urban Environment, 23-27 August 2004, Vancouver, BC, Canada.*

Lee, R. W., Kim, J. W., and Kim, D. W. (1985). Development of color pavement in Korea. *Journal of transportation engineering*, **111**(3), 292–302.

Levinson, R. and Akbari, H. (2002). Effects of composition and exposure on the solar reflectance of portland cement concrete. *Cement and Concrete Research*, **32**(11), 1679–1698.

Levinson, R., Akbari, H., and Berdahl, P. (2010). Measuring solar reflectancepart II: Review of practical methods. *Solar Energy*, **84**(9), 1745 – 1759.

McGuffie, K. and Henderson-Sellers, A. (2014). *The Climate Modelling Primer*. John Wiley & Sons.

Mohseni, A. (1998). LTPP seasonal asphalt concrete (AC) pavement temperature models. Technical Report FHWA-RD-97-103, Federal Highway Administration.

Mohseni, A. (2005). LTPP BIND. Federal Highway Administration, McLean, VA. http://www.fhwa.dot.gov/research/tfhrc/programs/infrastructure/pavements/ltpp/dwnload.cfm

NASA (2008). *Aerodynamics Research Revolutionizes Truck Design*. Government Printing Office.

OPSS (2013). OPSS.MUNI 1101: Material Specification for Performance Graded Asphalt Cement. Ontario Provincial Standard Specification.

Ozisik, M. (1985). Heat transfer: a basic approach. *MacGraw-Hill, New York, USA*.

Patten, J., McAuliffe, B., Mayda, W., and Tanguay, B. (2012). Review of aerodynamic drag reduction devices for heavy trucks and buses. Technical Report CSTT-HVC-TR-205, National Research Council Canada.

Pomerantz, M., Akbari, H., Berdahl, P., Konopacki, S., Taha, H., and Rosenfeld, A. (1999). Reflective surfaces for cooler buildings and cities. *Philosophical magazine B*, **79**(9), 1457–1476.

Pomerantz, M., Pon, B., Akbari, H., and Chang, S.-C. (2000). *The effects of pavements' temperatures on air temperatures in large cities.* Ernest Orlando Lawrence Berkeley National Laboratory.

Russia Today (2014). Plane sinks in melting asphalt at moscow airport. http://on.rt.com/lqxjr9.

Santamouris, M. (2007). Heat island research in europe: the state of the art. *Advances in building energy research*, **1**(1), 123–150.

Simulia (2011). Abaqus 6.11 theory manual. *Providence, RI, USA: DS SIMULIA Corp.*

Stull, R. B. (2000). *Meteorology for scientists and engineers: a technical companion book with Ahrens' Meteorology Today.* Brooks/Cole.

Tatum, J. (2011). *Stellar Atmospheres*, chapter Definitions of and Relations between Quantities used in Radiation Theory. University of Victoria, Victoria, BC.

Tran, N., Powell, B., Marks, H., West, R., and Kvasnak, A. (2009). Strategies for design and construction of high-reflectance asphalt pavements. *Transportation Research Record: Journal of the Transportation Research Board*, **2098**(1), 124–130.

Wang, H., Zhong, J., Feng, D., Meng, J., and Xie, N. (2013). Nanoparticles-modified polymer-based solar-reflective coating as a cooling overlay for asphalt pavement. *International Journal of Smart and Nano Materials*, **4**(2), 102–111.

Yang, J., Wang, Z., and Kaloush, K. H. (2013). Unintended consequences: A research synthesis examining the use of reflective pavements to mitigate the urban heat island effect. *Arizona State University National Center of Excellence for SMART Innovations.*

Yavuzturk, C., Ksaibati, K., and Chiasson, A. (2005). Assessment of temperature fluctuations in asphalt pavements due to thermal environmental conditions using a two-dimensional, transient finite-difference approach. *Journal of Materials in Civil Engineering*, **17**(4), 465–475.

Yilmaz, H., Toy, S., Irmak, M., Yilmaz, S., and Bulut, Y. (2008). Determination of temperature differences between asphalt concrete, soil, and grass surfaces of the city of Erzurum, Turkey. *Atmósfera*, **21**(2), 135–146.

Yuri, M. (1998). *Remote Sensing of Earth Radiation Budget.* The University of New Jersey.

Appendix A

Materials

AME Materials Engineering

Superpave Warm Mix Design Report

AME - Materials Engineering, 10 Perdue Court, Units 2 & 3, Caledon, Ontario, Canada, L7C 3M6
Phone: (905) 840-5914; Fax: (905) 840-7859, E-Mail: ame@amecorp.ca

BEST EMPLOYERS IN CANADA 2012

LAB MIX NUMBER	53110.001 SP12.5FC1	JOB MIX FORMULA NO.	
CONTRACT NUMBER	Various	HOT MIX TYPE/USE	SP12.5FC1 Warm Mix
		ITEM NO.	
HIGHWAY	Various Locations	LOCATION	Aecon - Hwy 7 Sharbot Lake
TESTING LAB	AME Materials Engineering, Caledon, Ontario	DATE SAMPLES REC'D	25-Jul-12
TEST DATA CERTIFIED BY:		DATE COMPLETED	14-Aug-12

Job Mix Formula - Gradation Percent Passing *

% AC	37.5	25	19.0	16.0	12.5	9.5	6.7	4.75	2.36	1.18	600	300	150	75
4.80	100	100.0	100.0	100.0	97.5	85.2		61.4	39.3	27.2	18.5	11.2	6.6	4.4

Traffic Category: C **Gyrations:** **N ini:** 7 **N des:** 75 **N max:** 115

Property	Requirements	Selected
%Gmm @ N des / Va	96.0 / 4.0	96.1 / 3.9
%Gmm @ N ini	89.0 Max	88.5
%Gmm @ N max	98.0 Max	97.0
% VMA (min)	14.0	14.5
% VFA	65-75	72.4
DP	0.6 to 1.2	1.0
TSR	80% Min	87.8

% AGG #1	37.0
% AGG #2	13.0
% AGG #3	17.0
%AGG #4	33.0
% AGG #5	-
% AGG #6	-
BRIQ. BRD	2.394
MRD	2.494

% RAP	-
% AC RAP	-

Consensus Properties

% CR Total	100.0
% CR 2 Face	100.0
% F & E (5:1)	0.6
FAA	46.1
Sand Equiv.	85

ASPHALT CEMENT

SUPPLIER	Grade
McAsphalt	PG 58-40P

ADDITIVE

SUPPLIER	TYPE	AS % of AC
Evotherm	3GV	0.30%

	SOURCE / INVENTORY NUMBER		SOURCE / INVENTORY NUMBER
AGGREGATE #1	12.5mm Stone / Danford Granite Quarry / K01-106	AGGREGATE #4	Manufactued Sand / Danford Granite Quarry / K01-106
AGGREGATE #2	Chip / Aecon Marmora Quarry / C01-058	AGGREGATE #5	
AGGREGATE #3	Screenings / Danford Granite Quarry / K01-106	RAP	

AGGREGATE DATA	AGG. SPECIFIC GRAVITY	AGG. ABSORP. (%)	AGGREGATE GRADING - PERCENT PASSING												
			37.5	25.0	19.0	16.0	12.5	9.5	4.75	2.36	1.18	600	300	150	75
AGG #1	2.625	0.5		100.0	100.0	100.0	93.1	59.7	5.1	2.2	2.0	1.8	1.5	1.3	1.1
AGG #2	2.972	0.4						100.0	88.6	12.6	2.2	1.1	0.8	0.6	0.5
AGG #3	2.636	0.4						100.0	87.0	61.9	47.0	35.7	24.7	15.3	9.0
AGG #4	2.626	0.4						100.0	99.4	77.8	52.8	32.8	16.5	7.9	4.8
AGG #5															
RAP															

Coarse Agg. Gsb	2.639	Fine Agg. Gsb	2.678	Combined Gsb	2.663

*JMF Adjusted to Allow for 1.0 % Fines Returned to the Mix

Remarks: **Mix Comp Temp=Recomp Temp=125C; Briq. Wt.=4800gms; Abs%<2 no sealing required; AC extraction by LS-282; Mix design mixing Temp = 135C.**

Reviewed By: ______________________ Date: __________

Figure A.1: AME Superpave 12.5mm FC1 Mix design

AME Materials Engineering

Superpave Mix Design Report

AME - Materials Engineering, 10 Perdue Court, Units 2 & 3, Caledon, Ontario, Canada, L7C 3M6
Phone: (905) 840-5914; Fax: (905) 840-7859, E-Mail: ame@amecorp.ca

BEST EMPLOYERS IN CANADA 2012

LAB MIX NUMBER	18000.024 SP19mm	JOB MIX FORMULA NO.	
CONTRACT NUMBER	Various	HOT MIX TYPE/USE	SP 19mm
		ITEM NO.	
HIGHWAY	Various	LOCATION	Aecon - Brampton Plant
TESTING LAB	AME Materials Engineering, Brampton Ont.	DATE SAMPLES REC'D	02-Apr-12
TEST DATA CERTIFIED BY:		DATE COMPLETED	01-May-12

Job Mix Formula - Gradation Percent Passing *

% AC	37.5	25	19.0	16.0	12.5	9.5	6.7	4.75	2.36	1.18	600	300	150	75
4.80	100	100.0	93.8	88.1	82.4	68.7		49.6	39.9	26.9	17.6	11.2	7.2	4.2

Traffic Category: E Gyrations: N ini: 9 N des: 125 N max: 205

Property	Requirements	Selected
%Gmm @ N des / Va	96.0 / 4.0	96.0 / 4.0
%Gmm @ N ini	89.0 Max	87.0
%Gmm @ N max	98.0 Max	97.3
% VMA (min)	13.0	13.3
% VFA	65-75	69.9
DP	0.6 to 1.2	1.1
TSR	80% Min	94.0

% AGG #1	22.0
% AGG #2	29.0
% AGG #3	35.0
%AGG #4	14.0
% AGG #5	
% AGG #6	-
BRIQ. BRD	2.481
MRD	2.584

% RAP	-
% AC RAP	-

Consensus Properties

% CR Total	100.0
% CR 2 Face	100.0
% F & E (5:1)	0.2
FAA	48.3
Sand Equiv.	91

ASPHALT CEMENT

SUPPLIER	Grade
McAsphalt	70-28P

ADDITIVE

SUPPLIER	TYPE	AS % of AC
	N/A	

	SOURCE / INVENTORY NUMBER		SOURCE / INVENTORY NUMBER
AGGREGATE #1	19mm Stone / Dufferin Acton Quarry / G09-067	AGGREGATE #4	Screenings / Dufferin Milton Quarry / B12-127
AGGREGATE #2	HL3 Stone / Dufferin Acton Quarry / G09-067	AGGREGATE #5	
AGGREGATE #3	High Stability Sand / Dufferin Milton Quarry / B12-127	RAP	

AGGREGATE DATA	AGG. SPECIFIC GRAVITY	AGG. ABSORP. (%)	AGGREGATE GRADING - PERCENT PASSING												
			37.5	25.0	19.0	16.0	12.5	9.5	4.75	2.36	1.18	600	300	150	75
AGG #1	2.676	1.1		100.0	71.3	45.2	21.5	3.8	2.0	1.8	1.6	1.5	1.3	1.1	0.7
AGG #2	2.661	1.5		100.0	100.0	100.0	98.1	63.3	4.7	1.9	1.7	1.5	1.2	1.0	0.5
AGG #3	2.781	0.6						100.0	99.8	83.9	54.3	32.6	17.7	8.6	2.7
AGG #4	2.799	0.5						100.0	86.3	61.7	42.1	29.7	21.7	16.8	12.8
AGG #5															
RAP															

Coarse Agg. Gsb	2.674	Fine Agg. Gsb	2.770	Combined Gsb	2.722

*JMF Adjusted to Allow for 1.5 % Fines Returned to the Mix

Remarks: **Mix Comp Temp=Recomp Temp=150 °C; Briq. Wt.=4955gms; Abs%<2 no sealing required; AC extraction by LS-282; Mix design mixing Temp = 165 °C**

Reviewed By: ______________________ Date: __________

Figure A.2: AME Superpave 19mm Mix design

Appendix B

Additional temperature profile data

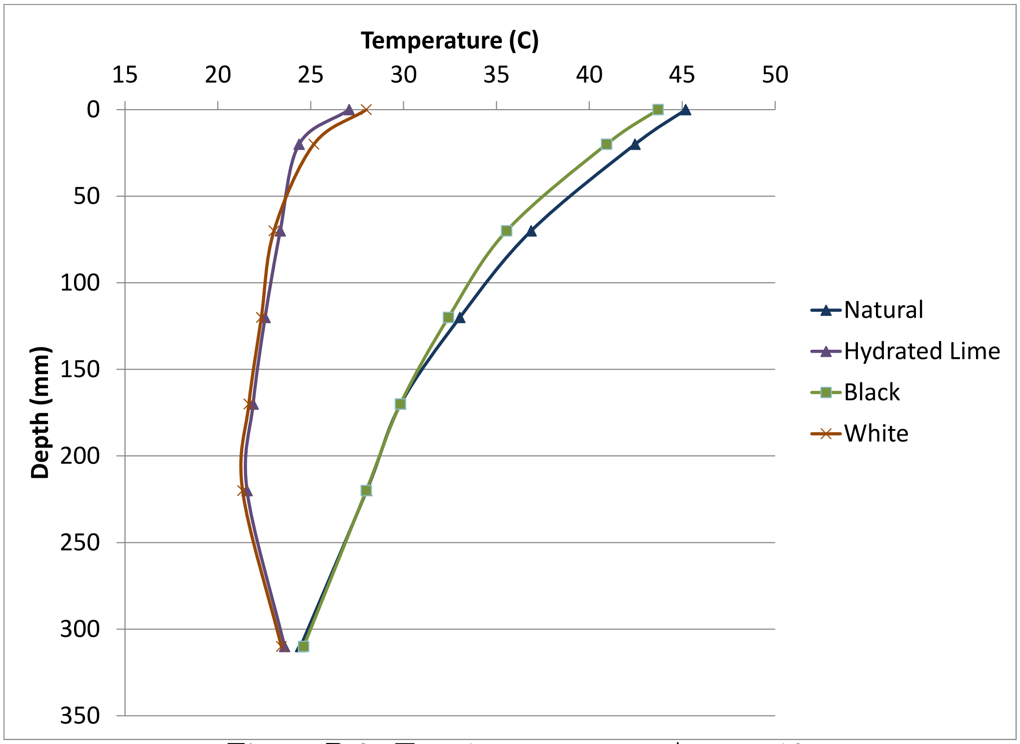

Figure B.3: Test 1 temperature August 10

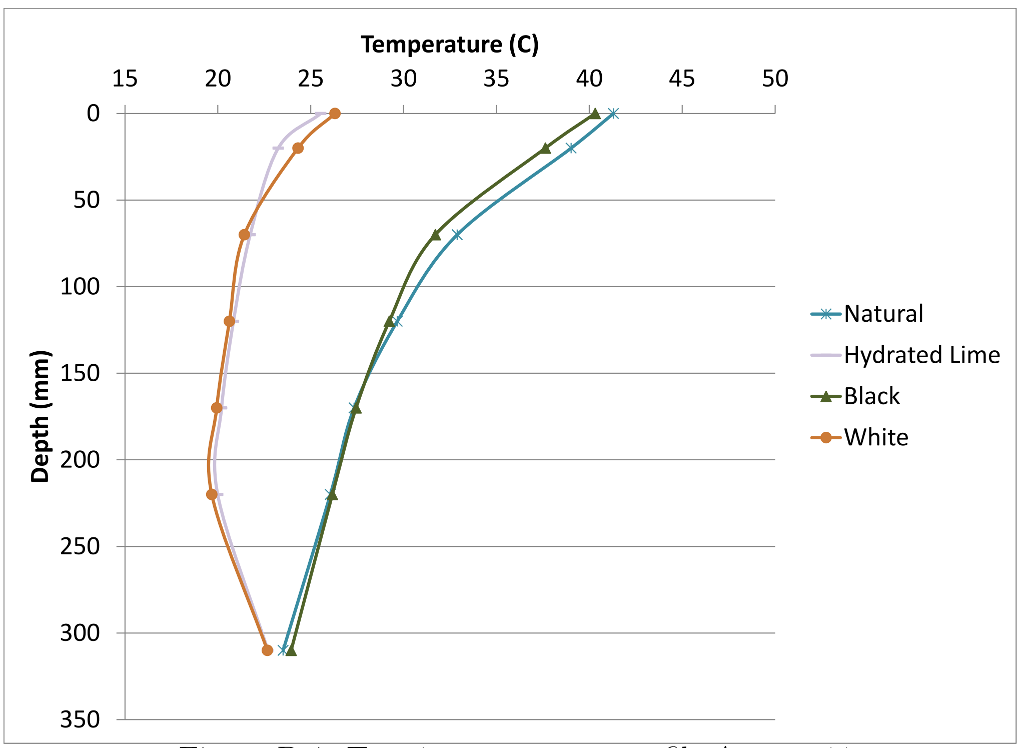

Figure B.4: Test 1 temperature profile August 11

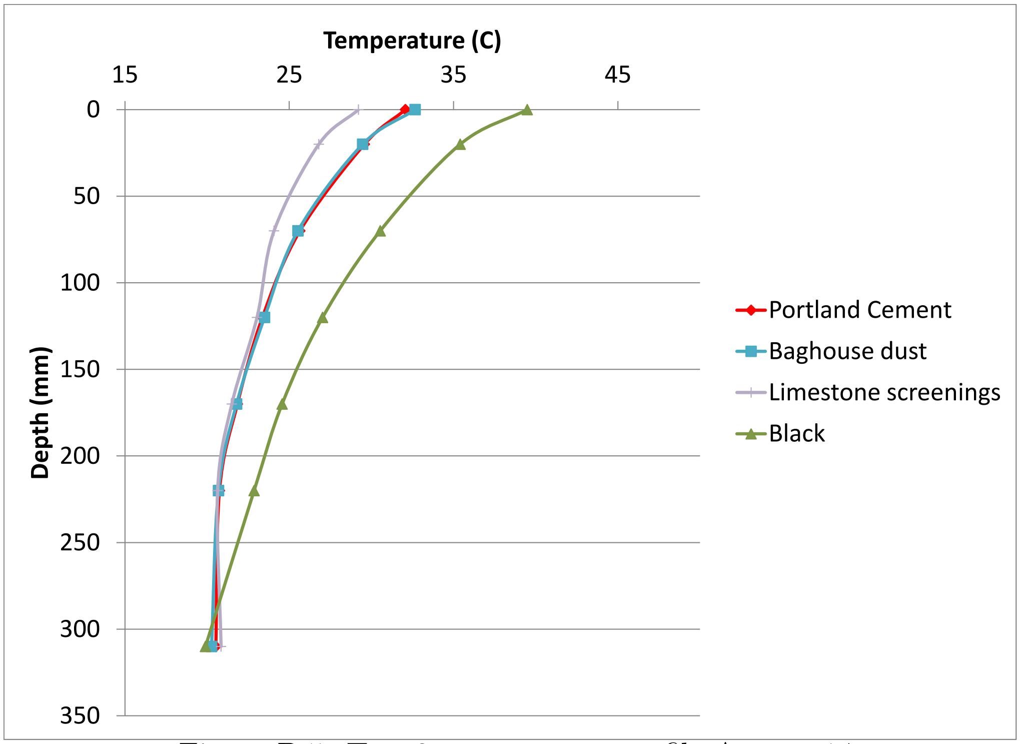

Figure B.5: Test 2 temperature profile August 14

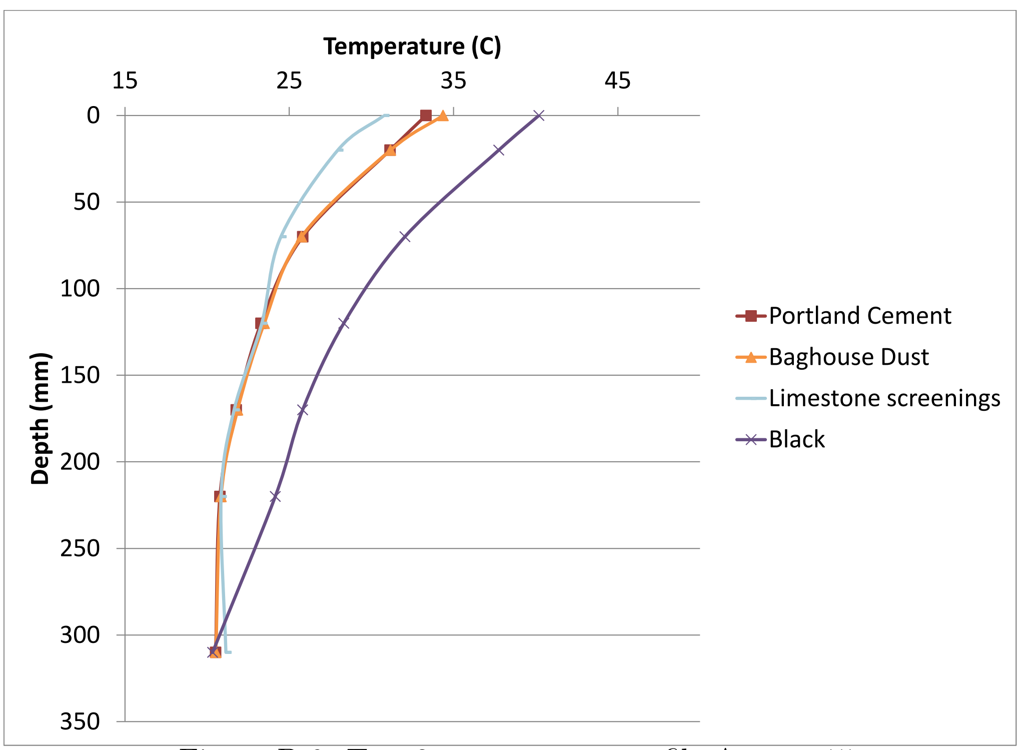

Figure B.6: Test 2 temperature profile August 15

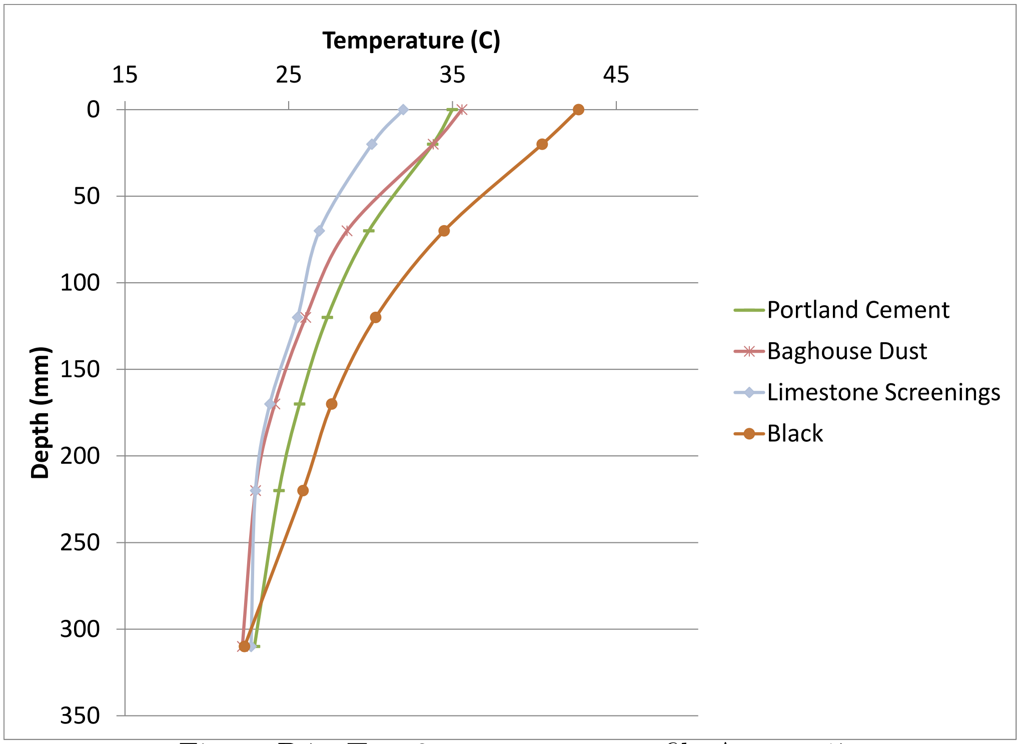

Figure B.7: Test 2 temperature profile August 17

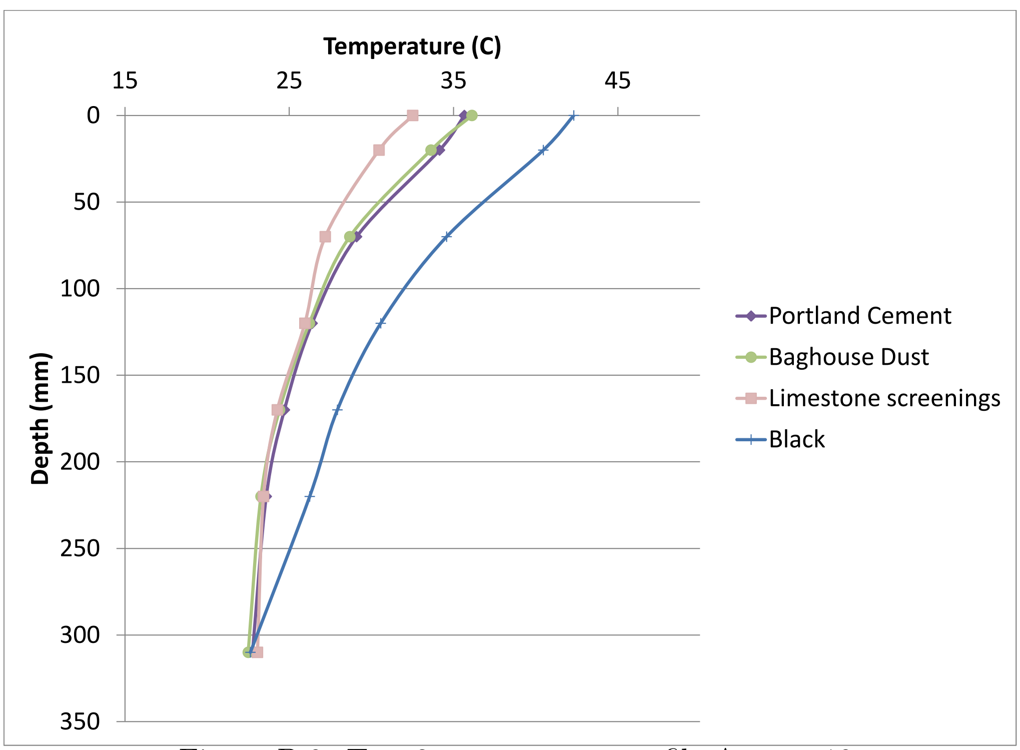

Figure B.8: Test 2 temperature profile August 18

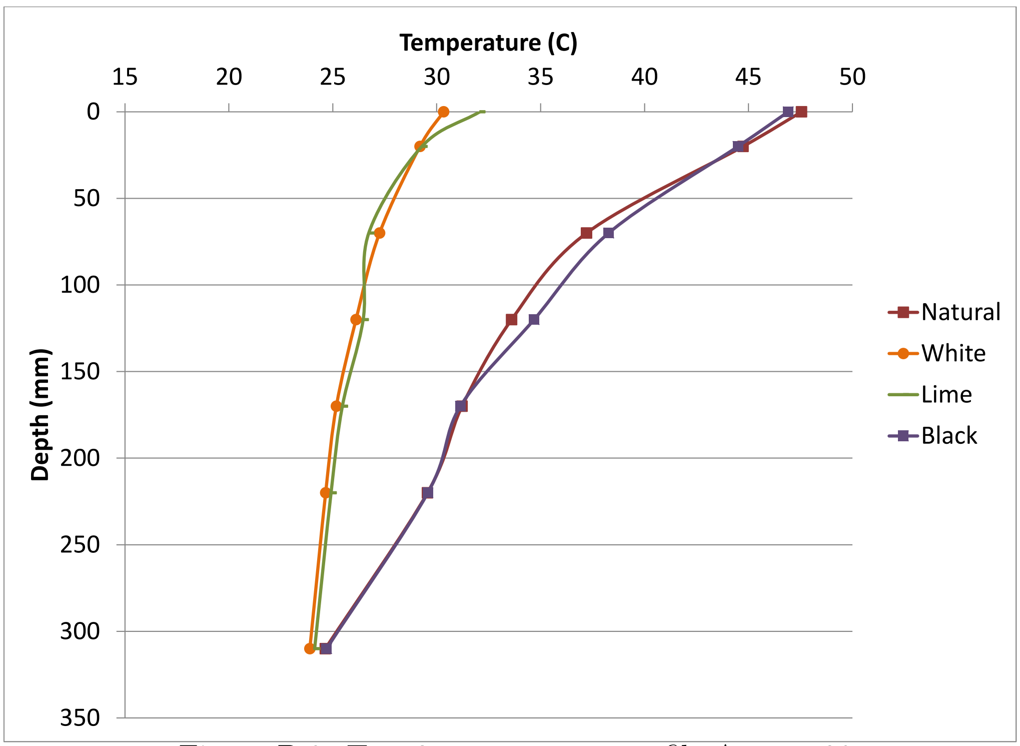

Figure B.9: Test 3 temperature profile August 20

Appendix C

Testing procedure for the durability of a surface in terms of albedo

This testing procedure covers a standardized method for determining the change of surface albedo with wear. It is a modification of the Wet Track Abrasion test outlined in ASTM D3910-11 (ASTM, 2011)

C.1 Apparatus

The testing apparatus is similar to that used in ASTM D3910-11. A planetary type mechanical mixer (Hobart N-50) is equiped with a weighted (2.3 kg) rubber hose holding device. A metal pan of adequate size to hold the test specimen is clamped in place and supported by wooden blocks. The apparatus is shown in Figure C.10. A full description of the required apparatus is given in ASTM D3910-11.

C.2 Preparation of specimen

Asphalt concrete specimens of 300mm diameter and 40mm thickness are used for this test. The specimens are prepared with asphalt pre-heated to 125°C, which are compacted into a mould by use of a 100mm tamper attached to an impact hammer (Milwaukee SDS-Max Demolition Hammer, model number 5446-21). The asphalt mix is polymer modified in order to increase the adhesion of surface coatings (see Section 3).

Surface treatments are applied to the completed specimens. Paints can be applied by roller or brush. Other surface coatings which are applied as a powder, such as hydrated lime, must be applied to a warm asphalt concrete surface (preferably polymer modified HMA). The specimens must first be placed in a pan or flat tray and preheated in an oven to 60°C. Do not remove the specimen from the tray while it is warm as it may fall apart.

The concentration of the coating to be applied is $150g/m^2$ for all materials used in this case, which comes to 11g total per 300mm diameter specimen.

Approximately half of the surface coating is dusted over the surface. This may be spread out with a soft brush if necessary. It is then compacted by laying a piece of wax paper over the surface and rolling with a steel rod. Alternatively, any other heavy cylinder can be used, such as a marble rolling pin. The wax paper is used to prevent the surface coating from sticking to the roller.

After the initial compaction, the remaining materials is spread on, taking care to make the coating even. The material may then again be brushed around for even coverage. Alternatively, the wax paper may be applied to the surface and gently slid around. The roller is then used for final compaction. The specimen is then left to cool overnight before it can be tested.

C.3 Test procedure

The first step is to determine the initial albedo of the specimen surface using the light meter method (see Section 4). After this, the wet track abrasion test can be conducted.

The specimen is placed into the pan and submerged in water at approximately 25°C. The specimen must soak for at least 1 hour. A fresh piece of abrasion standard hose is connected into the holding device, which is then attached to the mixer. The specimen is raised in place, clamped, and supported by the wooden blocks. Ensure that the back of the pan is in contact with the mixer stand. The mixer should be turned to low. The testing sequence can now be started.

In the initial test, the mixer is run for 5 minutes. After the test, the specimen is removed from the water bath and any loose material on the surface is brushed off. The specimen is then left to dry overnight. When fully dry, the albedo of the abraded surface is recorded as outlined above. Be sure to only record the albedo of the area that is abraded. A photograph of the surface should also be taken.

The test can then be repeated for 45 minutes. Be sure to place the same abraded location under the mixing head. The rubber hose used in the 5 minute test can be re-used for this test if the strings within the hose have not been exposed. Allow the specimen to dry and record the albedo as above.

If there was a change in albedo between the first two tests, then an additional 100 minute test is to be completed. In this case, a fresh piece of hose must be used. (The hose can be re-used by rotating it 90°C and using the fresh surface.) More time may

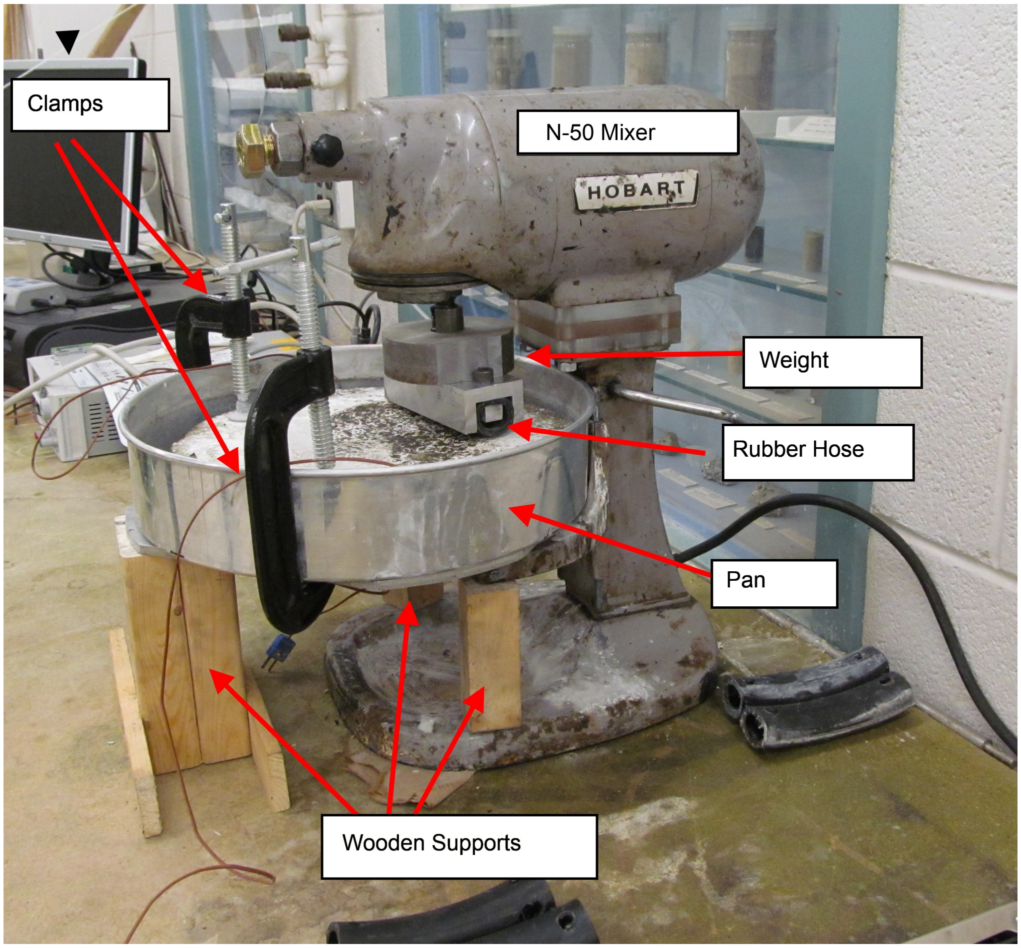

Figure C.10: Test Apparatus

be added if the albedo continues to change.

C.4 Report

Report the albedo recorded before testing as well as after accumulated test time of 5, 50 and 150 minutes.

Appendix D

Abaqus 6.11 Theory Manual Section 2.11.1 Uncoupled Heat Transfer Analysis

2.11.1 UNCOUPLED HEAT TRANSFER ANALYSIS

Product: Abaqus/Standard

The Abaqus/Standard capability for uncoupled heat transfer analysis is intended to model solid body heat conduction with general, temperature-dependent conductivity; internal energy (including latent heat effects); and quite general convection and radiation boundary conditions. This section describes the basic energy balance, constitutive models, boundary conditions, finite element discretization, and time integration procedures used.

Heat transfer in flowing materials (convection) is discussed in "Convection/diffusion," Section 2.11.3. Radiation heat transfer in cavities is discussed in "Cavity radiation," Section 2.11.4. All such heat transfer mechanisms can be present in a model.

Energy balance

The basic energy balance is (Green and Naghdi)

$$\int_V \rho \dot{U} dV = \int_S q\, dS + \int_V r\, dV, \tag{2.11.1–1}$$

where V is a volume of solid material, with surface area S; ρ is the density of the material; $\dot{U}$ is the material time rate of the internal energy; q is the heat flux per unit area of the body, flowing into the body; and r is the heat supplied externally into the body per unit volume.

It is assumed that the thermal and mechanical problems are uncoupled in the sense that $U = U(\theta)$ only, where θ is the temperature of the material, and q and r do not depend on the strains or displacements of the body. For simplicity a Lagrangian description is assumed, so "volume" and "surface" mean the volume and surface in the reference configuration.

Constitutive definition

This relationship is usually written in terms of a specific heat, neglecting coupling between mechanical and thermal problems:

$$c(\theta) = \frac{dU}{d\theta},$$

except for latent heat effects at phase changes, which are given separately in terms of solidus and liquidus temperatures (the lower and upper temperature bounds of the phase change range) and the total internal energy associated with the phase change, called the latent heat. When latent heat is given, it is assumed to be in addition to the specific heat effect (see Figure 2.11.1–1). For many cases it is reasonable to assume that the phase change occurs within a known temperature range, which can be specified by the user. However, in some cases it may be necessary to include a kinetic theory for the phase change to model the effect accurately (an example would be the prediction of crystallization in a polymer casting process).

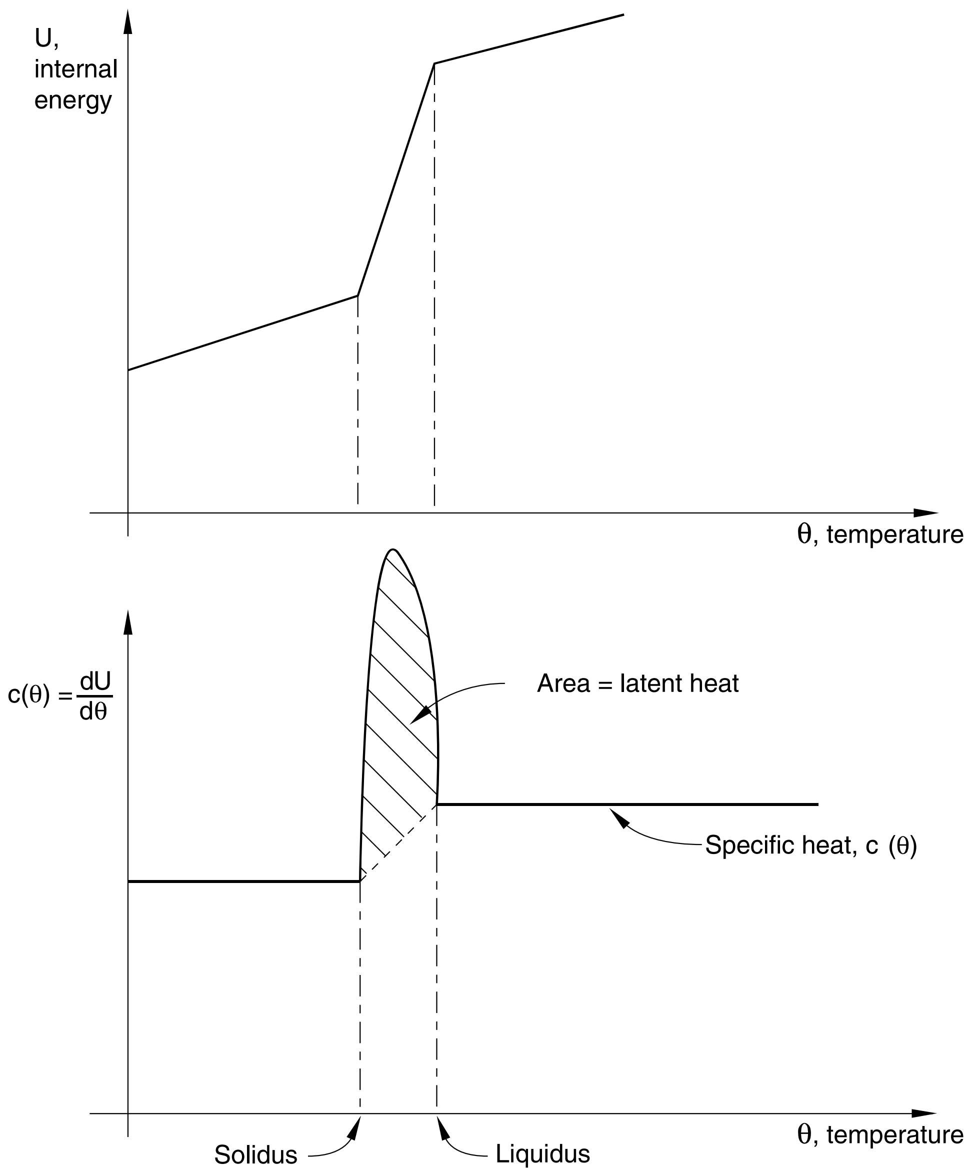

Figure 2.11.1–1 Specific heat, latent heat definition.

For such cases the user can model the process in considerable detail, using the solution-dependent state variable feature in Abaqus, with user subroutine **HETVAL**.

Heat conduction is assumed to be governed by the Fourier law,

$$\mathbf{f} = -\mathbf{k}\frac{\partial \theta}{\partial \mathbf{x}}, \tag{2.11.1–2}$$

where $\mathbf{k}$ is the conductivity matrix, $\mathbf{k} = \mathbf{k}(\theta)$; $\mathbf{f}$ is the heat flux; and $\mathbf{x}$ is position. The conductivity $\mathbf{k}$ can be fully anisotropic, orthotropic, or isotropic.

Boundary conditions

Boundary conditions can be specified as prescribed temperature, $\theta = \theta(\mathbf{x}, t)$; prescribed surface heat flux, $q = q(\mathbf{x}, t)$ per area; prescribed volumetric heat flux, $q = r(\mathbf{x}, t)$ per volume; surface convection: $q = h(\theta - \theta^0)$, where $h = h(\mathbf{x}, t)$ is the film coefficient and $\theta^0 = \theta^0(\mathbf{x}, t)$ is the sink temperature; and radiation: $q = A\Big((\theta - \theta^Z)^4 - (\theta^0 - \theta^Z)^4\Big)$, where A is the radiation constant (emissivity times the Stefan-Boltzmann constant) and θ^Z is the value of absolute zero on the temperature scale being used. Surfaces can also participate in cavity radiation effects. The cavity radiation formulation in Abaqus is described in "Cavity radiation," Section 2.11.4.

Spatial discretization

A variational statement of the energy balance, Equation 2.11.1–1, together with the Fourier law, Equation 2.11.1–2, is obtained directly by the standard Galerkin approach as

$$\int_V \rho \dot{U} \delta\theta \, dV + \int_V \frac{\partial \delta\theta}{\partial \mathbf{x}} \cdot \mathbf{k} \cdot \frac{\partial \theta}{\partial \mathbf{x}} dV = \int_V \delta\theta \, r \, dV + \int_{s_q} \delta\theta \, q \, dS, \tag{2.11.1–3}$$

where $\delta\theta$ is an arbitrary variational field satisfying the essential boundary conditions. The body is approximated geometrically with finite elements, so the temperature is interpolated as

$$\theta = N^N(\mathbf{x})\,\theta^N, \quad N = 1, 2, \ldots,$$

where θ^N are nodal temperatures. The Galerkin approach assumes that $\delta\theta$, the variational field, is interpolated by the same functions:

$$\delta\theta = N^N \delta\theta^N.$$

First- and second-order polynomials in one, two, and three dimensions are used for the N^N. With these interpolations the variational statement, Equation 2.11.1–3, becomes

$$\delta\theta^N \Big\{ \int_V N^N \rho \dot{U} dV + \int_V \frac{\partial N^N}{\partial \mathbf{x}} \cdot \mathbf{k} \cdot \frac{\partial \theta}{\partial \mathbf{x}} dV = \int_V N^N r \, dV + \int_{S_q} N^N q \, dS \Big\},$$

and since the $\delta\theta^N$ are arbitrarily chosen, this gives the system of equations

$$\begin{aligned}\int_V N^N \rho \dot{U} dV + \int_V \frac{\partial N^N}{\partial \mathbf{x}} \cdot \mathbf{k} \cdot \frac{\partial \theta}{\partial \mathbf{x}} dV \\ = \int_V N^N r \, dV + \int_{S_q} N^N q \, dS.\end{aligned} \tag{2.11.1–4}$$

This set of equations is the "continuous time description" of the geometric approximation.

Time integration

Abaqus/Standard uses the backward difference algorithm:

$$\dot{U}_{t+\Delta t} = (U_{t+\Delta t} - U_t)(1/\Delta t). \tag{2.11.1–5}$$

This operator is chosen for a number of reasons. First of all, we choose from one-step operators of the form

$$f_{t+\Delta t} = f_t + \big((1-\gamma)\dot{f}_t + \gamma \dot{f}_{t+\Delta t}\big)\Delta t$$

because of their simplicity in implementation (for example, no special starting procedures are needed) and well-understood behavior. For $\gamma < 1/2$ such operators are only conditionally stable for linear heat transfer problems. We prefer to work with unconditionally stable methods, because Abaqus is most commonly applied to problems where the solution is sought over very long time periods (compared to the stability limit for the explicit form of the operator, $\gamma = 0$), and so choose $\gamma \geq 1/2$. Of these operators the central difference method, $\gamma = 1/2$, has the highest accuracy. However, that form of the operator tends to produce oscillations in the early time solution that are not present in the backward difference form. Thus, we use $\gamma = 1$: backward difference. Introducing the operator, Equation 2.11.1–5, into the energy balance Equation 2.11.1–4 gives

$$\begin{aligned}\frac{1}{\Delta t}\int_V N^N \rho (U_{t+\Delta t} - U_t) dV + \int_V \frac{\partial N^N}{\partial \mathbf{x}} \cdot \mathbf{k} \cdot \frac{\partial \theta}{\partial \mathbf{x}} dV \\ - \int_V N^N r \, dV - \int_{S_q} N^N q \, dS = 0.\end{aligned} \tag{2.11.1–6}$$

This nonlinear system is solved by a modified Newton method. The method is modified Newton because the tangent matrix (the Jacobian matrix)—that is, the rate of change of the left-hand side of Equation 2.11.1–6 with respect to $\theta^N_{t+\Delta t}$—is not formed exactly. The formation of the terms in this tangent matrix is now described.

The internal energy term gives a Jacobian contribution:

$$\frac{1}{\Delta t}\int_V N^N \rho \left.\frac{dU}{d\theta}\right|_{t+\Delta t} N^M dV.$$

$(dU/d\theta)|_{t+\Delta t}$ is the specific heat, $c(\theta)$, outside the latent heat range, and is $c + L/(\theta_L - \theta_S)$ if $\theta_L > \theta_{t+\Delta t} > \theta_S$ at the integration point, where θ_L and θ_S are the liquidus and solidus temperatures and L is the latent heat associated with this phase change.

In severe latent heat cases this term can result in numerical instabilities, as the stiffness term $dU/d\theta$ is small outside the solidus-liquidus temperature range and is very stiff inside that rather narrow range. To avoid such instabilities in those cases this term is modified to a secant term during the early iterations of the solution to a time step. Since the modification occurs only in cases involving latent heat, it affects only those problems.

The conductivity term gives a Jacobian contribution:

$$\int_V \frac{\partial N^N}{\partial \mathbf{x}} \cdot \mathbf{k}\Big|_{t+\Delta t} \cdot \frac{\partial N^M}{\partial \mathbf{x}} dV + \int_V \frac{\partial N^N}{\partial \mathbf{x}} \cdot \frac{\partial \mathbf{k}}{\partial \theta}\Big|_{t+\Delta t} \cdot \frac{\partial \theta}{\partial \mathbf{x}}\Big|_{t+\Delta t} N^M dV.$$

The second of these terms is typically small, since the conductivity usually varies only slowly with temperature. Because of this, and because the term is not symmetric, it is usually more efficient to omit it. This term is omitted unless the unsymmetric solver is chosen. Prescribed surface fluxes and body fluxes can also be temperature dependent and will then give rise to Jacobian contributions.

With film and radiation conditions, the surface flux term gives a Jacobian contribution:

$$\int_S N^N \frac{\partial q}{\partial \theta}\Big|_{t+\Delta t} N^M dS.$$

For film conditions, $q = h(\theta)(\theta - \theta^o)$,

$$\frac{\partial q}{\partial \theta} = \frac{\partial h}{\partial \theta}(\theta - \theta^o) + h,$$

while for radiation, $q = A(\theta^4 - \theta^{o4})$,

$$\frac{\partial q}{\partial \theta} = 4A\theta^3.$$

These terms are included in exactly this form in the Jacobian. The modified Newton method is then

$$\begin{aligned}\Bigg[\frac{1}{\Delta t}\int_V N^N \rho \frac{dU}{d\theta}\Big|_{t+\Delta t} N^M dV &+ \int_V \frac{\partial N^N}{\partial \mathbf{x}} \cdot \mathbf{k}|_{t+\Delta t} \cdot \frac{\partial N^M}{\partial \mathbf{x}} dV \\ &+ \int_S N^N \left(\frac{\partial h}{\partial \theta}(\theta - \theta^o) + h + 4A\theta^3\right) N^M dS\Bigg] \bar{c}^M \\ &= \int_V N^N r \, dV + \int_{S_q} N^N q \, dS - \frac{1}{\Delta t}\int_V N^N \rho (U_{t+\Delta t} - U_t) \, dV \\ &- \int_V \frac{\partial N^N}{\partial \mathbf{x}} \cdot \mathbf{k} \cdot \frac{\partial \theta}{\partial \mathbf{x}} dV,\end{aligned}$$

with $\theta^N_{t+\Delta t, i+1} = \theta^N_{t+\Delta t, i} + \bar{c}^N, i =$ iteration number.

(2.11.1–7)

For purely linear systems Equation 2.11.1–7 is linear in $\overline{c}^M$ and, hence, in $\theta^N_{t+\Delta t}$, so a single equation solution provides the $\theta^N_{t+\Delta t}$. Since the method usually is only a minor modification of Newton's method, convergence is rapid.

Abaqus/Standard uses an automatic (self-adaptive) time stepping algorithm to choose Δt. This is based on a user-supplied tolerance on the maximum temperature change allowed in a time increment, and the increment is adjusted according to this parameter, as well as the convergence rate of Equation 2.11.1–7 in nonlinear cases.

The first-order heat transfer elements (such as 2-node link, 4-node quadrilateral, and 8-node brick) use a numerical integration rule with the integration stations located at the corners of the element for the heat capacitance terms. This means that the Jacobian term associated with the internal energy rate is diagonal. This approach is especially effective when strong latent heat effects are present. The second-order elements use conventional Gaussian integration. Thus, second-order elements are to be preferred for problems when the solution will be smooth (without latent heat effects), whereas the first-order elements should be used in nonsmooth cases (with latent heat).

The HEATCAP element is available for modeling lumped heat capacitance at a point. The associated concentrated film and concentrated radiation loading options are specified by the user. These loading options are also allowed in coupled temperature-displacement, coupled thermal-electrical, and coupled thermal-electrical-structural analyses.

Reference

- "Uncoupled heat transfer analysis," Section 6.5.2 of the Abaqus Analysis User's Manual